DOCTOR OF PHILOSOPHY

Mode spectrum of laser diodes subject to optical feedback

Perkins, Dave

Award date:
2004

Awarding institution:
Bangor University

Mode Spectrum of Laser Diodes Subject to Optical Feedback

Mode Spectrum of Laser Diodes Subject to Optical Feedback

University of Wales,

Bangor.

Submitted September 2004,

by

David Edward Perkins

for a

Doctorate of Philosophy

To Bethan and my Parents

Summary

Semiconductor laser diodes are are used in numerous applications. Laser diodes must be coupled to some form of external optical system for them to be any use, this can be achieved in many ways, but a the coupling usually results in some of the light being reflected back into the laser's facet. The laser is extremely susceptible to external stimuli, this is of course why they can so easily be modulated and are ideal for optical communication systems, but this also means that the unintended reflections cause dramatic changes in the laser's dynamics. A consequence of this effect has meant that considerable efforts have been made in to research of dynamics of laser diodes subject to optical feedback.

The usual approach to a theoretical study of laser diodes is to make some assumptions about the laser's output and parameters. However, every assumption removes some of the potential power of the model, this is done to reduce the computational requirements, which would otherwise be prohibitive. One fundamental assumption made is the light emitted from the laser is at one frequency, said to operate in the single mode limit, however it has been observed that most devices are actually multimode. The ap-

parent and well acknowledged conundrum is addressed in this work. The computational needs are met through the use of a purpose built cluster from commodity components. The model used is a recast version of the 1980's Coupled Cavity approach developed by Ebeling and Coldren.

The main results of this work are summarised here:

- A new spatial harmonic coupled cavity model is presented, offering a a single continuous variable of a complex frequency.
- By varying the external reflectivity and thus changing the level of reflected light into the cavity a catastrophic loss of mode discrimination occurs.
- Variation of sub-wavelengths of the external cavity induce a modulation in the mode lifetime, and at loss of mode discrimination this modulation does not occur.
- The critical point of loss of mode discrimination varies linearly with external cavity length. As such it is possible to define a short cavity limit, within which only certain phenomena occur, because at longer cavity lengths the feedback level is so small that it prohibitive.
- Large external cavities see the dielectric medium of the laser diode as a perturbation in the cold cavity limit. At a certain level of feedback all the modes can be regarded as compound cavity modes, rather than laser modes and external cavity modes.
- Laser diodes subject to optical feedback in the long cavity limit are seen as a dielectric perturbation to the external cavity modes. The addition of optical gain however, in the laser diode can overcome this effect and the laser diode's mode can regain dominance.

- A Beowulf cluster was developed for this work, and through the use of Java as the cluster Middle-ware is used to perform all the numerical simulations using legacy Fortran code.

Acknowledgements

I like to thank Dr. Paul S. Spencer for his continuing support and supervision of this work.

I would also like to acknowledge discussions with Prof. Paul Rees, which kept me on the straight and narrow. I would like to thank all the members of the Optoelectronics Group for numerous helpful discussions, with special thanks to Dr. Guy Barlow for his expertise in waveguide theory. I would also like to thank Rob Sheperd for offering his advice in computing with helpful discussions of a technical and not so technical nature.

I would like to thank Non and Derek Taylor for offering me the required solitude in their home for finalising this thesis.

I would like to acknowledge the funding of this work by the *Engineering and Physical Science Research Council* (EPSRC).

A final thank you to all the staff at the University of Wales, Bangor, School of Informatics for providing excellent resources.

David Perkins

Sept 2004

Contents

List of Figures

Chapter 1

Introduction

1.1 Semiconductor Lasers

Advances in technology over the last two decades have brought about increased demands on media storage and communications. To achieve the ever increasing drive towards ubiquitous computing the use of semiconductor laser diodes in optical storage devices such as DVDs (Digital Versatile Disks) and optical communication systems is inevitable. Although semiconductor lasers are already widely used, there is still plenty of scope for further exploitation. One of the primary factors that has limited utilisation is the inherent sensitivity of the laser diode to external stimuli. Small perturbations in the surrounding environment can destabilise a laser diode, resulting in fluctuations in both wavelength and output power [1]. Improved manufacturing techniques and packaging now offer a degree of immunity to laser diodes, but at the expense of increased manufacturing costs.

It has been observed both experimentally and theoretically that by deliberately changing the environment around the semiconductor laser diode it is possible to also take

advantage [2, 3, 4, 5, 6] of the natural sensitivity. For instance by controlling the optical feedback it is possible to increase the coherence of the laser and improve stability. It is also true that optical feedback effect can be detrimental and can lead to what is called *Coherence Collapse*, which is seen as large fluctuations in the laser diode's output power [7].

This thesis aims to increase the appreciation of laser instabilities and under-pin the dynamical models by further analysis and understanding of the laser's longitudinal mode structure.

1.2 Distributed Systems

The modern digital computer era began in 1945 and initially the development was slow and very expensive. In the mid-1980s, however, two fundamental advancements in technology gave rise to the dramatic pace of development we are familiar with today. The first was the *Central Processing Unit* (CPU), and the second was the *Local Area Network* (LAN). Increased processing power gave computers a sufficient level of abstraction from the computers inner workings to let less experienced users employ them to improve there own output. The LAN enabled these still relatively expensive machines (including printers, data storage and computers) to be linked together, thus allowing the sharing of information and the sharing of CPUs across the network. The result of these developments was to make computing more available and accessible to a wider group. The use of more powerful machines via remote connection gave rise to idea of combining computing power to perform calculations faster; the genesis of *Distributed Systems*. The definition of a distributed system is: *'A distributed system is a collection of independent computers that appear to its user a single coherent system'* [8].

Along side the LAN came the development of the *Wide Area Network* (WAN), this let computers over large distances or in different buildings be connected together. The spread of interconnected computers lead eventually to the Internet as we know it today. The rapidly increasing size and speed of the Internet has brought about the relatively new and on-going development of 'Grid' and 'e-Science' technologies [9].

The reduction in the cost of computers also led to more rapid development of Distributed Systems; costs went from one machine cycle per second costing one million pounds to one hundred pounds buying 10 million machine cycles per second (if the car had been developed at the same rate as the computer then a Rolls-Royce would now cost one pound and do a billion miles to the gallon).

As machine cycles became even cheaper, the idea of sharing these valuable resources was lost for a while, the computers were still interconnected but Distributed Systems were very much overlooked. It was not long before the potential power of combining all these now much more powerful machines was identified and thus the discipline of 'Distributed Systems' was rediscovered.

A particular area within the field of distributed systems is that of cluster development, whereby a cluster of dedicated computers are networked to produce a much larger and more powerful computer to that of its constituent component computers. For many years this was a very specialised field, primarily due to the costs involved. However, a breakaway area of cluster development looked at using commodity components that were relatively low cost to develop high performance clusters, this particular type of cluster is called a *Beowulf cluster* [10]. The Beowulf cluster uses a distributed memory architecture and as a consequence is only suitable for specific types of problem that have a large *computation to communication ratio* (see Chapter 7).

The development of Distributed Systems is not only of academic interest but goes

a long way toward aiding further research in many disciplines by offering unrivaled computing resources. The ever rising ceiling of available computing power gives the scientist the ability to remove simplifying assumptions that previously reduced the computational overhead of the problem and run simulations that would previously have had prohibitive computational needs. This thesis details the development and use of a Beowulf cluster for execution of computationally intensive numerical problems. Both the hardware and the software required to establish a usable and fully transparent system is presented to allow a previously prohibitive problems to be solved.

1.3 Multi-Discipline

As can be seen from the previous two sections, both areas of research offer many potential avenues for development, but it is when the two disciplines are combined to allow advanced research into a physical problem using a distributed system as the tool, that both areas greatly benefit.

The work presented in this thesis uses a purpose built Beowulf cluster to execute simulations of semiconductor lasers, and perform analysis of the longitudinal modal structures.

1.4 Objectives

The primary objective of this work is to study the coupled cavity model's modal structure. Having ascertained the salient features of the modal structure in the 'cold-cavity' limit the work then needs to establish the relevance and context of the results, this will be achieved through the addition of gain in the laser diode's active region.

The secondary objective is to observe any relationships between the static and dynamic solutions. This may allow dynamical boundaries to be defined by the static solutions.

The third objective of the work is to examine the advantages of using a distributed system for the processing of the numerical models. This also requires a full appreciation of the parallel processing paradigm.

1.5 Thesis Outline

Firstly, general semiconductor laser design is introduced, followed by an overview of the available semiconductor laser theoretical models. This then sets the scene to present the recast coupled cavity model used throughout this thesis. A technique is also presented for solving the coupled cavity model called the Argument Principle Method. The method of solution on the cluster, of the *new* recast coupled cavity model is tested and shown to give a true and accurate results, this is achieved through the examination of a solitary laser configuration of the coupled cavity model. The effects of coherent optical feedback are then studied and seen to show significant variations in the modal structure for parameter variation.

Having until now just looked at the model in the cold cavity limit, the laser diode is then pumped, the effects of this *optical gain* has been studied to further develop the model. NB: All new results are presented on a separate page from the text.

A more detailed overview of the distributed system used to calculate the solutions of the model is also given. The thesis is then concluded with suggestions as to the future direction for further work.

1.6 Contributions

The main contributions made in this thesis are outlined below:

- A new spatial harmonic coupled cavity model is presented, offering a a single continuous variable of a complex frequency.
- By varying the external reflectivity and thus changing the level of reflected light into the cavity a catastrophic loss of mode discrimination occurs.
- Variation of sub-wavelengths of the external cavity induce a modulation in the mode lifetime, and at loss of mode discrimination this modulation does not occur.
- The critical point of loss of mode discrimination varies linearly with external cavity length. As such it is possible to define a short cavity limit, within which only certain phenomena occur, because at longer cavity lengths the feedback level is so small that it prohibitive.
- Large external cavities see the dielectric medium of the laser diode as a perturbation in the cold cavity limit. At a certain level of feedback all the modes can be regarded as compound cavity modes, rather than laser modes and external cavity modes.
- Laser diodes subject to optical feedback in the long cavity limit are seen as a dielectric perturbation to the external cavity modes. The addition of optical gain however, in the laser diode can overcome this effect and the laser diode's mode can regain dominance.
- A Beowulf cluster was developed for this work, and through the use of Java as

the cluster Middle-ware is used to perform all the numerical simulations using legacy Fortran code.

References

[1] C.H. Henry and R.F. Kazarinov. Instability of semiconductor lasers due to optical feedback from distant reflectors. *IEEE J. Quantum Electron.*, QE-22(2):294–301, February 1986.

[2] G.P. Agrawal. Line narrowing in a single-mode injection laser due to external optical feedback. *IEEE J. Quantum Electron.*, QE-20(5):468–471, May 1984.

[3] R.W. Tkach and A.R. Chraplyvy. Regimes of feedback effects in 1.5-μm distributed feedback lasers. *J. Lightwave Tech.*, LT-4(11):1655–1661, November 1986.

[4] P. Besnard, B. Meziane, and G. M. Stephan. Feedback phenomena in a semiconductor laser induced by distant reflectors. *IEEE J. Quantum Electron.*, 29(5):1271, May 1993.

[5] K. Petermann. External optical feedback phenomena in semiconductor lasers. *IEEE J. Quantum Electron.*, 1(2):480–489, June 1995.

[6] J. Sacher, W. Elsasser, and E.O. Gobel. Nonlinear dynamics of semiconductor laser emission under variable feedback conditions. *IEEE J. Quantum Electron.*, 27(3):373–379, March 1991.

[7] D. Lenstra, B.H. Verbeek, and A.J. Den Beof. Coherence collapse in single-mode semiconductor lasers due to optical feedback. *IEEE J. Quantum Electron.*, QE-21(6):674–679, June 1985.

[8] J.M. Crichlow. *The Essence of Distributed Systems*. Essence of Computing. Prentice Hall, 1st edition, 2000. ISBN: 0130-15167-X.

[9] W. Gentzsch. Grid computing, a vendor's vision. *2nd IEEE/ACM International Symposium of Cluster Computing and the Grid*, pages 323–324, May 2002.

[10] D.J. Becker, T. Sterling, D. Savarese, J.E. Dorband, U.A. Ranawake, and C.V. Packer. Beowulf: A parallel workstation for scientific computation. *Proceedings of the 1995 International Conference on Parallel Processing(ICPP)*, 1:11–14, August 1995.

Chapter 2

Laser Theory

2.1 Introduction

The front page of an Los Angles newspaper on 8th July 1960 read "Los Angles scientist has invented the Death-Ray". This 'death ray', or ruby laser, had been demonstrated by Theodore(Ted) H. Maiman on the 16th May, 1960. It was, despite a valiant attempt to convince them otherwise, still a 'military tool' in the eyes of the press. The press were uninterested in its other, and more probable applications, and there the laser claimed its sci-fi role as a lethal weapon. Maiman's work on solid state lasers, which began in 1959 was based on a paper written by Arther L. Schawlow and Charles H. Townes, "Infrared and Optical Masers," [1] in *The Physics Review* in 1958 [1], which used the mechanism of stimulated emission shown previously in 1952 by Basov and Prohorov, from the microwave to optical region of the electromagnetic spectrum.

Through the 1960s the laser race was on, in December 1960 the first gas laser was demonstrated [3]. Then in 1962 several groups reported lasing action in semiconductors[4,

[1]Maiman's paper was originally submitted to *Physical Review Letters* but they rejected it, eventually the work was published in *Nature* [2], on 6th August 1960.

5, 6] using a *Fabry-Perot* optical cavity. In 1963 it was suggested that the semiconductor laser diode might be improved by of a sandwiched semiconductor active layer between semiconductor alloys with relatively wider band gaps [7, 8], which what is now commonly referred to as a *heterostructure* laser diode. The first successful demonstration of heterostructure laser diode operation at room temperature occurred in 1969 [9], but this was still under pulsed operation. Continuous wave (CW) operation was obtained one year later in 1970 [10, 11]. This semiconductor heterostructure laser diode design is still widely studied and used today.

The great steps forward made in laser technology have been accompanied by increasing exploitation of lasers in both industrial and domestic application. These range from laser machinery, to surgical instruments, and laser printers are almost ubiquitous in most modern homes.

Type	**Material**	**Wavelength**	**Use**
Excimer Gas	Argon Fluoride	(UV)193nm	Industrial Cutting/Drilling
Excimer Gas	Xenon Chloride	(UV)308nm	Invasive Surgery
Gas	Nitrogen	(UV)337nm	Spectroscopy
Gas	Argon	(BLUE)488nm	Display, Light Shows
Gas	Xenon	(White)multi	Invasive Surgery
Gas	Helium Neon	(Green)543nm	Alignment
Metal Vapor	Gold	(RED)627nm	Cosmetic Surgery
Solid State	Erbium:YAG	(MIR)2940nm	Dentistry
Solid State	Chromium Sapphire (Ruby)	(NIR)694nm	Cosmetic Surgery
Dye	Rhodamine	(VIS)600nm	Invasive Surgery
Semiconductor	Gallium Arsenide	(NIR)840nm	Comms, Printing, CD, DVD
Semiconductor	Gallium Aluminum Arsenide	(VIS/NIR)670-830nm	Displays, Comms
Semiconductor	Indium Phosphide	(VIS/NIR)1300-1550nm	Telecoms

Table 2.1: *Some example lasers and the their applications. There are considerable variations in wavelength*

As can be seen from Table 2.1, the possible applications are only limited by our imagination. It is, however, the semiconductor laser diode that is of interest here, and there are some striking differences between the semiconductor laser and gas and solid state lasers. The physical size of devices is significantly different: a typical helium-neon laser, as used for barcode scanning in supermarket checkouts is of the order of a quarter of a meter (0.25), whereas a semiconductor laser is of the order of a quarter of a millimeter ($0.25 \times 10^{-}3$m); three orders of magnitude different in length. Another large difference is in the amount of light that is emitted to the outside world. Conventional lasers typically emit 1% to 5% of the total light intensity, this is called a *closed* cavity system, whereas the laser diode emits light in the order of 70% and is called an *open* cavity system, this is why laser diodes are particularly interesting. The laser diode being an *open* system has a two fold effect, not only does more light get emitted but the laser diode is more susceptible to external stimuli and the surrounding environment.

In addition, semiconductor laser diodes have the ability to simply be modulated by using an electrical current, this is why they are of particular interest in the field of optical communications where modulation is 'the name of the game'. It has already been mentioned that the wavelength of the device is primarily down to the materials that are used to fabricate the laser diode. To appreciate how this relationship between the wavelength and material properties works, an understanding semiconductor materials is required.

2.2 Semiconductor Material System

Each different type of laser whether gas, dye or semiconductor, offers unique features that make it effective for specific applications. Figure 2.1 shows typical applications for

different types of semiconductor lasers.

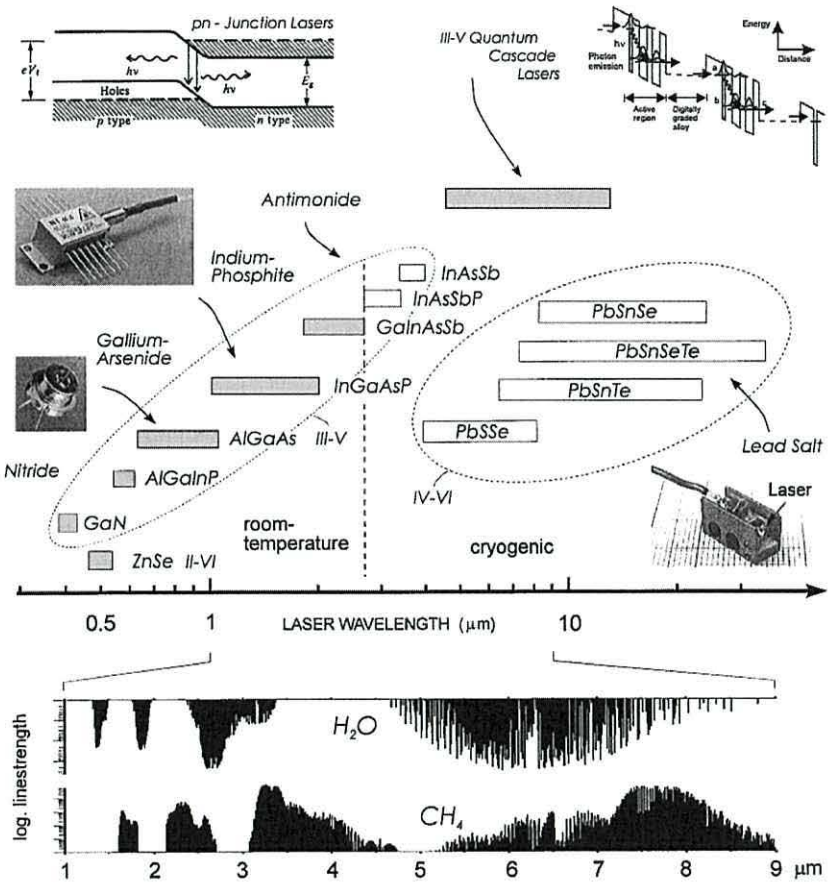

Figure 2.1: *A graph depicting the broad range of available wavelength for different active laser mediums and their applications.*

The range of possible applications of semiconductor laser diodes is attributable to this large band of potential wavelengths available by using different materials, ranging from near ultraviolet to far infrared, Fig. 2.2 shows how small variations in the alloy material composition of a Indium-Phosphide based system can be used to control the band-gap and hence the lasing wavelength, and also the lattice constant.

Semiconductor lasers are fundamentally based around a p-n junction, hence the name laser diode. If two similar pieces of semiconductor, one n-type (excess carriers)

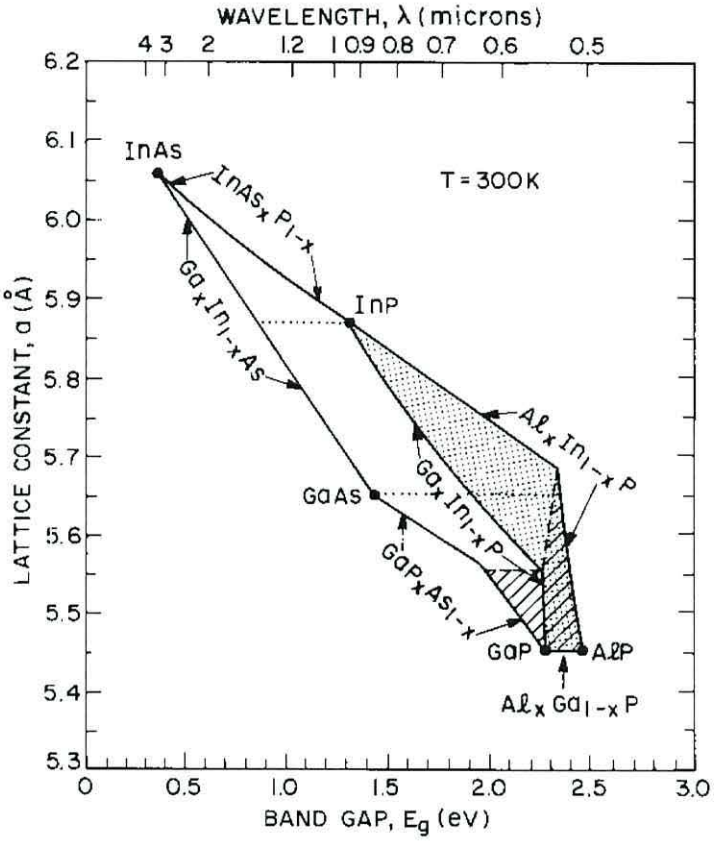

Figure 2.2: *Band gap and lattice constant for* $In_{1-x}Ga_xAs_{1-y}P_y$ *(clear region) and* $(Al_xGa_{1-x})_yIn_{1-y}P$ *(shaded regions). (Diagram source [12])*

and one p-type (excess holes) are examined the two Fermi energy levels are initially discontinuous, this is shown in Fig. 2.3. However, if a p-n junction is constructed the Fermi-level must remain continuous, Fig. 2.4, and as a consequence the electrons and holes diffuse across the junction, thus causing potential barrier, the junction is then said to be in a state of equilibrium. Applying a forward bias to the diode reduces the potential barrier and in doing so creates an 'overlap' region where both holes and electrons exist allowing recombination, and as a consequence, give out photons of light with the designated energy (equivalent to that of the band gap, $E_g = E_c - E_v$) see Fig. 2.5.

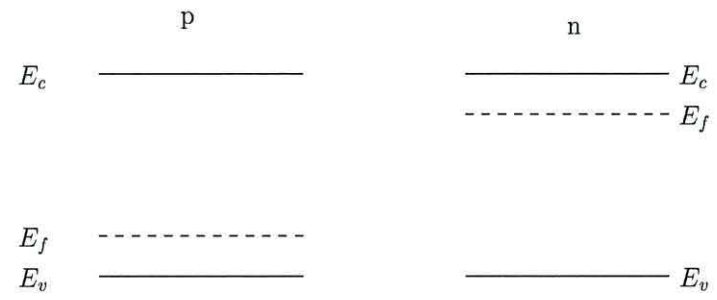

Figure 2.3: *The band diagram of a separate n and p type semiconductors*

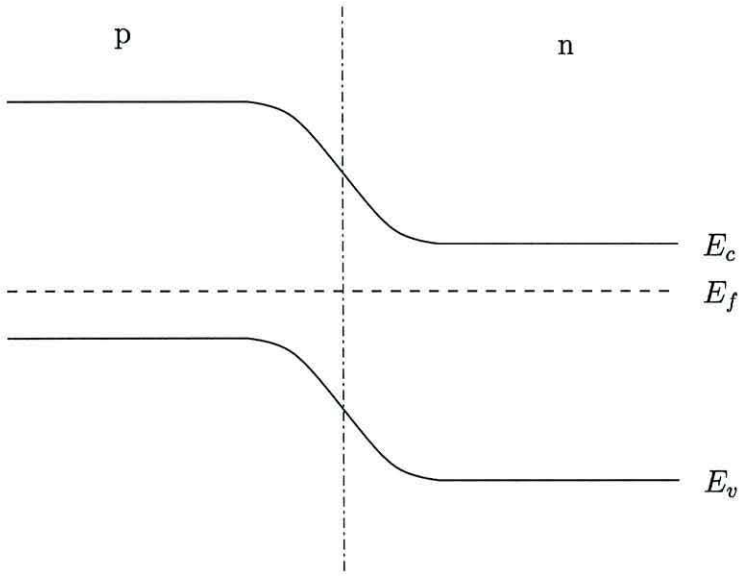

Figure 2.4: *The band diagram of a p-n junction in the equilibrium state*

The region of recombination, the active region, is easily shown by the quasi-Fermi levels, they define the active region of the laser diode, the active region is relatively small for a *homojunction* of the order of $0.1\mu m$. As there is a very small area where the electron-hole pairs (EHP) can recombine, they do so very quickly, so to be able to obtain sustained or continuous operation a large electrical current must be used. The use

of large currents leads to the the devices operating at high temperatures and continuous operation can only be sustained under cryogenic cooling alternatively pulsed operation can be achieved at higher temperatures. The primary cause is a lack of a mechanism to confine sufficient charge carriers to the active region to allow *continuous wave* (CW) operation. To over come this carrier confinement problem a *heterojunction* must be used.

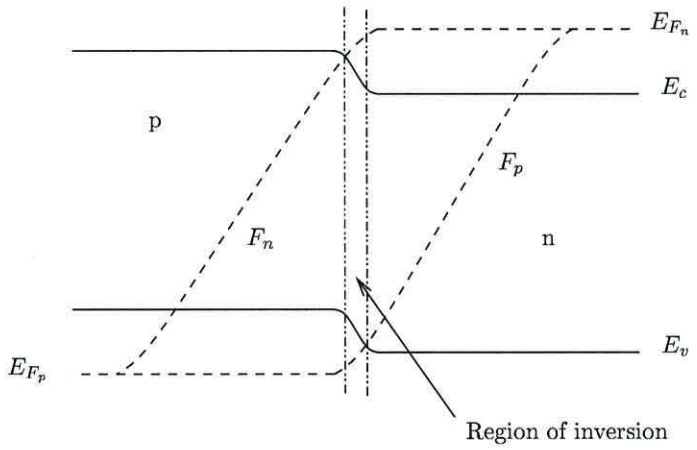

Figure 2.5: *A homojunction with a forward bias applied.*

An active layer sandwiched between layers which have larger band-gaps, but are also lattice matched allows much greater confinement. Figure 2.6 shows the single-heterojunction band diagram with no bias applied, the Fermi level is again equal throughout the entire device. It is important that the Fermi level in the n-type cladding is within the conduction band to allow a build up of charge carriers to form. Under forward bias conditions the holes and electrons can freely enter the active region, but are unable to cross over to the other side due to the potential barrier made by the band gap difference shown in Fig. 2.7. The forward bias then allows a sustained build up of the electron and

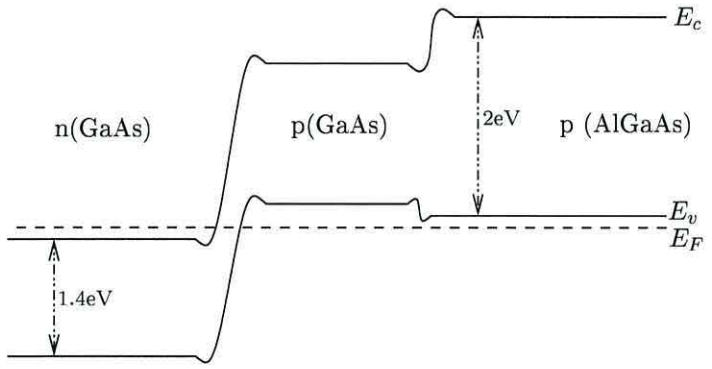

Figure 2.6: *A single-heterojunction band diagram at equilibrium.*

hole populations in the conduction and valence band respectively, the electrons and are then able to recombine to emit a photon of light. The overall effect of the heterostructure allows for a much reduced threshold and room temperature CW operation.

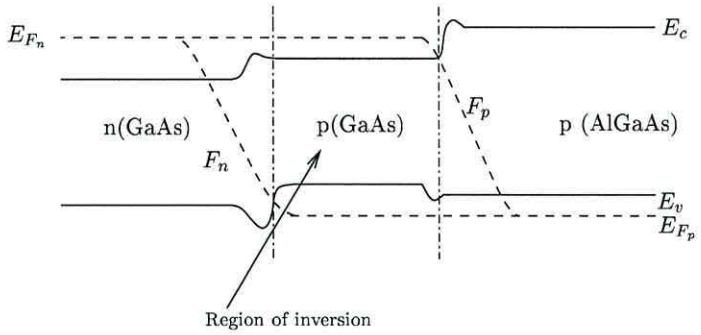

Figure 2.7: *A single-heterojunction band diagram with forward bias applied.*

Figure 2.7 shows a energy band diagram of a forward bias single-heterojunction laser diode, the smallest photon energy is equivalent to the band gap, E_g, as it is not possible for a electron to loose less energy to make the transition from the conduction

band to the valence band, the material may be regarded as transparent. However, it is possible for an electron at the top of the conduction band or at the quasi-Fermi level F_n, to transcend to the valence band or further to the other quasi Fermi level F_p. Population inversion is obtained when the quasi-Fermi level separation is greater than the band gap,

$$E_g \leq (F_n - F_p). \tag{2.1}$$

When the laser diode is place under forward bias, the effect of the build up of EHPs allows for the recombination to produce photons of light. The single-heterojunction laser diode can be improved to offer greater confinement and reduced a current requirement through the use of additional semiconductor layers: the *double-heterojunction.*

2.3 Geometry of the Laser Cavity

Assuming that a material structure is such that the conditions for optical gain are met, then the structure must be contained in a manner to allow standing wave. A simple yet effective means of achieving this is through the use of a Fabry-Perot cavity. The Fabry-Perot (FP) cavity is formed by cleaving the semiconductor structure normal to the heterojunction, the effect of the cleaved facets is to create two partially reflective dielectric mirrors which will reflect sufficient light back into the laser diode cavity to overcome losses and ensure lasing action.

Figure 2.8 shows a FP laser cavity of length L, defined by two mirrors formed by a cleaved facets. The cavity is filled with a semiconductor medium which has a refractive index, n, and therefore has an optical length nL. The mirrors are situated at $z = 0$ and $z = L$ and have power reflectivities of R_1 and R_2 respectively. Establishing a standing-

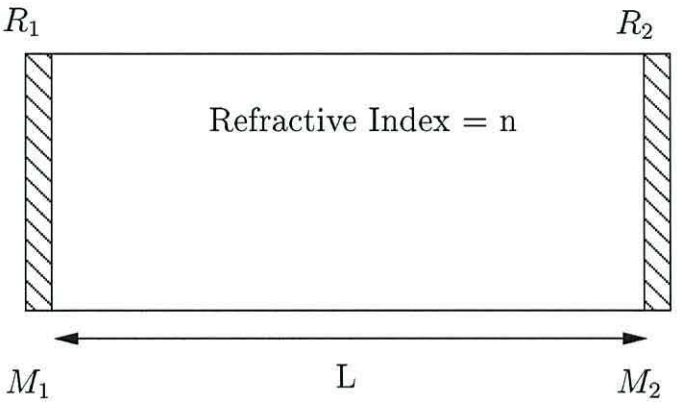

Figure 2.8: *A Fabry-Perot cavity bounded by two mirrors.*

wave, or longitudinal lasing mode within the cavity requires the reflected light wave to satisfy the *phase condition*, namely,

$$\lambda = \frac{2nL}{m} \tag{2.2}$$

where λ is the wavelength and m is an integer, this can be rewritten in terms of frequency,

$$\nu = \frac{mc}{2Ln} \tag{2.3}$$

where c is the speed of light.

Equation (2.3) indicates that there are an infinite number of wavelengths that satisfy the phase condition and thus are longitudinal modes of the cavity. In practice the finite spectral width of the optical gain ensures only a finite number of modes can possibly lase. Figure 2.9 shows a typical mode spectrum of a Fabry-Perot laser diode, well above threshold. Multiple longitudinal modes are supported because of the relatively

weak frequency selectivity of the Fabry-Perot cavity and the broad gain spectrum of the lasing medium.

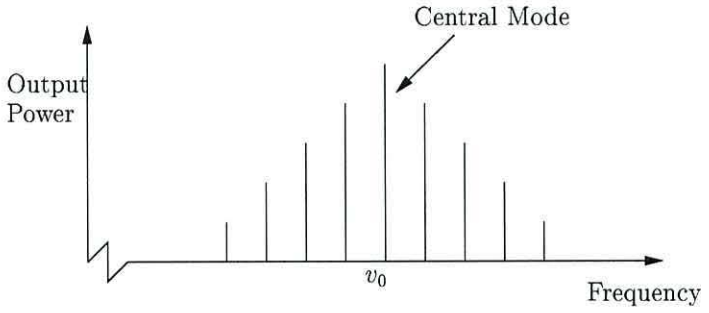

Figure 2.9: *A laser output spectrum with strong electrical pumping.*

The FP cavity laser diode is a very simple device to manufacture and as a consequence they are widely used. In a bid to induce single mode operation, which is a necessity in lots of applications, alternative cavity designs have been developed that have greater selectivity.

In-plane or *planar* lasers can be made to be much more longitudinal mode selective, this can be achieved by the addition of a *grating* to the end of the FP cavity, the grating has the effect of creating a frequency selective reflector. A grating is a periodic series of perturbations in the direction of propagation. These perturbations are arranged so that the reflections add constructively at particular frequencies. At the Bragg wavelength a small amount of light is reflected at each grating interface. If the grating is sufficiently long reflectivities approaching unity can be achieved.

Hence the cleaved facet mirrors of a FP cavity can be replaced with a passive grating to increase frequency selectivity of the device. If the grating is distributed over a passive region to form Bragg reflections, the devices are known as *Distributed Bragg Reflector*

(DBR) lasers. However to add the grating to the planar laser diode requires there to be a transition from the active to the passive region(s), and fabrication of such a device is difficult because the transition can have unwanted discontinuities. As such these devices are expensive and only generally used in specific applications. One technique to overcome this problem is to place the grating completely within the active region, removing the need to have a transition from active to passive regions, this type of laser is called a *Distributed Feed Back* (DFB) laser.

In the case of planar lasers the preferred method of adding a grating is to include it in the active region because of more straightforward fabrication [13].

A particular type of semiconductor laser diode that has the primarily been developed for single mode operation is the *Vertical Cavity Surface Emitting Laser* or VCSEL, see Fig. 2.10. This type of laser emits the light normal to the active region plane, and as a consequence of laser's cavity geometry and material parameters, single mode operation is obtained. The VCSEL typically uses either grating for reflections, and because of the geometry of the laser, are above and below the active region. The cavity is able to be made to be of the order of one wavelength thick, this is the dominant feature of the VCSEL, with the addition of a grating makes the VCSEL single mode, provided that small lateral size and appropriate shape is used to achieve single lateral and polarisation mode.

2.3.1 Transverse Mode Structure

The output of the laser diode has a beam profile, this beam profile is defined by the *transverse modes*. The transverse modes supported by the waveguiding formed by the index changes induced by the heterojunction and the lateral ridge structure.

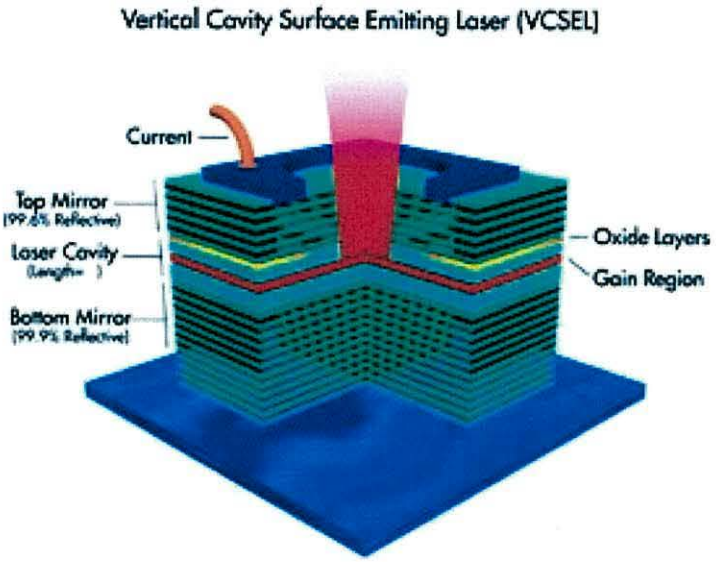

Figure 2.10: *A VCSEL laser cross-sectional drawing*

The large aspect ratio between the length and transverse dimensions of the laser diode make it possible to treat the transverse modes and longitudinal modes separately. The standard approach calculates the transverse modes by assuming the lasing wavelength is known.

Subsequent calculations can then be undertaken to deduce the confinement factor. The confinement factor is effectively a weighted factor that accounts for the fact that not all of the optical field is contained within the active region. By scaling the material gain by the confinement factor the effective, or modal gain, seen by the optical field can be calculated. Hence, the influence of the transverse modal profile has on the device characteristic can be, in most cases modeled by the confinement factor.

2.3.2 Lasing Threshold

A condition to determine the lasing threshold can be established by investigating at the wave propagation within the FP cavity, as depicted in Fig. 2.8. If it is said that the net optical gain is $g - \gamma$, where g is the gain and γ is losses, and that at $z = 0$ or mirror one (M_1) the wave power is P_{f0}. The forward traveling wave is defined as:

$$P_f(z) = P_{f0}e^{(g-\gamma)z}, \tag{2.4}$$

In order to derive the lasing condition of the first longitudinal mode the field amplitudes will be considered, the forward traveling E-field is denoted as $E_f(z)$ where $P_f = |E_f|^2$, giving,

$$E_f(z) = E_{f0}e^{\frac{1}{2}(g-\gamma)z}. \tag{2.5}$$

The wave traveling back from mirror two (M_2) is similarly defined as,

$$E_b(z) = E_{b0}e^{\frac{1}{2}(g-\gamma)(L-z)}, \tag{2.6}$$

the two waves are related by the reflection coefficients, R_1 and R_2, where the field reflectivities are defined by $R_1 = |r_1|^2$ and $R_2 = |r_2|^2$ and giving,

$$E_{f0} = r_1 E_b(0), \tag{2.7}$$

$$E_{b0} = r_2 E_f(L). \tag{2.8}$$

Using these two relationships, (2.7) and (2.8) an expression for a lasing condition is found,

$$r_1 r_2 e^{2(g-\gamma)L} = 1, \tag{2.9}$$

rearranging, gives an expression for the threshold gain of a device,

$$g_{th} = \gamma + \frac{1}{2L} ln\left(\frac{1}{R_1 R_2}\right). \tag{2.10}$$

A combination of the material parameter and the FP cavity then give appropriate condition for a semiconductor laser diode to lase.

2.4 Summary

Semiconductor lasers are remarkably small devices (e.g.chip size: $100\mu m \times 200\mu m \times 300\mu m$) and as as such emit very high frequencies, this along with the fact that they can be directly modulated through the mechanism of stimulated emission, either optically or electrically, makes them suitable as high frequency coherent light sources hence there wide acceptance for optical communication systems. Their considerable use in the telecommunication industry as well as other industrial application has meant that improving the laser diodes and reducing cost is of great importance.

The laser diode is made from a semiconductor material, and as such the effect of stimulating the electrons causes photons of light to be emitted. By creating a cavity around the semiconductor, standing waves are able to form, the the optical gain can be exploited to generate a light source. There are numerous ways of improving the laser diode design, the semiconductor structure can be adjusted to give gain at required frequencies, but also the resonant cavity can be changed to achieve single mode or multimode operation.

References

[1] A.L. Schawlow and C.H. Townes. Infrared and optical masers. *Phys. Rev.*, 112:1940, 1958.

[2] T.H. Mainman. Stimulated optical radiation in ruby. *Nature*, 187:493, 1960.

[3] A. Javan, Jr. W.R. Bennett, and D.R. Herriott. Population inversion and continous optical maser oscillation in gas discharge containing a he-ne mixture. *Phys. Rev. Lett.*, 3:106–110, Feburary 1961.

[4] R.N. Hall, G.E. Fenner, J.D. Kingsley, T.J. Soltys, and R.O. Carlson. Coherent light emission from gaas junctions. *Phys. Rev. Lett.*, 9:366–368, November 1962.

[5] M.I. Nathan, W.P. Dumke, G. Burns, Jr F.H. Dill, and G. Lasher. Stimulated emission of radiation from gaas p-n junctions. *Appl. Phys. Lett.*, 1(3):62, November 1962.

[6] T.M. Quist, R.H. Rediker, R.J. Keyes, W.E. Krag, B. Lax, A.L. McWhorter, and H.J. Zeigler. Semiconductor maser of gaas. *Appl. Phys. Lett.*, 1(4):91, December 1962.

[7] H. Kroemer. A proposed class of heterojunction lasers. *Proc IEEE*, 51:1782–1783, 1963.

[8] Z.I. Alferov and R.F. Kazarinov. Semiconductor laser with electric pumping. *Inverntors Certificate 181737*, 1963. Application NO. 950840, priority as of March 30, 1963.

[9] I. Hayashi, M.B. Panish, and P.W.Foy. A low-threshold room-temperature injection laser. *IEEE J. Quantum Electron.*, QE-5:211–212, April 1969.

[10] I. Hayashi, M.B. Panish, P.W. Foy, and S. Sumski. Junction lasers which operate continously at room temperature. *Appl. Phys. Lett.*, 17(3):109–111, August 1970.

[11] Z. Alferov, V. Andreev, D. Garbuzov, Y. Zhilyaev, E. Morozov, E. Portnoi, and V. Trofim. Room temperature operation of heterojunction laser. *Fiz. Tekh. Poluprovodnikov*, 4(1826), 1970. Translation: Sov. Physics. Semiconductor 4. 1573, 1971.

[12] G.P. Agrawal and N.K. Dutta. *Long-Wavelength Semiconductor Lasers*. Computer Science and Engineering Series. Van Nostrand Reinhold Company Inc., 1986.

[13] L.A. Coldren and S.W. Corzine. *Diode Lasers and Photonic Integrated Circuits*. Wiley, 1995. ISBN: 0-471-11875.

Chapter 3

Laser Dynamics

3.1 Introduction

As a consequence of easy direct modulation and the instabilities of laser diodes much research has be carried out on the dynamics of semiconductor laser diodes. Of particular interest are the effects external optical feedback, to make use of the laser output the light must be coupled to an external device or medium (optic fiber for example), despite precautions some of the light will be reflected back into the laser cavity. Optical feedback changes the dynamics of laser diodes, transiting different regimes of behaviour [1]. Most studies assume the laser diode to be a single mode device but it has however, been observed that the devices tend to have multimode spectrum.

Initially a simple phenomenological approach is presented to develop the rate equations for a solitary laser diode, this model is frequency independent and only calculates the rate of change of photons and charge carriers in the assumed mode.

The essential effects of coherent optical feedback are included in the electric field rate equation model developed by Lang and Kobayashi in 1980 [2]. When the model

is used in the single mode limit, it sees the optical feedback as a perturbation to the lasing mode, but in fact the application of optical feedback does in general increase the number of longitudinal modes, to accommodate this the model can be extended to accommodate multiple longitudinal modes. This is however under *a priori* assumption about the number of possible modes and there respective wavelengths and threshold gains. The primary drawback of this type of model is that it is only valid for low to moderate levels of external optical feedback.

The discrepancy that most models assume a single lasing mode but a multimode spectrum is observed experimentally, is addressed through the use of the *Coupled Cavity* model. The inherent multimode nature of laser diodes is encompassed directly into the model, and also allows higher levels of feedback to be studied, giving further insight into the laser diodes characteristics. The coupled cavity approach makes no assumptions about the modal structure or how many modes satisfy the lasing condition. The coupled cavity approach developed by Ebeling and Coldren [3] has been demonstrated by Pierce *et al* [4] to quantitatively reproduce the observed experimental results.

A drawback and cause of the lack of use of multimode models is the computational overhead associated with the calculations, not only do the rate equations demand large amounts of computing power, but before the temporal simulations can be commenced, the frequencies and the lifetimes of each of the modes must be found.

The work presented in this thesis uses the coupled cavity approach to study the modal structure of a multimode laser diode subject to coherent optical feedback, the aim being to eliminate possible erroneous assumptions about the modal structure. This chapter is intended to set the stage for the investigation into the modal structure and introduce methods to calculate the number of possible lasing modes and find their wavelengths and lifetimes.

3.2 Solitary Laser Diode

Within the laser's cavity there are two primary quantities of concern, the *carrier* density, N, and the *photon* density, S. Establishing how these two quantities vary with time allows further understanding into laser diode characteristics. A simple phenomenological approach is taken to the development of the required rate equations. Initially a rate equation for the carriers within the active region of the laser shall be developed, followed by the development of a rate equation for the photon density.

The number of carriers (electrons) within the active region can either increase, through the process of *Generation* or decrease through the process of *Recombination.* These two processes form the basis of the rate equations, they also provide a starting point for the phenomenological development of the rate equations. It can be said that the rate of change of the carriers, N, is equal to the combined effect of the generation and recombination of carriers,

$$\frac{dN}{dt} = G_{gen} - R_{rec}, \tag{3.1}$$

here G_{gen} is the generation rate of electrons and R_{rec} is the rate of recombining electrons per unit volume in the active region. The carrier generation is produced by a current density J across the active region, of thickness d, thus,

$$G_{gen} = \frac{J}{qd}, \tag{3.2}$$

q is the electronic charge. The rate of recombination is somewhat more complicated and can be split into several mechanisms. There is a *spontaneous* recombination rate, R_{sp}, this occurs when some energy is lost and some electrons drop back into the valance

band, a photon will be produced but the contribution is small by comparison to the stimulated emission (this only occurs if lasing). There needs to also be a *non-radiative* recombination, R_{nr}, and there is some *carrier leakage*, R_l, both of these processes reduce the carrier density but do not contribute to the photon density. Finally and perhaps most importantly, the *stimulated* recombination, R_{st}, this is the source of photon generation once the laser is above threshold, or once population inversion has been achieved. The recombination can thus be written,

$$R_{rec} = R_{sp} + R_{nr} + R_l + R_{st}. \tag{3.3}$$

It is possible to describe all the *natural* processes, taking place through the creation of a *carrier lifetime*, τ_e, this allows a rate of decay of carriers due to natural processes to be written,

$$\frac{dN_{nat}}{dt} = R_{sp} + R_{nr} + R_l = \frac{N}{\tau_e}, \tag{3.4}$$

so int the first approximation (in a more accurate model, τ_e itself decreases with N due to the importance of bimolecular and possibly Auger emission in lasers) the total recombination taking place is written using equation (3.3) and equation (3.4) as,

$$R_{rec} = \frac{N}{\tau_e} + R_{st}. \tag{3.5}$$

Now by taking the separate expressions of the rate of recombination and generation it is possible to write a simple, first version of the rate equation for the carriers,

$$\frac{dN}{dt} = \frac{J}{qd} - \left(\frac{N}{\tau_e} + R_{st}\right) = \frac{J}{qd} - \frac{N}{\tau_e} - R_{st}. \tag{3.6}$$

To complete the full model the rate equation for change in photons density, S, must be developed. Within a laser cavity the primary contributing factor to the photon density is the the stimulated recombination process, for every recombination a photon is generated. In the case of a Fabry-Perot cavity the photons of interest are the ones emitted at a resonant mode frequency (related to cavity length and band gap of the material), so it is true to say that the spontaneously emitted photons make a minimal contribution to the resonant modes as they are emitted across the entire range of possible frequencies and in all directions, so very few are emitted at the resonant frequency of interest, they must still, however, be taken into account.

The confinement factor, *Gamma* determines the extent to which the active region is within the transverse mode profile and thus the magnitude of the gain within the waveguide region of the laser diode. As in the case of the carrier rate equation it is now possible to write a simple expression for the rate of change of photons within the laser cavity,

$$\frac{dS}{dt} = \Gamma R_{st} + \Gamma \beta_{sp} R_{sp} - \frac{S}{\tau_p}, \tag{3.7}$$

where β_{sp} is the *spontaneous emission factor*. In the case of uniform mode coupling this is the reciprocal of the number of optical modes within the bandwidth of the spontaneous emission. Again a *photon lifetime*, τ_p has been used to account for the natural photon decay processes.

Equations (3.6) and (3.7) are the almost complete coupled rate equations for a semiconductor laser diode. To complete them the value of R_{st} must be related to the gain and photon density. If it is assumed that the laser diode is above threshold and that the confinement factor is one ($\Gamma = 1$), total confinement, then if the initial photon density is S and after a small distance through the active region, Δz, the photon density is $S + \Delta S$,

this growth can be described as gain per unit length, g by,

$$S + \Delta S = S e^{g\Delta z}. \tag{3.8}$$

If Δz is sufficiently small then $e^{g\Delta z} \approx (1 + g\Delta z)$. Also the distance moved can be defined in terms of a velocity for a time, t, thus $\Delta z = v_g \Delta t$, where v_g is the group velocity. Substituting back into equation (3.8) the increase in the photon density is

$$\Delta S = S g v_g \Delta t, \tag{3.9}$$

this now allows a generation term to be expressed,

$$\left(\frac{dS}{dt}\right)_{gen} = R_{st} = \frac{\Delta S}{\Delta t} = v_g g S. \tag{3.10}$$

Now having an expression for the stimulated photon emission, which of course is equal to the stimulated carrier recombination, the rate equations are nearly complete. It is possible to express the spontaneous photon emission as an effective spontaneous current, J_{sp} just as the pumping current was defined. Combining all these adjustments, the coupled rate equations for a semiconductor laser diode can be written,

$$\frac{dN}{dt} = \frac{J}{qd} - \frac{N}{\tau_e} - v_g g S, \tag{3.11}$$

$$\frac{dS}{dt} = \Gamma v_g g S + \frac{J_{sp}}{qd} - \frac{S}{\tau_p}. \tag{3.12}$$

These two equations still require further development to make use of them, however, these further modifications depend upon the intended use, for instance a carrier density dependence of gain must be included. It has been suggested that the gain varies as a

function linear function of carrier density [5] and can be approximated by,

$$g \approx a(N - N_{tr}) \tag{3.13}$$

where a is the differential gain and N_{tr} is the transparency carrier density.

Using equations (3.11), (3.12) and (3.13) a small signal analysis can be performed, this results in some of the characteristic parameters associated with semiconductor lasers.

The laser diode has some similar output responses to that of a RLC circuit, a variation in the electrical pumping causes a change in the output that has damped oscillations or *relaxation oscillations* as they are known, this occurs at a resonant frequency called the *relaxation resonance frequency* and is related to the system parameters. Here an overview of the means of determining these parameters from the rate equations is presented.

If a direct current (DC) J_0, with a small alternating current (AC) J_1, superimposed is applied to the laser diode then the lasers steady state carrier density and photon density would respond similarly, the drive frequency is ω, thus:

$$J = J_0 + J_1 e^{j\omega t}, \tag{3.14}$$

$$N = N_0 + N_1 e^{j\omega t}, \tag{3.15}$$

$$S = S_0 + S_1 e^{j\omega t}. \tag{3.16}$$

In order to make use of the steady state conditions equations (3.14),(3.15) and (3.16) and rate the equations (3.11) and (3.12) must be rewritten to include the linear gain

approximation from equation (3.13),

$$\frac{dN}{dt} = \frac{J}{qd} - \frac{N}{\tau_e} - v_g a(N - N_{tr})S, \tag{3.17}$$

$$\frac{dS}{dt} = \Gamma v_g a(N - N_{tr})S + -\frac{S}{\tau_p}. \tag{3.18}$$

The varying values of J, N and S can be substituted into equations (3.17) and (3.18) and because at steady state the differential goes to zero, and $a(N_0 - N_{tr})$ is just g_{th} and can be replaced by $(\Gamma v_g \tau_p)^{-1}$ [5], the rate equations can be written in a steady state form,

$$j\omega N_1 = \frac{J_1}{qd} - \frac{N_1}{\tau_e} - \frac{S_1}{\Gamma\tau_p} - v_g a N_1 S_0, \tag{3.19}$$

$$j\omega S_1 = \Gamma v_g a N_1 S_0. \tag{3.20}$$

To find the relaxation resonance frequency the two steady state equations (3.19) and (3.20) must be manipulated. Multiplying the two equations together and ignoring all but the third term on the right hand side of the first equation gives a value for the relaxation resonance frequency,

$$\omega_R^2 = \frac{v_g a S_0}{\tau_p}. \tag{3.21}$$

The relaxation resonance frequency effectively sets the maximum modulation frequency and hence approximately defines the modulation bandwidth [5].

3.3 External Optical Feedback

Soon after the development of the laser diode it was realized that when using the laser for certain applications, some of the output light would unintentionally be reflected back into the laser cavity. The effect of this optical feedback was to destabilize the

laser, it was then of course deemed vital that further understanding of optical feedback be achieved. Lang and Kobayashi made the first attempt at explaining weak optical feedback in 1980 [2]. Their model describes the evolution of an electric field of a single mode laser diode. The first rate equation model presented in section 3.2 does not include optical frequency, it concentrates on modeling how the changes in the photon and carrier densities occurs and assumes the optical frequency is known and does not vary. To fully describe the effect of optical feedback variation in the instantaneous optical frequency need to be modeled. The optical feedback can be modeled using a time delayed field term with a coupling strength, κ.

The Lang and Kobayashi rate equation is written, assuming a single lasing frequency of a solitary laser, ω_0, as

$$\frac{d}{dt}E(t) = \frac{1}{2}(1 + i\alpha)\,G(N)\,(N(t) - N_{th})\,E(t) + \frac{\kappa}{\tau_e}E(t-\tau)e^{-i\omega_0(t-\tau)}, \tag{3.22}$$

where $G(N)$ is the gain term, τ_e is the carrier lifetime, τ is the external cavity round trip time, $N(t)$ is the instantaneous carrier density and N_{th} is the threshold carrier density. The use of the alpha factor, α (popularized by Henry [6]) gives a convenient phenomenological means of quantifying the amplitude and phase coupling that occurs in semiconductors.

3.3.1 Steady State Analysis

Steady state analysis provides deeper insight in to the effects of parameter variation within the Lang-Kobayashi equations. By defining the electric field, $E(t)$, as a slowly varying amplitude and phase,

$$E(t) = E_0(t)e^{i\phi(t)}, \tag{3.23}$$

the complex electric field equations can be written as two purely real equations for the amplitude and phase,

$$\frac{dE_0(t)}{dt} = \frac{1}{2}G_N(N(t) - N_{th})E_0(t) + \left(\frac{\kappa}{\tau_{in}}\right)E_0(t-\tau)cos(\omega_0 t + \Delta(t)), \quad (3.24)$$

$$\frac{d\phi(t)}{dt} = \frac{\alpha}{2}G_N(N(t) - N_{th}) + \frac{\kappa E_0(t-\tau)}{\tau_{in}E_0(t)}sin(\omega_0 t + \Delta(t)), \quad (3.25)$$

where $\Delta(t) = \phi(t) - \phi(t-\tau)$, and N_{th} is the threshold carrier density of the solitary laser. There have been many studies into extending this steady state analysis to examine various aspects of the equations [7, 8, 9, 10, 11, 12, 13, 14, 15, 16], they have shown that the steady state analysis of the system results in a set of coupled equations that describe how the gain (through the carrier density) and the lasing frequency are effected by the external optical feedback. The solutions are found by assuming $E_0(t) = E_0(t-\tau) = E_s$, $N(t) = N_s$ and $\phi(t) = \Delta\omega_s t = (\omega_s - \omega_0)t$. Substituting these into equations (3.24,3.25) and setting the derivatives to zero gives,

$$\omega_0 - \omega_s = \frac{\kappa}{\tau_{in}}\sqrt{1+\alpha^2}sin(\omega_s\tau + arctan\alpha), \quad (3.26)$$

$$N_s = N_{th} - \frac{2\kappa}{G_N\tau_{in}}cos(\omega_s\tau). \quad (3.27)$$

The gain modulation can also be expressed by rearranging equation (3.27) to give,

$$G_N(N_{th} - N_S) = \frac{2\kappa}{\tau_{in}}cos(\omega_S\tau) = (\tilde{g}) \quad (3.28)$$

It is clear in equation (3.26) that the alpha factor plays a significant role in the resultant values for the fixed point solutions. Figure 3.1 shows a plot of the transcendental equation (3.26) as a function of increased optical feedback. Each colour represents a

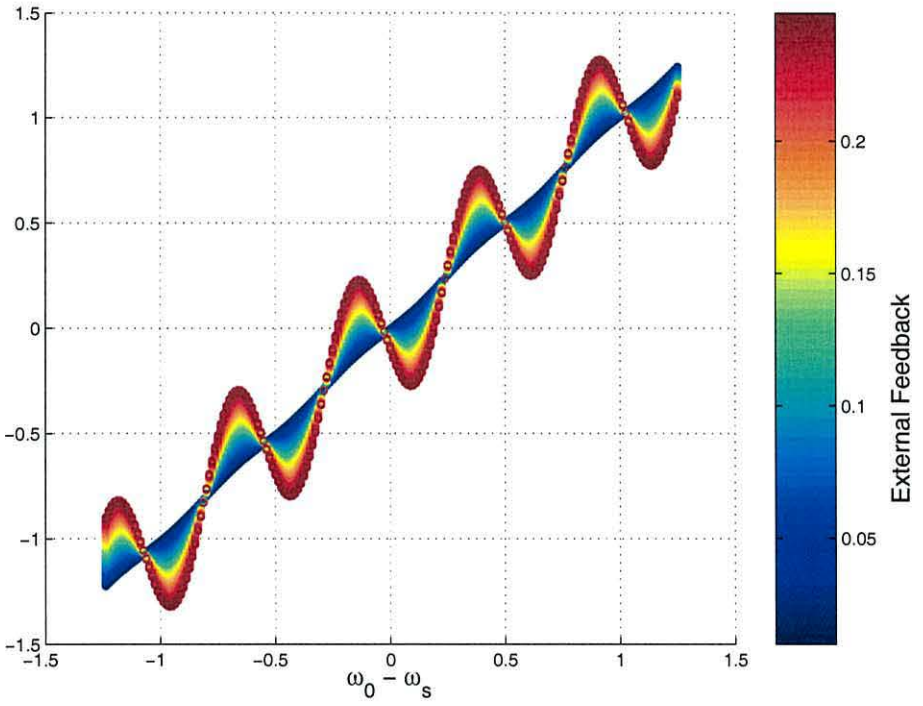

Figure 3.1: *Round trip phase change versus optical frequency for varying levels of feedback, represented by different colours. As the feedback level is increased the number of solutions around the solitary mode increase. It can be clearly seen that for zero and very weak feedback that only a single solution exists: the solitary mode.*

particular feedback level. It can be seen that increasing the feedback level increases the number of solutions. The solutions are often referred to as compound-cavity modes, they can be split in to *anti-modes* and *modes*. Anti-modes are the compound-cavity modes where the curve intersects zero with a negative gradient, and the modes are where the solutions intersect with a positive gradient. This distinction of modes and anti-modes can be more precisely expressed, by taking the derivative with respect to ω_s of equation (3.26)the curvature can be determined and hence the modes satisfy the

following condition [7]:

$$\frac{d\omega_0}{d\omega_s} = 1 + \frac{\kappa\tau}{\tau_{in}}\sqrt{1+\alpha^2}cos(\omega_s\tau + arctan(\alpha)) > 0 \tag{3.29}$$

Combining equations (3.26) and (3.29) gives a means of identifying the possible lasing modes. Feedback increases the number of possible solutions and each of which has its own gain threshold. For a fixed feedback level the threshold carrier density, and hence the optical power can be shown to be significantly affected by the external cavity length. The photon density for all the modes taken together is given by,

$$P_s = |E_s|^2 = \frac{1}{G_N(N_s - N_0)}\left(\frac{J}{ed} - \frac{N_s}{\tau_s}\right). \tag{3.30}$$

One of the primary limitations of the Lang-Kobayashi model is that it is not valid for strong external optical feedback, this is because the model assumes only a small perturbation from the solitary laser operating point.

3.3.2 Regimes of Feedback

A paper by *Tkach and Chraplyvy* in 1986, [1] outlined the now well known regimes of external optical feedback for external cavity laser diodes. Varying the level of external optical feedback allows control over which of the dynamical regimes the laser operates. Figure 3.2 shows the five regimes of dynamical external laser diode operation as a function of the feedback power and the cavity length. An overview of the salient features of each of the regimes is given below.

Regime I is where low levels of feedback are injected back into the laser cavity, typically of the order of $-80dB$ (less than 10^{-7}). The effect upon the laser's spectrum

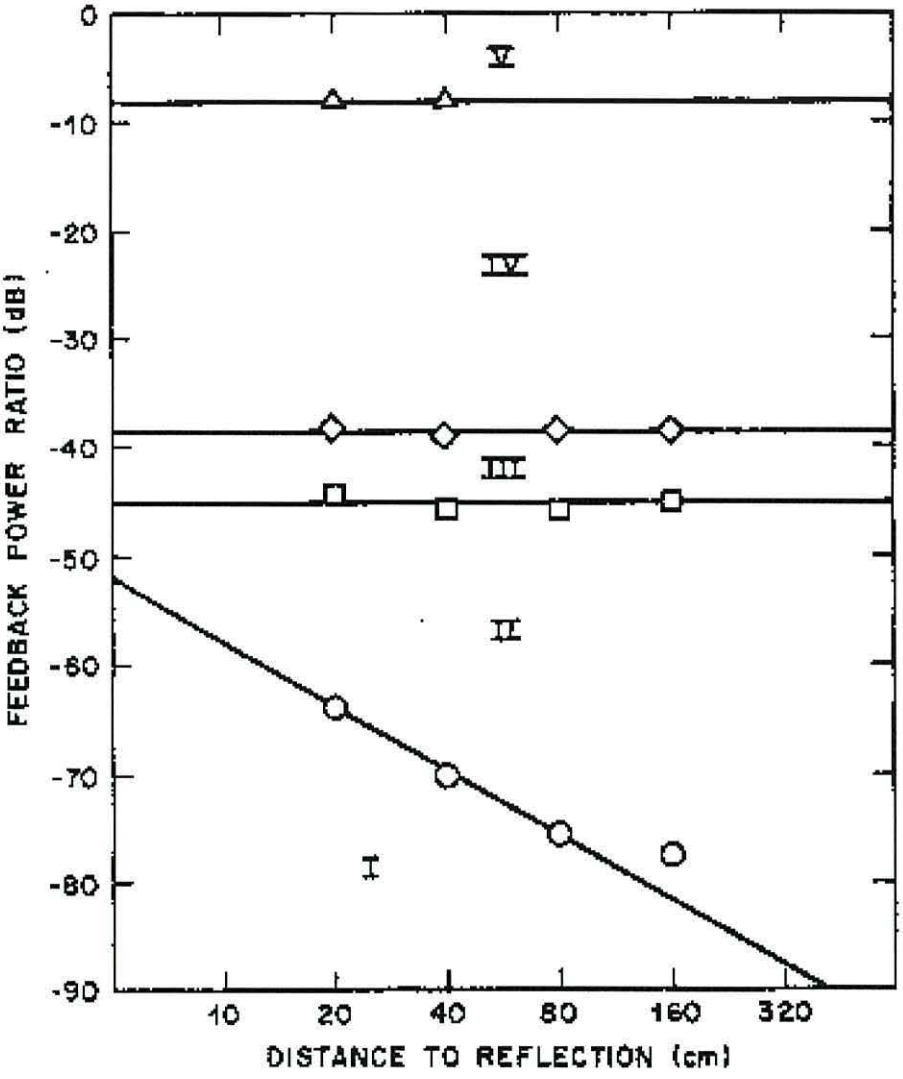

Figure 3.2: *The five regimes of external cavity laser diode operation.(Diagram Source [1])*

is a reduction or broadening of the laser's linewidth (up to 30%, [6]), the in-phase case decreases the linewidth and the out-phase case increases the linewidth [17]. The phase can also cause the threshold gain and lasing frequency to change. The levels of feedback are extremely low, so in many cases it is caused by any unintended reflections, perturbations or misalignment, this regime is generally not

used in any applications because the level of feedback can easily fluctuate and can cause the lasers dynamics to change. The narrowest linewidth single mode laser in this regime can be described using a "thermodynamic" potential model, which is based on neglecting all the power fluctuations [18, 19], a consequence of these calculations it that the deepest potential well, most stable external cavity mode is the mode with the narrowest linewidth [20].

Regime II is transited from *Regime I* with the characteristic line broadening, the original single mode in the first regime is split into two or more rapidly hopping modes, this is accompanied by a considerable increase in phase noise, attributable to the differing threshold gains of the modes. The modes do not lase simultaneously but instead a single mode hops frequency. As further feedback is added the hopping frequency and mode split further increase.

Regime III is characterized by a stable single mode operation, this is achieved as the feedback phase causes the mode of the smallest threshold gain lases, called the *Maximum Gain Mode*, unlike in *Regime I* where the mode with minimum linewidth lases [21]. Work by Levine *et al* [22] on the maximum gain mode and minimum linewidth mode has indicated that the maximum gain mode will be the only stable external cavity mode under larger levels of feedback. However. it is not always possible to put the system in this state. The very small range under which this regime exists ($-38dB$ to $-45dB$ or variation of $10^{-4}\%$), means that it is very sensitive to variations in the external feedback, this means that keeping the laser in the regimes is tremendously difficult, hence it is inappropriate for most applications, and not always observed experimentally.

Regime IV is called the coherence collapse regime; typically 1% to 10% of feedback

is required to operate the laser diode in this regime, it has also been seen that the coherence length of the laser is significantly reduced, by as much as a thousand times; this results in coherence lengths of less than 10mm, [11]. Once a certain feedback is reached the laser enters a dynamically unstable state. The linewidth broadens by several orders of magnitude, by operation on multiple modes and a broader band of noise [23, 24]. Frequency and amplitude fluctuations in the coherence collapse regime make the laser useless for conventional communications, however, it has been shown to allow data to be chaotically encrypted for secure communications [25, 26, 27].

Regime V is the regime in which strong optical feedback is applied to the laser diode. It is characterized by a very narrow linewidth for stable single mode operation along with low noise intensity [24]. In order to operate the laser in this regime the system must at least have 10% of the emitted power reflected back into the laser cavity, it is within this region that the laser is dominated by the external cavity and is some times called a *External Cavity Diode Laser* (ECDL).

3.3.3 Short and Long Cavity Limits

The regimes of laser dynamics described in the previous section are not as clear cut as one would ideally like, this is reflected by the fact that a two parameter space is presented, Fig. 3.2, made up of feedback ratio and distance to reflection. As a consequence of the possible laser diode parameter sets, there have been numerous studies [10, 20, 24] into defining the regime boundaries more accurately, it is however worth noting that in general the five dynamical regimes are possible; the questions is what conditions will ensure the dynamics are as expected?

Figure 3.2 shows that the feedback required to operate in *Regime II* decreases with increasing external cavity length. However, all the other boundaries appear to be independent of the external cavity length. This is only true if the external cavity length is much greater than the laser diode cavity. In practice this condition is usually met. However, in the case of reflection from within the laser package itself (or indeed in integrated devices) this condition ($l_{ext} >> l_{cavity}$) is no longer satisfied and different behaviour has been observed.

This delineation between these two limits (short and long cavity) is not easily quantified. The commonly accepted boundary between the two regimes was first put forward by Schunk and Petermann [20] and states that short cavity operation is observed if

$$\omega_r \tau_{ext} < 1 \tag{3.31}$$

where ω_r is the relaxation resonance frequency of the solitary laser. Hence the boundary is dependent on the injection carriers as well as the external cavity length. If the inequality is satisfied the reflected signal returns before a full cycle of the relaxation oscillation can take place.

An alternative definition makes use of the feedback coefficient, C [10, 20, 24],

$$C = \frac{\tau_{ext}}{\tau_D} \frac{1 - R_2}{\sqrt{R_2}} \sqrt{1 + \alpha^2} \sqrt{f_{ext}}, \tag{3.32}$$

where R_2 is the facet reflectivity, α is the linewidth enhancement factor, τ_D is the round trip time for the lasers cavity, likewise, τ_{ext} is the roundtrip time for the external cavity(proportional to the cavity length) and f_{ext} is the feedback fraction, this is equivalent to the feedback power ratio discussed in the previous section, and is defined as

$f_{ext} = P_r/P_l$ where the subscripts, r and l are reflected power and output power respectively. Short cavity operation is produced if,

$$C < 1, \tag{3.33}$$

(ie before multiple external cavity modes can exist)

Figure 3.3, shows a plot of the feedback fraction f_{ext} against the external cavity roundtrip time τ_{ext}. A plot of $C = 1$ is shown and offers a good approximation to the short-long cavity limit boundary, is allows a definite boundary below which the laser will always be stable ($C < 1$) and above which the laser is able to enter other regimes of dynamics. In conclusion to this section, the boundary of the short and long cavity limit is not precise, but a good approximation can be made. The critical difference between the short and long cavity operation, is that coherence collapse is not induced in the short cavity limit. The device is always stable.

3.4 Multimode Models

The rate equation model introduced in the beginning of this chapter models the rate of change of a quantity of charge carrier and photons of light, there is an assumed lasing frequency for the CW operation. The Lang and Kobayashi rate equation model then includes the lasing frequency in the model through the use of a slowly varying electric field. However, both these models assume that there is only one lasing mode. It is, however, possible to modify them to take into account multiple longitudinal modes. The single mode model with low to moderate levels of feedback have been shown to offer good approximations to the salient features of the experimental

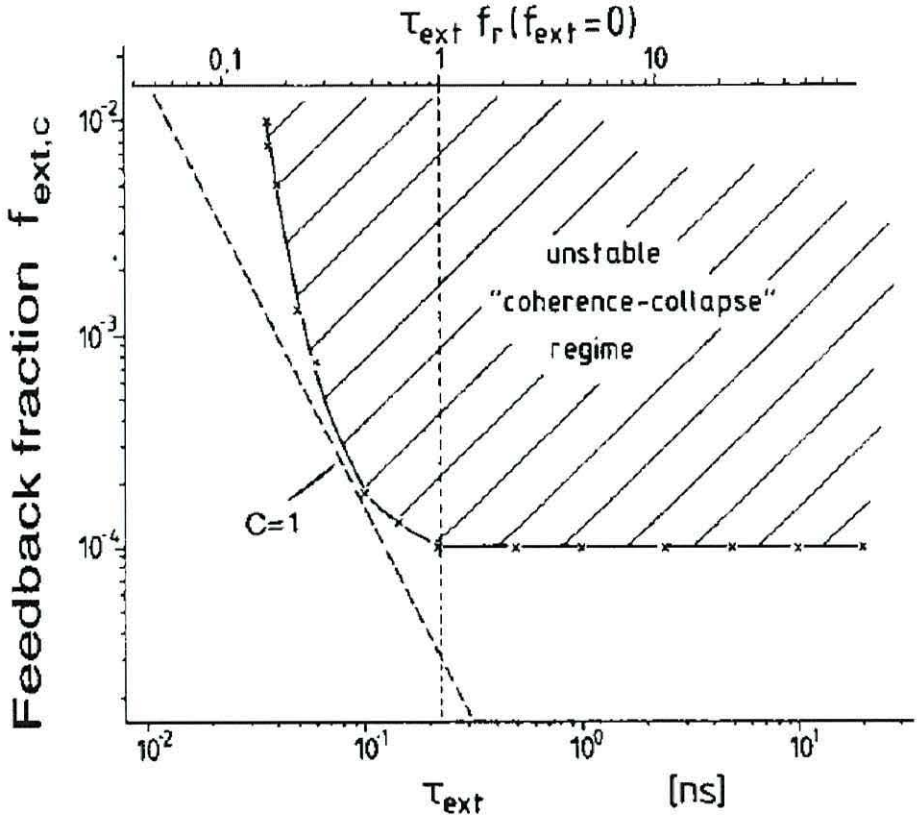

Figure 3.3: *Feedback fraction f_{ext}, above which "coherence collapse" occurs found from numerical calculation. f_r corresponds to the relaxation resonance frequency (f_r = 4.4GHz in this example). The dashed line corresponds to a feedback coefficient, C = 1.(Diagram Source [20])*

results [28, 10, 11, 1, 29, 30, 31, 8, 32, 33, 23, 34, 9]. The experimental results do however show a multimode spectrum [35], this is significant when within or close to coherence collapse regime [11], of laser semiconductor laser dynamics where the features are fundamentally expected to be multimode.

3.4.1 Multimode Lang-Kobayashi

The Lang-Kobayashi model can be extended to include multiple modes. Ryan *et al* [36], used a multimode Lang-Kobayashi model which was shown to model modulated laser diodes subject to weak optical feedback in single mode [37, 38] and in multimode [39, 40] operation. The modified Lang-Kobayashi model can be written in the following manner [36],

$$\frac{dE_m}{dt} = \frac{1}{2}(1 - i\alpha)(G_m - \gamma_m)E_m + \zeta_m^{int} + F_m(t) + \kappa_m E_m(t - \tau)e^{i\omega\tau}, \quad (3.34)$$

$$\frac{dN}{dt} = \frac{I}{q} - \frac{N}{\tau_e} - \sum_{j=1}^{M} G_j|E_j|^2 + F_N(t), \quad (3.35)$$

where

$$G_m(N) = a(N - N_0) - \delta G_m, \quad (3.36)$$

$$\zeta_m^{int} = -\frac{1}{2}\left(\beta_m P_m + \sum_k \theta_{mk} P_k\right)E_m + \sum_k \kappa_{mk} E_{2k-m}^{\star} E_k^2. \quad (3.37)$$

In equation (3.35) $E_m(t)$ is the complex amplitude of the mth mode oscillating at a frequency ω_m, G_m is the mode gain, γ_m is the mode dependent cavity loss, ζ_m^{int} account for interactions between the modes, τ is the external roundtrip time and F_m account for the random noise generated by the spontaneous emission. The complex field is written in terms of amplitude and phase as $E_m = \sqrt{P_m}e^{i\phi}$, where P_m is the photon number and ϕ is the phase. In equation (3.35) N is the number of electrons, I is the injection current, q the electronic charge, τ_e the carrier lifetime. In equation (3.36), a is the gain parameter, N_0 is the transparency density, δG_m is the gain margin, θ_{mk} is the cross-saturation parameter, and κ_{km} is the four wave mixing parameter [36].

3.4.2 Iterative Model

The iterative approach based on the traveling wave description is an alternative approach to modeling laser diodes subject to optical feedback. Such an approach was initially developed by Sporleder [41] and then extended by Mork [42]. The main difference from the Lang-Kobayashi model is that higher levels of feedback can be applied as multiple round trips of the external cavity are included. It can also be easily be modified to include multimode laser cavity operation. The iterative model employs difference equations and uses the time interval of the internal round trip time τ_{in}, the equation are written in the following form [42],

$$\begin{aligned} E_m(t+\tau_{in}) &= \left\{E_m(t) + \kappa E_m(t-\tau)e^{-j\Omega_m\tau}\right\} \times \\ &\quad e^{\frac{1}{2}\tau_{in}[(1-i\alpha)G_N(N(t)-N_{th})+G_2(\omega_m,N)]} + \tau_{in}F_E(t). \end{aligned} \tag{3.38}$$

where G_2 are the terms describing the spectral variation of gain, and the rate equation for carriers,

$$\frac{dN}{dt} = J - \frac{N(t)}{\tau_e} - \sum_m G(\omega_m, N)|E_m(t)|^2, \tag{3.39}$$

where all the terms have there usual meaning.

3.4.3 Coupled Cavity Model

Extensions of the Lang-Kobayashi or the Iterative model to include multiple longitudinal modes assume the longitudinal modes to be equally spaced in wavelength or frequency, and that the application of external optical feedback acts as a perturbation to each of the modes. This requires an assumption about the number of longitudinal modes and their wavelength before any simulations can be undertaken.

The coupled cavity model [4] includes the effects of optical feedback in a very different way, the model draws from the early theory of Lamb and Scully on the whole universe mode theory of lasers [43, 44]. The theory was originally developed to look at how Fabry-Perot modes and external modes couple with narrow linewidth lasers, and examined their power leakage [45]. In contrast Ebeling's coupled cavity analysis assumes finite external cavity lengths, and the resulting output spectrum shows distinct modes. Unlike in the Lang-Kobayashi and Iterative approaches no initial assumptions are made about the number of cavity modes or their wavelengths.

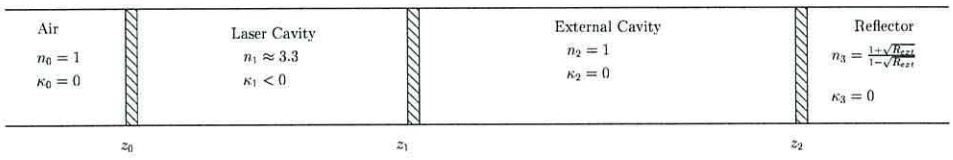

Figure 3.4: *Laser diode with external reflector as a coupled cavity system. The refractive index of each cavity is denoted by n_m and gain by κ_m.*

Figure 3.4 shows a coupled laser diode cavity (z_0 to z_1) coupled to an external air cavity (z_1 to z_2) which is created through the use of a dielectric mirror at z_2, the value of the refractive index, n_3 is chosen to yield an identical reflectivity to the proposed external reflector (having a reflectivity of R_{ext}) through the relationship,

$$n_3(\omega) = \frac{1 + \sqrt{R_{ext}(\omega)}}{1 - \sqrt{R_{ext}(\omega}}. \tag{3.40}$$

The laser diode is bounded at the other end by a *semi-infinite* air cavity. It is possible that the reflectivity of the dielectric mirror may have a frequency dependence, and must be written as shown in equation (3.40), but from this point it will be assumed that the reflectivity is frequency independent and written as R_{ext}. The system shown in Fig.3.4 and

described here is the system of interest in this thesis, but the technique is adaptable to model almost any system of cavities, other devices such as distributed feedback (DFB) lasers or integrated devices can be modeled through appropriate additional matrices and appropriate parameters.

The coupled cavity model is founded on using a one-dimensional plane wave derivation, this greatly simplifies the equations to be handled. It is of course important that the model allows for the transverse modes to be accommodated, this can be achieved phenomenologically using an effective index calculation.

The longitudinal modes are calculated using Ebeling and Coldren's [3] method, self-consistently with the optical susceptibility. The possible modes that exist must have the wavelength and threshold gain calculated. This is carried out under the assumption that the sinusoidally varying electromagnetic field are traveling in both directions in each of the cavities described above. The electric field component satisfies the wave equation

$$\frac{d^2E_m}{dz^2} + k_m^2 E_m = 0, \tag{3.41}$$

where the complex propagation constants are defined as:

$$k_m = \frac{\omega}{c}(n_m + i\kappa_m). \tag{3.42}$$

where n_m is the refractive index of the m^{th} section and κ_m is related to the gain, g_m by the expression,

$$\kappa_m = \frac{c}{\omega}\frac{g_m}{2}. \tag{3.43}$$

The development of the coupled cavity analysis starts by equating the electromagnetic fields at the cavity boundaries. A derivation of this model can be found in Appendix A.

In short the model is derived from an equation for the forward and backward traveling waves at a given boundary. The total electric field is written as,

$$E(z) = Ae^{-jkz} + Be^{jkz} \tag{3.44}$$

After applying the usual electromagnetic interface conditions, any given configuration can be described using a matrix formalism. Here the system shown in figure 3.4, is describe with the matrix notation,

$$\begin{pmatrix} A_3 \\ B_3 \end{pmatrix} = Q(z_2)Q(z_1)Q(z_0)\begin{pmatrix} A_0 \\ B_0 \end{pmatrix} \tag{3.45}$$

where $Q(z_m)$ represents a single boundary at z_m and is of the form:

$$Q(z_m) = \begin{pmatrix} \frac{k_{m+1}+k_m}{2k_{m+1}} e^{i(k_{m+1}-k_m)z_m}, & \frac{k_{m+1}-k_m}{2k_{m+1}} e^{i(k_{m+1}+k_m)z_m} \\ \frac{k_{m+1}-k_m}{2k_{m+1}} e^{-i(k_{m+1}+k_m)z_m}, & \frac{k_{m+1}+k_m}{2k_{m+1}} e^{-i(k_{m+1}-k_m)z_m} \end{pmatrix}$$

The expression must then be solved, this can be achieved by setting $A_0 = 1$, and $A_3 = 0$ and solving the system for k_1. A non-generic solution can be determined on the basis that element $Q_{1,1} = 0$. In the case of a laser diode subject to optical feedback the following equation must be solved,

$$\frac{e^{ik_3z_2}}{8k_3k_0k_1}\{(k_3+k_0)e^{-ik_0(z_2-z_1)}\left[(k_3-k_1)^2e^{-ik_1z_1}-(k_1-k_0)^2e^{ik_1z_1}\right][-2i(k_3-k_0)(k_0^2-k_1^2)e^{ik_0(z_2-z_1)}sin(k_1z_1)\} = 0 \tag{3.46}$$

The solutions to the above expression can be then related to the lasing frequency, ω_{mode}

and threshold gain, g_{th} by the following relations:

$$\omega_{mode} = \frac{c}{n_1}\Re\{k_1\}, \tag{3.47}$$

$$g_{th} = -2\Im\{k_1\}, \tag{3.48}$$

where n_1 is treated as a constant at any one time. It is solving equation (3.46) that causes the greatest computational overhead, as the cavities get longer or the structure become complex this becomes prohibitive.

Alternative models have been proposed to study optical feedback in laser diodes that calculate the underlying mode structure of the compound cavity, [4]. In particular, Pierce *et al.* [4] made use of the coupled cavity approach developed by Ebeling *et al.* [3] to show that the Chraplyvy and Tkach [1] classification of the regimes of operation was reproduced using the a multimode coupled cavity model. In the coherence collapse regime the simulations showed that the anticipated chaotic dynamics observed in the total optical power was associated with significant mode hopping in the spectral domain. Further developments of this type of model has been hampered by the computational overhead that accompanies this approach.

By making the simplifying assumption that the laser diode facet furthest from the external mirror has unity reflectivity, it can be shown that a 'boundary equation' can be derived from the coupled cavity approach. This boundary equation can then be used to determine the longitudinal mode structure of a laser diode with a external cavity, [46]. Using this approach Duarte and Solari have investigated the validity of the Lang-Kobayashi model in the short cavity limit by studying the bifurcations of the boundary equation. Their analysis revealed that the mode structure developed through a succession of saddle-node bifurcations, which caused modes to apparently appear and dis-

appear as the external reflectivity was increased. More importantly, they showed that as the external reflectivity was increased, that two distinct types of longitudinal mode structure could be identified. For low levels of optical feedback the modes cluster in 'islands' around the remnants of the solitary laser modes, and the solutions are qualitatively similar to those predicted by the Lang-Kobayashi model. However, beyond a certain external reflectivity the the islands begin to merge and this effectively establishes the limit of validity of the Lang-Kobayashi equation; since it requires consideration of multiple longitudinal modes. In the Duarte and Solari paper the maximum reflectivity, above which the Lang-Kobayashi model was still valid, was loosely stated as being around R=0.011. The authors speculated that this maximum reflectivity would be sensitive to the frequency dependence of semiconductor susceptibility, but would only be weakly dependent on the external cavity round-trip time.

In this thesis the question of the longitudinal mode structure will be considered in a more general configuration than that addressed in [46]. In particular, both of the laser facets will be assumed to be partially reflecting; the susceptibility of the semiconductor will also be assumed to frequency independent; and all external cavity sizes will be considered. By studying the 'cold cavity' limit it will be shown that there is a critical feedback level at which both phase discrimination and mode lifetime discrimination is lost (see chapter 4). This striking effect is only important when the external cavity and laser cavity are comparable and indicates that the sub-picosecond pulses predicted by the Lang-Kobayashi model, [47, 48] may ultimately be due to mode-locking. The critical feedback level was also found to decrease exponentially with external cavity length, which is in agreement with Duarte and Solari speculations [46].

Rate Equations

Along side the solution of (3.46) is a set of rate equations, one for the carrier density in the gain section,

$$\frac{dN}{dt} = \frac{J}{qd} - \frac{J_{spon}}{qd} - v_g \sum_l g(\omega_l) S_l - \frac{N}{\tau_e}, \tag{3.49}$$

and m equations for the photon densities, S_l, in each of the coupled modes,

$$\frac{dS_l}{dt} = v_g \Gamma g(\omega_l) S_l + \beta \frac{J_{spon}}{qd} - \frac{S_l}{\tau_l}. \tag{3.50}$$

In this system of equations J is the drive current, d is the active region width, q is the electronic charge, J_{spon} is equivalent to the spontaneous emission current, β is the spontaneous coupling factor, v_g is the modal group velocity, Γ is the confinement factor (assumed to be the same for all modes) and τ_e is the carrier lifetime.

3.5 Summary

Several theoretical models of laser diodes subject the feedback have been outlined. The Lang and Kobayashi model has been discussed, and its limitations identified. Some of the limitations are addressed by way of the iterative approach, through the addition of multiple round trips larger values of external feedback can be modeled.

In general the models described assume a single longitudinal mode is lasing (the single mode limit), but the observed behaviour usually suggests multimode operation. Subsequent work has extended the models to allow multimode simulation to be conducted, but these still operate under some assumptions about the system in advance, namely, that the modes are all equally spaced in frequency.

The conventional coupled cavity model was outlined and the method to determine the longitudinal mode spacing of the device emphasised. No assumptions about the mode spacing (modal structure) is made, thus a complete framework for a dynamical model can be determined.

References

[1] R.W. Tkach and A.R. Chraplyvy. Regimes of feedback effects in 1.5-μm distributed feedback lasers. *J. Lightwave Tech.*, LT-4(11):1655–1661, November 1986.

[2] R. Lang and K. Kobayashi. External optical feedback effects on semiconductor injection laser properties. *IEEE J. Quantum Electron.*, 16:347–355, 1980.

[3] K.J. Ebeling and L.A. Coldren. Analysis of multielement semiconductor lasers. *J.Appl Phys*, 54(6):2962–2968, June 1983.

[4] I. Pierce, P. Rees, and P. S. Spencer. Multimode dynamics in laser doides with optical feedback. *Phys. Rev. A*, 61:053801, 2000.

[5] L.A. Coldren and S.W. Corzine. *Diode Lasers and Photonic Integrated Circuits*. Wiley, 1995. ISBN: 0-471-11875.

[6] C.H. Henry. Theory of the linewidth of semiconductor lasers. *IEEE J. Quantum Electron.*, QE-18(2):259–264, February 1982.

[7] B. Tromborg, J.H. Osmundsen, and H. Olesen. Stability analysis for a semiconductor laser in an external cavity. *IEEE J. Quantum Electron.*, QE-20(9):1023–1032, September 1984.

[8] J. Mork, J. Mark, and B. Tromborg. Route to chaos and competition between relaxation oscillations for a semiconductor laser with optical feedback. *Phys. Rev. A*, 65:1999–2002, 1990.

[9] J. Mork, B. Tromborg, and J. Mark. Chaos in semiconductor lasers with optical feedback: Theory and experimental. *IEEE J. Quantum Electron.*, 28(1):93–108, January 1992.

[10] K. Petermann. *Laser Diode Modulation and Noise*. Kluwer Academic, 1988. isbn 90-277-2672-8.

[11] D. Lenstra, B.H. Verbeek, and A.J. Den Beof. Coherence collapse in single-mode semiconductor lasers due to optical feedback. *IEEE J. Quantum Electron.*, QE-21(6):674–679, June 1985.

[12] P. Besnard, B. Meziane, and G. M. Stephan. Feedback phenomena in a semiconductor laser induced by distant reflectors. *IEEE J. Quantum Electron.*, 29(5):1271, May 1993.

[13] C.H. Henry and R.F. Kazarinov. Instability of semiconductor lasers due to optical feedback from distant reflectors. *IEEE J. Quantum Electron.*, QE-22(2):294–301, February 1986.

[14] H. Li, J. Ye, and J.G. McInerney. Detailed analysis of coherence collapse in semiconductor lasers. *IEEE J. Quantum Electron.*, 29(9):2421–2432, September 1993.

[15] N. Kikuchi Y. Lui and J. Ohtsubo. Controlling dynamical behaviour of a semiconductor laser with external optical feedback. *Phys. Rev. E*, 65:2697–2700, 1995.

[16] N. Kikuchi, Y. Liu, and J. Ohtsubo. Chaos control and noise suppression in external cavity semicondutor lasers. *IEEE J. Quantum Electron.*, 33(1):56–65, January 1997.

[17] G.P. Agrawal. Line narrowing in a single-mode injection laser due to external optical feedback. *IEEE J. Quantum Electron.*, QE-20(5):468–471, May 1984.

[18] J. Mork and B. Tromborg. The mechanism of mode selection for an external cavity laser. *IEEE Phot. Tech. Lett.*, 2(1):21–23, January 1990.

[19] J. Mork, M. Semkow, and B. Tromborg. Measurement and theory of mode hopping in external cavity lasers. *Elec. Lett.*, 26(9):609–610, September 1990.

[20] N. Schunk and K. Petermann. Stability analysis for laser diodes with short external cavities. *IEEE Phot. Tech. Lett.*, 1(3):49–51, March 1989.

[21] K. Petermann. External optical feedback phenomena in semiconductor lasers. *IEEE J. Quantum Electron.*, 1(2):480–489, June 1995.

[22] A.M. Levine, G.H.M. van Tartwijk, D. Lenstra, and T. Erneux. Diode lasers with optical feedback: Stability of the maximum gain mode. *Phys. Rev. A*, 52:R3436–R4339, 1995.

[23] J. Wang and K. Petermann. Noise analysis of semiconductor lasers within the coherence collapse regime. *IEEE J. Quantum Electron.*, 27(1):3–9, January 1991.

[24] G.A. Acket, D. Lenstra, A.J. Den Beof, and B.H. Verbeek. The influence of feedback intensity on longitudinal mode properties and noise in index-guided semiconductor lasers. *IEEE J. Quantum Electron.*, QE-20(10):1163–1169, October 1984.

[25] L.M. Pecora and T.L. Carroll. Driving systems with chaotic signals. *Phys. Rev. A*, 44:2374–2383, 1991.

[26] R. Roy and K.S. Thornburg. Experimental synchronization of chaotic lasers. *Phys. Rev. Lett.*, 72(3):2009–2012, March 1994.

[27] S. Sivaprakasam and K.A. Shore. Message encoding and decoding usingchaotic external-cavity diode lasers. *IEEE J. Quantum Electron.*, 36(1):35–39, January 2000.

[28] G.P. Agrawal and N.K. Dutta. *Long-Wavelength Semiconductor Lasers*. Computer Science and Engineering Series. Van Nostrand Reinhold Company Inc., 1986.

[29] G.C. Dente, P.S. Durkin, K.A. Wilson, and C.E.Moeller. Chaos in the coherence collapse of a semiconductor laser. *IEEE J. Quantum Electron.*, 24(12):2441–2447, December 1988.

[30] N. Schunk and K. Petermann. Numerical analysis of the feedback regimes for a single mode semiconductor laser with external feedback. *IEEE J. Quantum Electron.*, 24(7):1242–1247, July 1988.

[31] B. Tromborg and J. Mork. Stability analysis and the route to chaos for laser diodes with optical feedback. *IEEE Phot. Tech. Lett.*, 2(8):549–552, August 1990.

[32] J.S. Cohen, F. Wittgrefe, M.D. Hoogerland, and J.P. Woerdman. Optical spectra of a semiconductor laser with incoherent optical feedback. *IEEE J. Quantum Electron.*, 26(6):982–990, June 1990.

[33] J. Park, D. Seo, and J.G. McInerney. Self-pulsations in strongly coupled asymmetric external cavity semiconductor lasers. *IEEE J. Quantum Electron.*, 26(8):1353–1362, August 1990.

[34] J. Sacher, W. Elsasser, and E.O. Gobel. Nonlinear dynamics of semiconductor laser emission under variable feedback conditions. *IEEE J. Quantum Electron.*, 27(3):373–379, March 1991.

[35] M. Giudici C. Green G. Giacomelli G. Huyet, S. Balle and J.R. Tredicce. Low frequency fluctuations and multimode operation of a semiconductor laser with optical feedback. *Optics Commun.*, 149:341–347, April 1998.

[36] G.R. Gray A.T.Ryan, G. Agrawal and E.C. Gage. Optical-feedback-induced chaos and its control in multimode semiconductor lasers. *J. Quantum Electron.*, QE-30(3):668–680, March 1994.

[37] L.N. Langley and K.A. Shore. The effect of external optical feedback on the turn-on delay statistics of laser diodes under pseudorandom modulation. *IEEE Phot. Tech. Lett.*, 4(11):1207–1209, November 1992.

[38] L.N. Langley and K.A. Shore. The effect of external optical feedback on timing jitter in modulated laser diodes. *J. Lightwave Tech.*, 11(3):434–441, March 1993.

[39] A. Ritter and H. Haug. Theory of laser diodes with weak optical feedback ii: Limit-cycle behavior, quasi-periodicity, frequency locking and route to chaos. *J. Opt. Soc. Am. B*, 10:144, 1993.

[40] A. Ritter and H. Haug. Theory of laser diodes with weak optical feedback i: Small signal analysis and sidemode spectra. *J. Opt. Soc. Am. B*, 10:130, 1993.

[41] F. Sporleder. Traveling wave line model for laser diodes with external optical feedback. *Proc. URSI Int. Symp. on Electromagn. Theory, Santiago de Compostela, Spain*, pages 585–588, August 1983.

[42] J.Mork. *Nonlinear Dynamics and Stochastic Behaviour of Semiconductor Lasers.* PhD thesis, Technical University of Denmark, 1989. report No. S48.

[43] M.B. Spencer and Jr. W.E. Lamb. Laser with a transmitting window. *Phys. Rev. A*, 5(2):884–892, February 1972.

[44] R. Lang and M.O. Scully. Why is the laser line so narrow? a theory of single-quasimode laser operation. *Phys. Rev. A*, 7(5):1788–1797, May 1973.

[45] A.G. Fox and T. Li. Resonant modes in a maser interferometer. *J. Bell Syst. Tech.*, 40:453–458, 1961.

[46] A.A. Duarte and H.G. Solari. Metamorphosis of the monochromatic spectrum in a double-cavity laser as a function of the feedback rate. *Phys. Rev. A*, 58(1):614–619, July 1998.

[47] A.A. Tager and K. Petermann. High-frequency oscillations and self-mode locking in short external-cavity laser diodes. *IEEE J. Quantum Electron.*, 30(7):1553–1561, July 1994.

[48] D. Pieroux and T. Erneux. Strongly pulsating lasers with delay. *Phys. Rev. A*, 53(4):2765–2771, April 1996.

Chapter 4

Mode Spectrum of Passive Cavities

4.1 Introduction

The use of lasers in nonlinear dynamics was initiated by Haken in 1975,[1], who showed that there is a strong mathematical resemblance between the dynamics of some types of lasers and turbulent fluid flow, seen in the seminal paper by Lorenz on the unpredictability of atmospheric dynamics [2]. Since then numerous types of lasers have been used to investigate nonlinear dynamics. Of particular interest in this regard are semiconductor lasers because they are unusually sensitivity to external stimuli and both experimentally and theoretically studies have shown that these systems exhibits a rich variety of nonlinear dynamical phenomena, such as, chaos, intermittency, low frequency fluctuations [3, 4, 5, 6, 7, 8, 9, 10, 11, 12, 13, 14, 15, 16, 17, 18, 19, 20].

Numerous studies of the Lang-Kobayashi coupled set of nonlinear equations have been undertaken, using various techniques: small signal analysis [21], bifurcation theory [6], asymptotic approach [14]; and much is now known of the nature and types of solutions these models predict. The Lang-Kobayashi model has proved to be remark-

ably successful in describing all the gross features that have so far been observed experimental. This is all the more remarkable, since once a laser diode has been destabilized it is known that it generally supports multiple longitudinal modes.

The use of dynamical models sometimes comes at the sacrifice of study of the boundary conditions or modal structures, this chapter presents a new coupled cavity model that allows a rigorous analysis of the longitudinal mode structure of a multimode laser diode with optical feedback. The necessity to develop a new coupled cavity approach came from the fact that the traditional version uses a discontinuous independent variable, so to allow a satisfactory technique of solving the system requires a continuous independent variable.

The coupled cavity model presented in the previous chapter by Pierce *et.al.* [22], developed a multimode dynamical model that calculated the underlying mode structure of a laser diode subject to optical feedback, using a coupled cavity approach, and confirmed that this model adhered to Chraplyvy and Tkach's [15] classification of the regimes of operation. However, the emphasis by Pierce *et.al.* was on the dynamics of the system and little attention was placed on how the mode structure of the system developed as the characteristics of the external cavity were changed. The study also considered a relative small external cavity round-trip time. As the external cavity size increases the number modes that have to be monitored increases significantly, this problem has hampered further development of this type of multimode model.

The computational overhead increases with cavity length because a larger number of closely spaced roots of a complex function need to be found. Additional complications are also introduced because in the standard coupled cavity approach [22, 23] the independent variable of the calculations is the complex wavenumber, which, being a discontinuous variable within the cavity configuration, restricts the root finding tech-

niques that can be applied to the problem. This issue can be addressed by recasting the model in terms of spatial harmonic plane waves rather than with the more usual temporal harmonic waves. This has the effect of introducing a continuous independent variable for the whole system, namely, a complex frequency, ω. This new approach finds the complex frequency of all the modes that can be supported by a given structure. In recasting the model the Argument Principle Method (APM) is applied to find the solutions of the model [24]. The APM is able to count the number of roots in a defined region and then calculate their locations to a high degree of accuracy. Applying the APM guarantees that all of the modes are found within the region of interest to a finite degree of accuracy.

The derivation of the modified coupled cavity model is outlined in the next section and then validated against a test structure. This new approach is then used to investigate how the mode structure of a system consisting of a dielectric and air cavity is influenced by the main system variable. Finally the results are discussed in relation to the closely related configuration of a laser diode subject to external optical feedback.

4.2 Theory

The conventional coupled cavity technique is a well known approach that can be used to determine the spatial modes supported by a particular structure at a given optical frequency. In the conventional approach the optical frequency is the known quantity, which is then subsequently used to determine the unknown wavenumbers that can be supported by the structure, meaning that the independent variable is discontinuous. To overcome this short-coming, the model will be recast to allow the use of a continuous variable (complex frequency) to allow the solutions to be more easily obtained.

Starting with the one dimensional Electromagnetic (EM) - wave equation, the derivation of this modified coupled cavity formalism will be briefly outlined,

$$\frac{\partial^2 E_x(z,t)}{\partial z^2} - \mu_0\sigma\frac{\partial E_x(z,t)}{\partial t} - \mu_0\epsilon\frac{\partial^2 E_x(z,t)}{\partial t^2} = 0. \tag{4.1}$$

where σ is the conductivity, μ_0 is the permeability of free space and ϵ is the the permitivity of the medium.

At the beginning of the derivation the significant differences between the two models becomes obvious. Instead of expressing the fields as a temporal harmonic dependent on space, they are now expressed as spatial harmonics dependent upon time. The EM field is separable and can be expressed in terms of a spatial harmonic function, and an as yet unknown temporal function,

$$E_x(z,t) = E_x(t)e^{jkz} \tag{4.2}$$

Substituting equation (4.2) into equation (4.1) and rearranging leads to the following spatial harmonic wave equation,

$$\mu\epsilon\frac{\partial^2 E_x(t)}{\partial t^2} + \mu\sigma\frac{\partial E_x(t)}{\partial t} + k^2 E_x(t) = 0. \tag{4.3}$$

Unlike the standard formalism no further simplifications can be made at this stage and the solutions are now sought of the form,

$$E_x(t) = Ae^{-j\omega t} + Be^{j\omega t} \tag{4.4}$$

Here A and B are arbitrary constants representing the magnitude of the forward and backward propagating waves, and the complex optical frequency, ω, is assumed to be

of the form,

$$\omega = \omega_r - j\omega_i \tag{4.5}$$

Using equation (4.3) the real and imaginary part of the optical frequency can be related to the material parameters of the medium, by substituting equation(4.4) into equation (4.3) gives,

$$\omega = \sqrt{\frac{k^2}{\mu\epsilon} - \frac{\sigma^2}{4\epsilon^2}} + j\frac{\sigma}{2\epsilon}. \tag{4.6}$$

An expression for the wavenumber k, can also be obtained,

$$k = \sqrt{\mu\epsilon\omega^2 - i\sigma\omega\mu} = \frac{n}{c}\sqrt{\omega^2 - \frac{i\sigma\omega}{\epsilon}} \tag{4.7}$$

Making the usual assumption that the power is proportional to the modulus squared of the E-field, it is straightforward to show that the mode life time is proportional to the imaginary part of the optical frequency,

$$P(t) = P_0 e^{\frac{t}{\tau}} = |E_f|^2 = |A|^2 e^{2\omega_i t} \tag{4.8}$$

and equating the exponents, a reciprocal of the mode lifetime in a homogeneous medium can be expressed,

$$\frac{1}{\tau_{mode}} = 2\omega_i. \tag{4.9}$$

Having defined the $E_x(t)$ and related the optical frequency and wavenumber to the material parameters Maxwell's equations are now used to determine the magnetic field,

$$H_y(t) = \left(\frac{j\sigma + \epsilon\omega}{k}\right) A e^{-j\omega t} + \left(\frac{j\sigma - \epsilon\omega}{k}\right) B e^{j\omega t} \tag{4.10}$$

Hence, giving the two expressions for $E_x(t)$ and $H_y(t)$ that form the basis of the modified coupled cavity technique,

$$E_x(t) = Ae^{-j\omega t} + Be^{j\omega t} \tag{4.11}$$

$$H_y(t) = \left(\frac{j\sigma + \epsilon\omega}{k}\right)Ae^{-j\omega t} + \left(\frac{j\sigma - \epsilon\omega}{k}\right)Be^{j\omega t} \tag{4.12}$$

$$\tag{4.13}$$

The expressions so far obtained relate to an infinite homogeneous medium. The boundary between two semi-infinite homogeneous media will now be investigated.

4.2.1 Coupled Cavities

Use is now made of electromagnetic boundary conditions to obtain the coupled cavity model (the use of planewaves is made here; similar results can be expected for waveguide modes). These require the tangential components of the two electromagnetic fields to be continuous across a boundary, to match the EM field at the discontinuity between two semi-infinite media. Assuming the boundary between the two homogeneous materials is at a general temporal point $t = t_m$, and using the subscript m and $m+1$ to denote the quantities either side of the temporal boundary, the following expressions can be derived from $E_m = E_{m+1}$ and $H_m = H_{m+1}$, gives

$$A_{m+1} = A_m\left(\frac{p_m - q_{m+1}}{p_{m+1} - q_{m+1}}\right) + B_m e^{2j\omega t}\left(\frac{q_m - q_{m+1}}{p_{m+1} - q_{m+1}}\right) \tag{4.14}$$

$$B_{m+1} = A_m e^{-2j\omega t}\left(\frac{p_m - p_{m+1}}{q_{m+1} - p_{m+1}}\right) + B_m\left(\frac{q_m - p_{m+1}}{q_{m+1} - p_{m+1}}\right) \tag{4.15}$$

where,

$$p_m = \frac{j\sigma_m + \epsilon_m\omega}{k_m} \tag{4.16}$$

$$q_m = \frac{j\sigma_m - \epsilon_m\omega}{k_m} \tag{4.17}$$

Equation (4.14) can also be expressed in a more compact matrix form,

$$\begin{pmatrix} A_{m+1} \\ B_{m+1} \end{pmatrix} = Q(t_m) \begin{pmatrix} A_m \\ B_m \end{pmatrix}, \tag{4.18}$$

where the matrix elements are of the form,

$$Q(t_m) = \begin{pmatrix} \alpha & \beta \\ \gamma & \delta \end{pmatrix} \tag{4.19}$$

and,

$$\alpha = \frac{p_m - q_{m+1}}{p_{m+1} - q_{m+1}}, \tag{4.20}$$

$$\beta = \frac{q_m - q_{m+1}}{p_{m+1} - q_{m+1}} e^{2j\omega t_m}, \tag{4.21}$$

$$\gamma = \frac{p_m - p_{m+1}}{q_{m+1} - p_{m+1}} e^{-2j\omega t_m}, \tag{4.22}$$

$$\delta = \frac{q_m - p_{m+1}}{q_{m+1} - p_{m+1}} \tag{4.23}$$

This matrix system may now be applied to any number of boundaries by multiplying the matrix of each material section. The boundary positions, $t_0, t_1 ... t_m, t_{m+1}$, are simply calculated using:

$$t_m = \frac{L_m n_m}{c} + t_{m-1} \tag{4.24}$$

Usually the first boundary would be set to zero, $t_0 = 0$.

It is useful at this point to draw comparisons with the standard approach developed by Ebeling. Both definitions, the standard and modified coupled cavity formalisms derived from the linear homogeneous wave equation (Shown again for clarity):

$$\frac{\partial^2 E_x(z,t)}{\partial z^2} - \mu\sigma\frac{\partial E_x(z,t)}{\partial t} - \mu\epsilon\frac{\partial^2 E_x(z,t)}{\partial t^2} = 0. \tag{4.25}$$

Table 4.1, outlines a direct comparison between the models, it also show a full outline of the modified coupled cavity model.

Once the overall matrix that relates the fields at either end of the structure has been obtained, suitable boundary conditions need to be applied. In most cases it is assumed that no external field is incident on the compound cavity structure ($B_m = A_{m+1} = 0$). Using this boundary condition the matrix equation can be rearranged to give an equation whose roots correspond to the modes of the structure. The roots of the equation are then solved using the Argument Principle Method.

The Argument Principle Method [25](APM) is a technique used to calculate the number of zeros, and their locations within an area of interest, in the complex plane of an analytic function. The calculation requires a complex contour within which the APM will count the number of zeros. Once the number of zeros is known a summation of the function for each zero is calculated, these summations are then used to construct an equivalent polynomial, which is known to have zeros in the same places as the function of interest. This can then be solved using standard numerical methods.

The argument principle method states that for any closed curve, C on a complex plane of z that:

$$S_m = \frac{1}{2\pi i}\oint_C z^m \frac{f'(z)}{f(z)}dz, \tag{4.26}$$

Temporal	Spatial
E-Field:	
$E_x(z,t) = E_x(z)e^{j\omega t}$	$E_x(z,t) = E_x(t)e^{jkz}$
Equations:	
$\frac{\partial^2 E_x(z)}{\partial z^2} + k^2 E_x(z) = 0$	$-k^2 E_x(t) - \mu\sigma\frac{\partial E_x(t)}{\partial t} - \mu\epsilon\frac{\partial^2 E_x(t)}{\partial t^2} = 0.$
Wavenumber:	
$k = \frac{\omega}{c}\hat{n}$	$k = \frac{n}{c}\sqrt{\omega^2 - \frac{j\sigma\omega}{\epsilon}}$
Matrix:	
$Q(t_m) = \begin{pmatrix} \alpha', & \beta' \\ \gamma', & \delta' \end{pmatrix}$	$Q(t_m) = \begin{pmatrix} \alpha, & \beta \\ \gamma, & \delta \end{pmatrix}$
$\alpha' = \frac{k_{m+1}+k_m}{2k_{m+1}}e^{i(k_{m+1}-k_m)z},$	$\alpha = \frac{p_m - q_{m+1}}{p_{m+1} - q_{m+1}},$
$\beta' = \frac{k_{m+1}-k_m}{2k_{m+1}}e^{i(k_{m+1}+k_m)z},$	$\beta = \frac{q_m - q_{m+1}}{p_{m+1} - q_{m+1}}e^{2j\omega t_m},$
$\gamma' = \frac{k_{m+1}-k_m}{2k_{m+1}}e^{-i(k_{m+1}+k_m)z},$	$\gamma = \frac{p_m - p_{m+1}}{q_{m+1} - p_{m+1}}e^{-2j\omega t_m},$
$\delta' = \frac{k_{m+1}+k_m}{2k_{m+1}}e^{-i(k_{m+1}-k_m)z}.$	$\delta = \frac{q_m - p_{m+1}}{q_{m+1} - p_{m+1}}.$
Mode solutions:	
$\omega_{mode} = \frac{c}{\hat{n}}\Re\{k_1\}$	$\omega_{mode} = \Re\{\omega\}$
$g_{th} = -2\Im\{k_1\}$	$\frac{1}{\tau_{mode}} = 2\Im\{\omega\}$

Table 4.1: *The conventional and modified coupled cavity mode*

where S_m is the summation around contour C, $f(z)$ is the function of interest and $f'(z)$ is the derivative, m is an integer which ranges between 0 and the number of zeros found, n. Setting $m = 0$ equation (4.26) calculates the number of zeros within the closed curve C, it simplifies to,

$$S_0 = \frac{1}{2\pi i} \oint_C \frac{f'(z)}{f(z)} dz = n, \tag{4.27}$$

where n is the number of zeros within C. Having used equation (4.27) to calculate the number of zeros, the degree of the equivalent polynomial to be constructed is known. The polynomial can then be represented as,

$$p(z) = C_1 z^1 + C_2 z^2 + C_3 z^3 + ... + C_n z^n = \sum_{j=1}^{n} C_j z^j, \tag{4.28}$$

where C_j are the coefficients, of which there are n. These coefficients are found using the recurrence relation:

$$C_k = \frac{1}{(k-n)} \sum_{j=1}^{n-k} S_j C_{j+k}. \tag{4.29}$$

where $k = n, .., 2, 1$. By setting $C_n = 1$ and the recursive application of equation (4.29) the coefficients of the polynomial can be obtained. The equation $p(z) = 0$ with $p(z)$ calculated from equation (4.28) can now be solved using a standard numerical algorithm for root finding, such as *Laguerre's Method.*

In equations (4.26) and (4.27) the derivative, $f'(z)$ of $f(z)$ is required. To make the APM as generic as possible the derivative must be obtained through numerical methods, this can be achieved using the *Cauchy Integral Formula*:

$$f'(z_0) = \frac{1}{2\pi i} \oint_D \frac{f(z)}{(z - z_0)} dz, \tag{4.30}$$

where D is an arbitrary analytic contour around the point z_0. Alternatively $f'(z)$ can be analytically derived and directly used in the APM.

More details of the exact execution of this technique are outlined in Section 7.3, where the emphasis is placed on ensuring the contour integration is undertaken correctly.

4.3 Results

4.3.1 Fabry-Perot Cavity

In order to validate the model the mode spectrum of a simple Fabry-Perot cavity was calculated and then compared with the exact analytic solutions. Figure 4.1 shows a Fabry-Perot cavity formed by a homogeneous dielectric medium sandwiched between two semi-infinite air sections, each with unity refractive index, $n_0 = n_2 = 1$. The refractive index of the dielectric medium was assumed to be, $n_1 = 3.25$. Using the

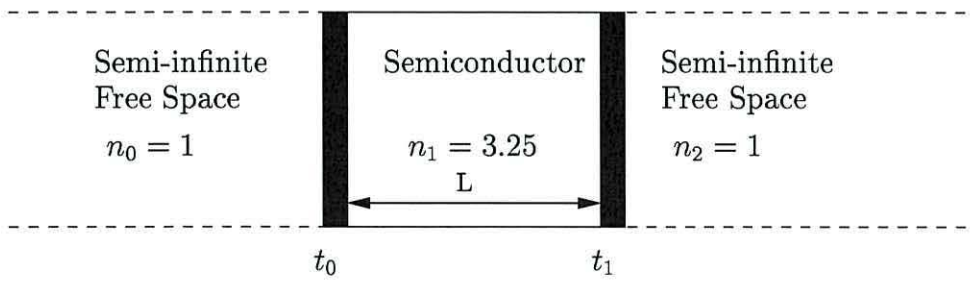

Figure 4.1: *A Fabry-Perot dielectric cavity bounded by two semi-infinite air sections*

formalism outlined above, a matrix (of the form (4.19)) can be used at each of the

boundaries to model the overall system, giving:

$$\begin{pmatrix} A_2 \\ B_2 \end{pmatrix} = Q(t_1)Q(t_0)\begin{pmatrix} A_0 \\ B_0 \end{pmatrix}. \tag{4.31}$$

Using the condition $A_2 = 0$ and $A_0 = 1$, ensures no external optical input into the laser and hence only longitudinal modes are found, the coefficient A_2 is then used as function f in the APM equations 4.26-4.30. The matrix equation can be solved in ω for the roots, these roots can then be related to the mode frequencies, ω_{mode} and the mode lifetimes, τ_{mode}, taken from equation. 4.6, gives:

$$\omega_{mode} = \Re\{\omega\} = \omega_r \tag{4.32}$$

$$\frac{1}{\tau_{mode}} = 2\Im\{\omega\} = 2\omega_i \tag{4.33}$$

Figure 4.2 shows a contour plot of the coupled cavity model, the matrix equations (4.31) magnitude is evaluated at regular intervals over a set region (the region usually corresponds to a defined contour used when applying the APM), the concentric eclipses correspond to a magnitude of the expression thus eluding to the location of the roots of the system.

The well known analytic expressions for the mode spacing and the mode lifetime of a Fabry-Perot cavity, [18], have been used to check the accuracy of the numerical calculations. The mode spacing and lifetime were calculated using,

$$\omega_{mode_m} = M\frac{\pi c}{nL}, \tag{4.34}$$

and,

$$\frac{1}{\tau_{mode}} = \frac{c}{2nL} ln\left(\frac{1}{R^2}\right), \tag{4.35}$$

where n is the refractive index of the medium, $n = 3.25$, L is the physical length of the laser diode,$L = 300\mu m$, c is the speed of light, $c = 3 \times 10^8 ms^{-1}$ and M is an integer value. Here R is the facet reflectivity, $R \approx 0.3$.

The stars (*) in Fig. 4.2 correspond to the predicted locations of the modes using the analytic equations above, (4.34) and (4.35). The figure clearly demonstrates that both matrix equation as a function of complex frequency ω, and the analytic solutions give identical results.

4.3.2 Coupled Fabry-Perot Cavities

The objective here is to study the 'cold-cavity' mode spectrum of the configuration shown in figure 4.3. The configuration consists of three partial dielectric mirrors which define two cavities, a dielectric cavity and an external air cavity. The dielectric cavity is assumed to be a semiconductor, while the other cavity is assumed to contain air. The effect that varying the size and the Q-factor of the external cavity has on the overall compound cavity mode structure is investigated. Also the effects of changing the refractive index of the dielectric cavity are studied. Variations in the reflectivity and the position of the right-hand mirror (at t_2) can be undertaken independently, whereas changes in the refractive index of the semiconductor effects both the optical length and the reflectivity of both the middle (at t_1) and left-hand mirror (at t_0) simultaneously.

The reflectivity of the right-hand mirror, R_{ext}, can be modified by changing the re-

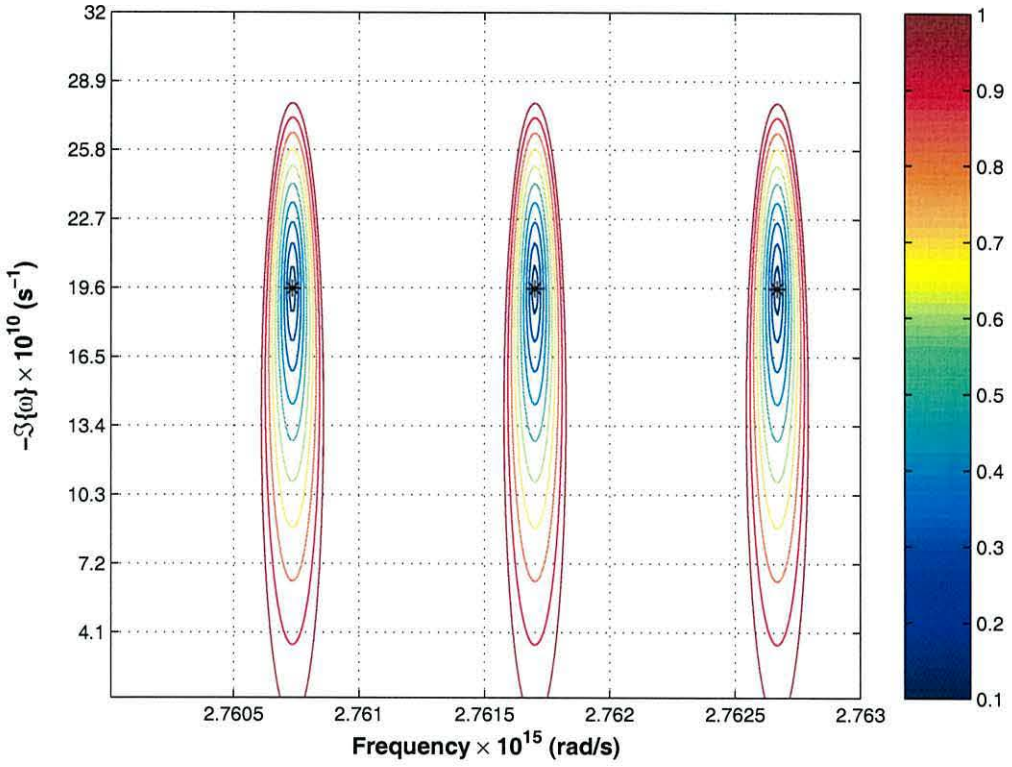

Figure 4.2: *A contour plot of the absolute value of the coefficient A_2 in equation 4.31 used to determine the modes of the system. The star (*) represents the modes calculated using the analytic Fabry-Perot equations.*

fractive index of the end semi-infinite region by using,

$$n_3 = \frac{1 + \sqrt{R_{ext}}}{1 - \sqrt{R_{ext}}}. \tag{4.36}$$

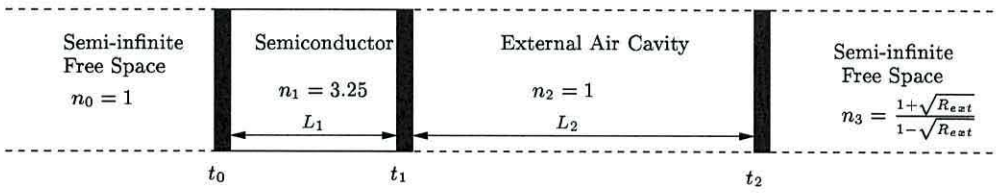

Figure 4.3: *Two coupled Fabry-Perot cavities bounded by a semi-infinite air region and a dielectric mirror.*

The mode spectrum of the compound cavity configuration shown in figure 4.3 can be determined using the modified coupled cavity approach outlined above, by cascading individual matrices, $Q(t_m)$, that defines each of the boundaries,

$$\begin{pmatrix} A_3 \\ B_3 \end{pmatrix} = Q(t_2)Q(t_1)Q(t_0)\begin{pmatrix} A_0 \\ B_0 \end{pmatrix}. \tag{4.37}$$

The initial boundary is set at zero, $t_0 = 0$, and the respective values of t_m are then calculated using (4.24). By assuming that $A_3 = 0$ and $A_0 = 1$ the APM can be used to find the roots of the resulting equation and thereby deduce the frequency mode spectrum within the area of interest.

4.3.3 Short Cavity Limit

Figure 4.4 shows the locations of the modes in a frequency space assuming an air cavity length of twelve times that of the dielectric cavity, $L_2 = 12L_1$. The modes designated as ω_0 and ω_4 are the modes due to the dielectric cavity, which we will refer to as dielectric modes. The remaining five modes can be attributable to the air cavity and are referred to as external cavity modes. The colour gradation in figure 4.4 represents increasing values of R_{ext}. At this stage it is instructive to define what is meant by *dominant mode*: a dominant mode is one where the lifetime is longer than that of any other mode within the spectral region of interest. Figure 4.4 depicts the typical mode bending that occurs in the *short cavity limit*. In this limit the dielectric cavity and external air cavity are almost comparable in optical length and it is the relative strength of the middle mirror, to that of the right-hand mirror, that determines the mode structure. The dielectric modes (ω_0 and ω_4) experience the most significant mode bending as R_{ext} is increased. At low values of external reflectivity the two cavities are only weakly coupled and the mode spacing of the whole structure is almost a linear superposition of the independent modes spacing of the dielectric cavity and the external air cavity. As the reflectivity of the external mirror is increased the coupling between the two cavities increases and the mode structure tries to evolves towards that of an idealised single compound cavity of optical length $(n_1L_1 + L_2)$. Consequently, the largest effect occurs between the dielectric mode and its nearest external cavity mode. The mode frequencies of these two modes always initially shift in such a way as to increase the frequency spacing between each other, figure 4.4. In contrast, the frequency of the external cavity furthest from dielectric modes, (eg. ω_2), undergoes virtually no frequency shift as R_{ext} increases.

The mode lifetimes of the external cavity modes increase more quickly with in-

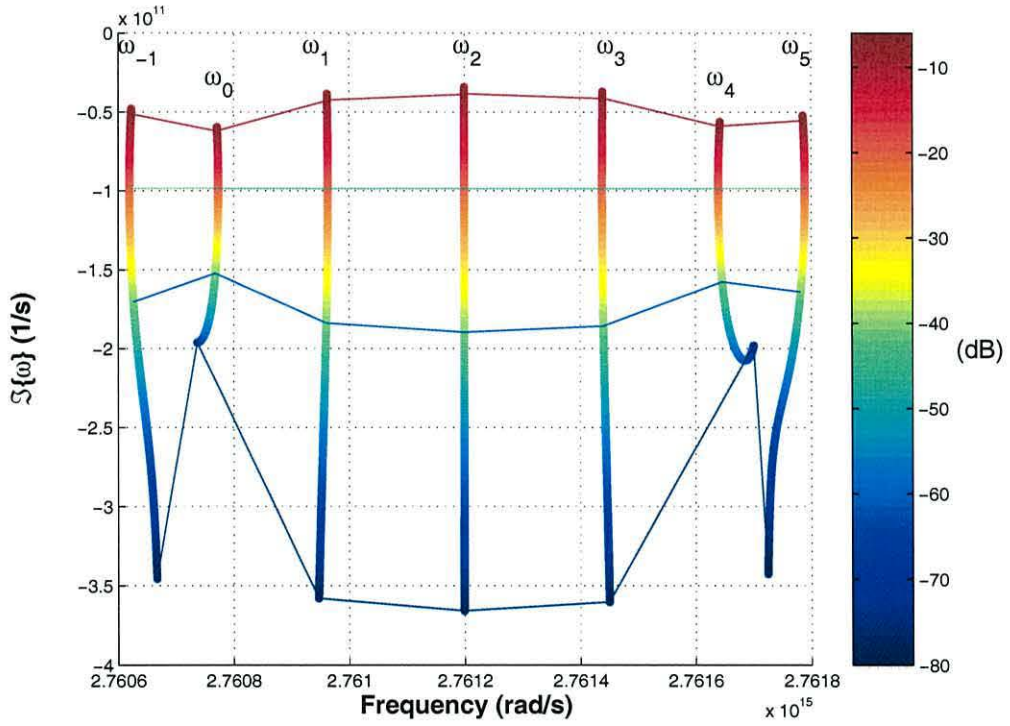

Figure 4.4: *Typical mode spectrum evolution with R_{ext}, in the short cavity limit ($L_2 = 12L_1$).*

creasing R_{ext} and eventually they have longer lifetimes than the dielectric modes. The horizontal lines, seen in figure 4.4, link all the modes at particular values of R_{ext} (-80dB, -41dB, 20.5dB and -6dB) and these clearly demonstrate the change in significance of the external cavity modes. Initially the mode lifetimes of the dielectric mode changes very little with R_{ext}, however there is a threshold value of R_{ext} above which the lifetime begins to change significantly. This threshold point ($R_{ext} = -65dB$) marks the transition at which the two cavities should no longer be viewed as almost independent entities, but must instead be viewed as a single compound structure. It is also interesting that the 'actual' mode bending relative to each of the other mode can be seen in Fig. 4.4, the two modes either side of the solitary laser mode are initially repelled by the solitary laser mode. However, at higher feedback levels the external cavity modes tend towards the solitary laser mode. Also, the solitary laser mode itself always initially moves away from the nearest external cavity mode. If nearest external cavity mode by chance, happens to be to the left of the solitary laser mode then the solitary laser mode bends to the right; the converse is true if the nearest external cavity happens to be to the right of the solitary laser mode.

4.3.4 Long Cavity Limit

The situation is dramatically different if there is significant asymmetry in the relative optical lengths of the two cavities. When the external cavity is much larger than the dielectric cavity, the external cavity modes dominate the mode structure even at very low external mirror reflectivities. In this *long cavity limit* the dielectric cavity must be viewed purely as a small perturbation to the much larger air cavity. The large disparity in the mode spacings, associated with the two cavities, limits the amount of mode bending

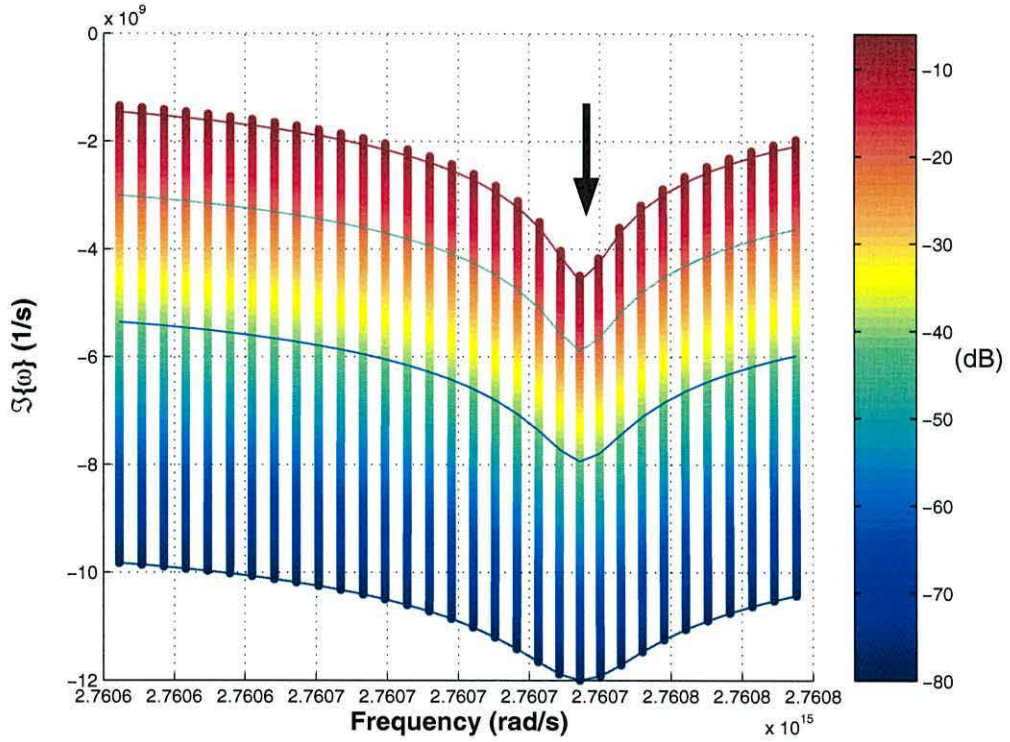

Figure 4.5: *Typical mode spectrum evolution with R_{ext} in the long cavity limit. In this case the external air cavity length is $500L_1$.*

that can occur because the average mode spacing is much smaller than in the short cavity limit.

The mode spectrum for the case when $L_2 = 500L_1$ is shown in figure 4.5 where only one dielectric mode has been included (see arrow). As expected the mode spacing is very small in comparison with that seen in figure 4.4 and the modes that originate from external air cavity all have longer mode lifetimes than the dielectric mode, even for very low values of R_{ext}.

4.3.5 Refractive Index Sensitivity

Varying the refractive index of the semiconductor has two effects: it changes the optical length of the dielectric cavity and it also changes the facet reflectivities. For very low mirror reflectivities, $R_{ext} = -80dB$, and short cavities, $L_2 = 12L_1$, increasing the refractive index causes the expected change in the characteristics of the dielectric modes, as shown in figure 4.6, for dielectric mode ω_0 of figure 4.4. Increasing the refractive index decreases the optical frequency and increases the mode lifetime. However, the external cavity modes are essentially unperturbed at this low value of R_{ext}. This is because the external cavity modes are only weakly coupled to the dielectric mode and view the refractive index change as a sub-wavelength movement of the boundary between the two cavities. Consequently, the external cavity modes oscillate as n_1 increases, with the small variations in the cavity length and effective reflectivity inducing phase effects which give rise to the behaviour seen in figure 4.7.

As the external mirror reflectivity is increased a point is reached were the two cavities are sufficiently strongly coupled that any change in the optical properties of the configuration perturbs all the modes. In effect the external air cavity modes no longer

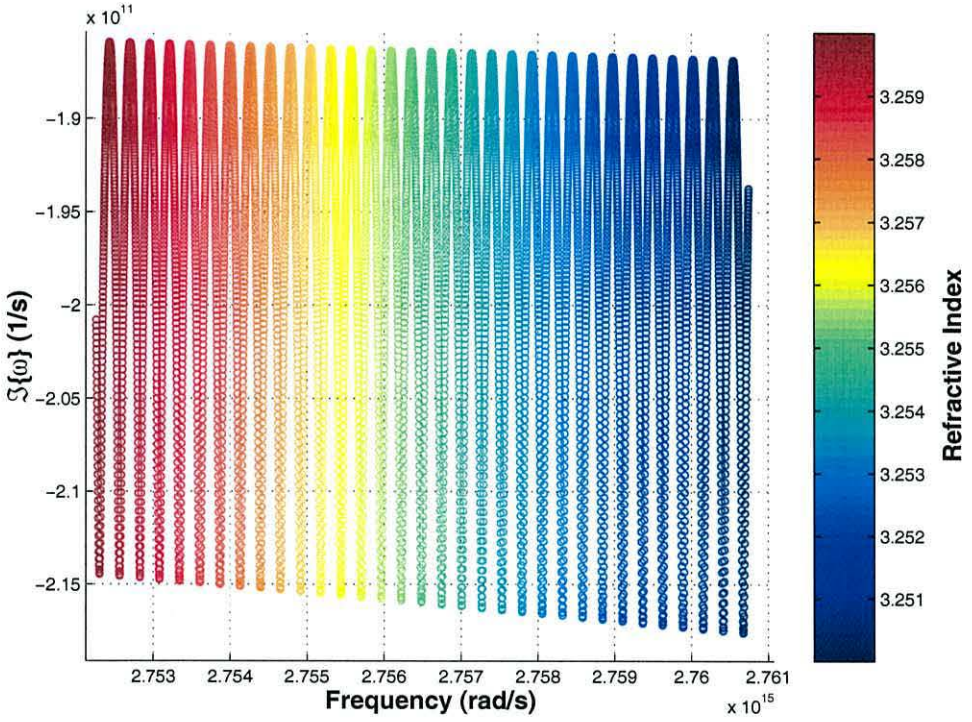

Figure 4.6: *The mode spectrum of a dielectric mode, ω_0, as the refractive index is increase in the short cavity limit ($L_2 = 12L_1$) and at a low external reflectivity ($R_{ext} = -80dB$).*

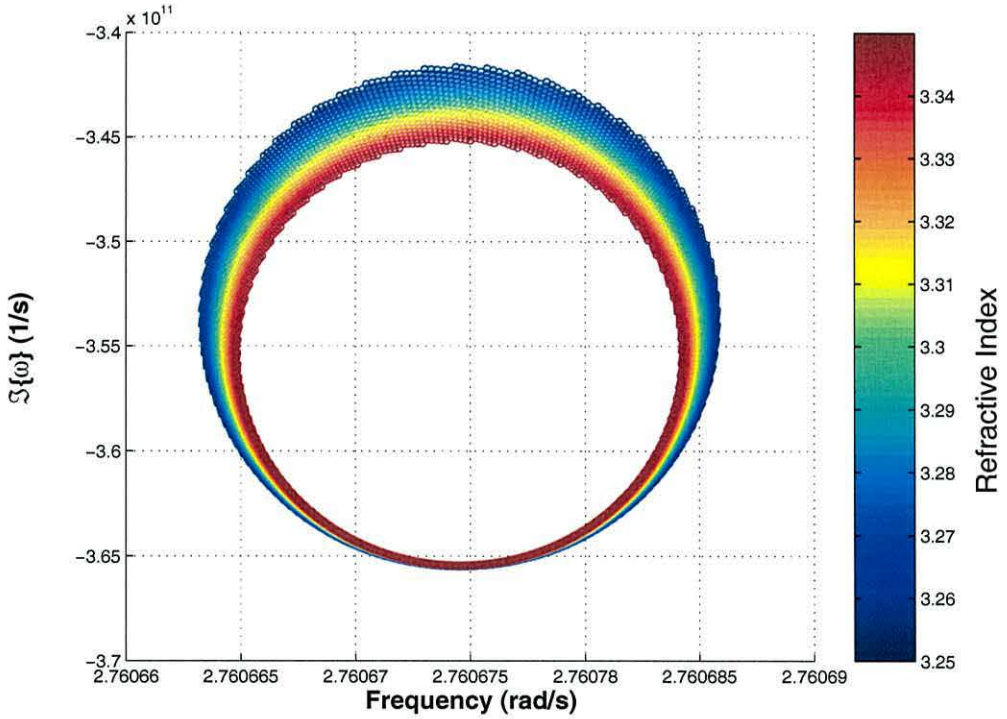

Figure 4.7: *The mode spectrum of an external cavity mode, ω_{-1}, as the refractive index of the dielectric cavity is increased, in the short cavity limit ($L_2 = 12L_1$) and at a low external reflectivity ($R_{ext} = -80dB$). The mode moves in an inward spiral for increasing refractive index.*

see the refractive index change as a sub-wavelength movement in the middle mirror, but as a significant change in their cavity. Hence, the mode spectrum evolves in a similar fashion to that of the dielectric mode, seen in figure 4.6. This transition occurs when the reflectivity of the external mirror is between $-66dB$ and $-65dB$, and corresponds to the region where the mode lifetimes of the dielectric modes begins to be markedly influenced by the external mirror reflectivity. This threshold reflectivity marks the point at which the system must be considered as one compound cavity rather than two weakly coupled separate cavities.

Figure 4.8 shows the evolution of an external cavity mode, in this case mode ω_{-1} (see figure 4.4), when the external mirror reflectivity is $-65dB$. This reflectivity is just above the critical transition point and hence the external cavity mode has evolved to become a compound cavity mode. However, as the refractive index is increased it reduces the coupling between the two cavities and forces the system back into the state where the two cavities are almost independent entities. Hence, the external compound cavity mode regresses back into being a external cavity mode, signified by the 'drop-out' seen in figure 4.8, as the refractive index increases.

For higher external reflectivities the two cavities are closely linked and hence a small change in the refractive index effects the mode frequencies and lifetimes of all the modes in a similar manner.

4.4 Discussion

The coupled cavity analysis above has assumed that the dielectric susceptibility of the semiconductor medium is frequency independent and has also assumed that there is no optical gain or loss in the cavity. This 'cold-cavity' limit has revealed some striking

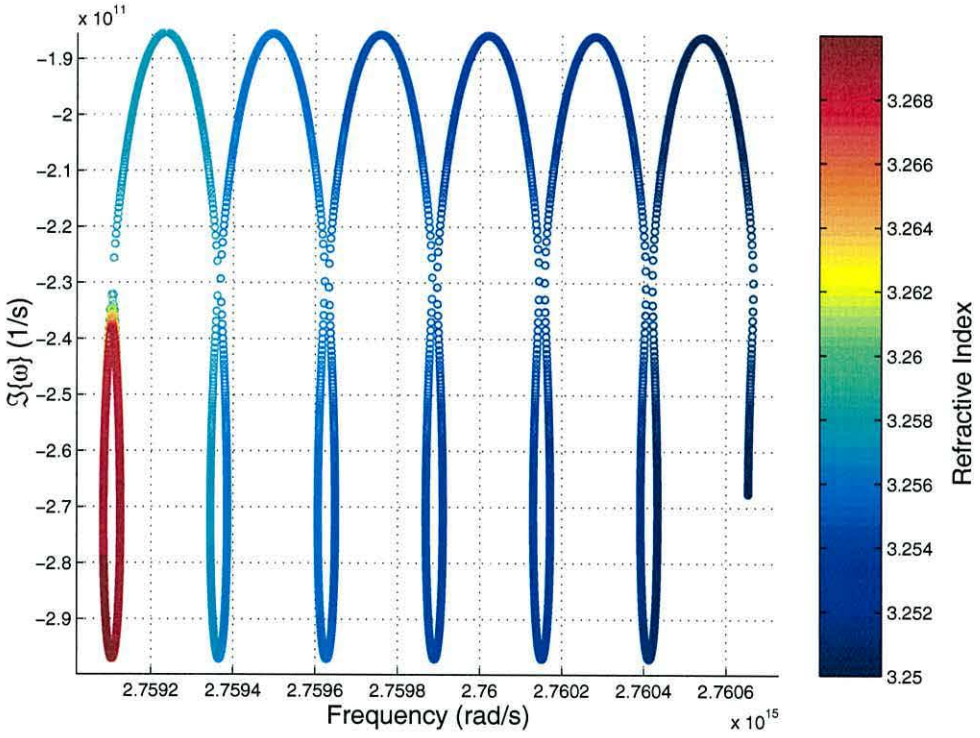

Figure 4.8: *Evolution of external mode ω_{-1} as a function of refractive index when the external mirror reflectivity is $-65dB$ and thus just above the threshold level.*

difference in the mode spectrum of the compound structure in the short and long cavity limits.

In the short cavity limit there is significant mode bending, see figure 4.4, this effect is a consequence of the interplay between the dielectric modes and the external cavity modes. A threshold external mirror reflectivity has also been identified where the modes structure is that of a compound cavity, while below this values the mode structure is really a superposition of the mode structures of two almost independent cavities. In the short cavity limit the modes loosely associated with the dielectric have much longer lifetimes than those of the external cavity modes, for all but the highest external mirror reflectivities and hence dominate the mode structure.

In contrast, in the long cavity limit, there is very little mode bending because the compound mode spacing is much narrower and this therefore limits the room available for mode bending effects. In addition, for all but the lowest external mirror reflectivities the modes that emanate from the external air cavity dominate the mode spectrum. (This marked difference in behaviour is reminiscent of the results in Helm's paper on the critical feedback level that delineates stable and unstable dynamics, [14], and its dependence on external cavity length.)

The lack of significance of the dielectric modes in the long cavity limit indicates that care must be taken when extrapolating this passive analysis to the case of a laser diode subject to optical feedback. The passive long cavity results underplay the significance of the dielectric modes because, when the optical gain is not present, the dielectric cavity is simply a small perturbation to a much larger air cavity. However, the short cavity results highlight how important the underlying mode structure is in integrated structures and also emphasizes how sensitive the mode frequencies and lifetimes are to the mirror reflectivity.

4.5 Summary

A modified version of the well-known coupled cavity model has been outlined and verified. This new approach allows the evolution of the spectral mode structure of multiple cavity configuration to be easily monitored, as the size of the cavities and the reflectivities of the dielectric mirrors are varied.

Using the modified coupled cavity model the underlying longitudinal mode structure of a dual cavity configuration has been investigated. A semiconductor laser diode subject to optical feedback in the cold cavity limit has shown that the longitudinal modes move with variations in the optical feedback and with changes in refractive index.

The results highlight significant differences in the mode structure for long and short cavities and stress the importance of mode structure effects in the short cavity limit.

References

[1] H. Haken. Analogy between higher instabilities in fluids and lasers. *Phys. Rev. A*, 53(77), 1975.

[2] E.V. Lorenz. Determineistic non-periodic flow. *J. Atmos. Sci.*, 20:130, 1963.

[3] J. Mork, J. Mark, and B. Tromborg. Route to chaos and competition between relaxation oscillations for a semiconductor laser with optical feedback. *Phys. Rev. A*, 65:1999–2002, 1990.

[4] J. Sacher, D. Baums, P. Panknin, W. Elsasser, and E.O. Gobel. Intensity instabilities of semiconductor lasers under current modulation, external light injection, and delayed feedback. *Phys. Rev. A*, 45(3):1893–1905, February 1992.

[5] A.M. Levine, G.H.M. van Tartwijk, D. Lenstra, and T. Erneux. Diode lasers with optical feedback: Stability of the maximum gain mode. *Phys. Rev. A*, 52:R3436–R4339, 1995.

[6] A.A. Duarte and H.G. Solari. Metamorphosis of the monochromatic spectrum in a double-cavity laser as a function of the feedback rate. *Phys. Rev. A*, 58(1):614–619, July 1998.

[7] N. Kikuchi Y. Lui and J. Ohtsubo. Controlling dynamical behaviour of a semiconductor laser with external optical feedback. *Phys. Rev. E*, 65:2697–2700, 1995.

[8] I. Fischer, O. Hess, W. Elsasser, and E. Gobel. High-dimensional chaotic dynamics of an external cavity semiconductor laser. *Phys. Rev. Lett.*, 73(16):2188–2191, October 1994.

[9] I. Fischer, G.H.M. van Tartwijk, A.M. Levine, W. Elsasser, E. Gobel, and D. Lenstra. Fast pulsing and chaotic itinerancy with a drift in the coherence collapse of semiconductor lasers. *Phys. Rev. Lett.*, 76(2):220–223, January 1996.

[10] R. Lang and K. Kobayashi. External optical feedback effects on semiconductor injection laser properties. *IEEE J. Quantum Electron.*, 16:347–355, 1980.

[11] D. Lenstra, B.H. Verbeek, and A.J. Den Beof. Coherence collapse in single-mode semiconductor lasers due to optical feedback. *IEEE J. Quantum Electron.*, QE-21(6):674–679, June 1985.

[12] Xing Pan Bajarne Tromborg, Henning Olesen and Shigeru Saito. Transmission line description of optical feedback and injection locking for fabry-perot and dfb lasers. *IEEE J. Quantum Electron.*, QE-23(11):1875–1889, November 1987.

[13] A.A. Tager and K. Petermann. High-frequency oscillations and self-mode locking in short external-cavity laser diodes. *IEEE J. Quantum Electron.*, 30(7):1553–1561, July 1994.

[14] J. Helms and K. Petermann. A simple analytic expression for the stable operation range of laser diodes with optical feedback. *IEEE J. Quantum Electron.*, 26(5):833–836, May 1990.

[15] R.W. Tkach and A.R. Chraplyvy. Regimes of feedback effects in 1.5-μm distributed feedback lasers. *J. Lightwave Tech.*, LT-4(11):1655–1661, November 1986.

[16] A. Ritter and H. Haug. Theory of laser diodes with weak optical feedback i: Small signal analysis and sidemode spectra. *J. Opt. Soc. Am. B*, 10:130, 1993.

[17] A. Ritter and H. Haug. Theory of laser diodes with weak optical feedback ii: Limit-cycle behavior, quasi-periodicity, frequency locking and route to chaos. *J. Opt. Soc. Am. B*, 10:144, 1993.

[18] K. Petermann. *Laser Diode Modulation and Noise*. Kluwer Academic, 1988. isbn 90-277-2672-8.

[19] G.H.M. van Tartwijk and D. Lenstra. Semiconductor lasers with optical feedback. *Quantum Semiclass. Opt.*, 7:87–143, 1995.

[20] G.H.M. van Tartwijk and G.P. Agrawal. Laser instabilities: a modern perspective. *Prog. Quant. Electron.*, 22:43–122, 1998.

[21] B. Tromborg, J.H. Osmundsen, and H. Olesen. Stability analysis for a semiconductor laser in an external cavity. *IEEE J. Quantum Electron.*, QE-20(9):1023–1032, September 1984.

[22] I. Pierce, P. Rees, and P. S. Spencer. Multimode dynamics in laser doides with optical feedback. *Phys. Rev. A*, 61:053801, 2000.

[23] K.J. Ebeling and L.A. Coldren. Analysis of multielement semiconductor lasers. *J.Appl Phys*, 54(6):2962–2968, June 1983.

[24] L.C. Botten, M.S. Graig, and R.C. McPhedran. Complex zeros of analytic functions. *Comput. Phys. Commun.*, 29:245–259, 1983.

[25] E. Anemogiannis and E.N. Glytsis. Multilayer waveguides: Efficient numerical analysis of general structures. *J. Lightwave Tech.*, 10(10):1344, October 1992.

Chapter 5

Mode Lifetime Sensitivity of Passive Coupled Cavity

5.1 Introduction

The external cavity length and the external mirror reflectivity will be the principal variables of this study. The formalism outlined in chapter 4 is used to track the trajectories of individual mode, as the external reflectivity has been gradually increased from $-80dB$ to $-6dB$. Typically the modes that would fall within the gain envelope of a semiconductor laser are of interest, thus have accordingly restricted the complex frequency space monitored.

5.2 Results

In this chapter the imaginary part of the complex frequency will be studied. As in chapter 4 an example for a fixed external reflectivity, the complex roots for a 300μm laser cavity with a refractive index of 3.25 with an external cavity which is twelve times

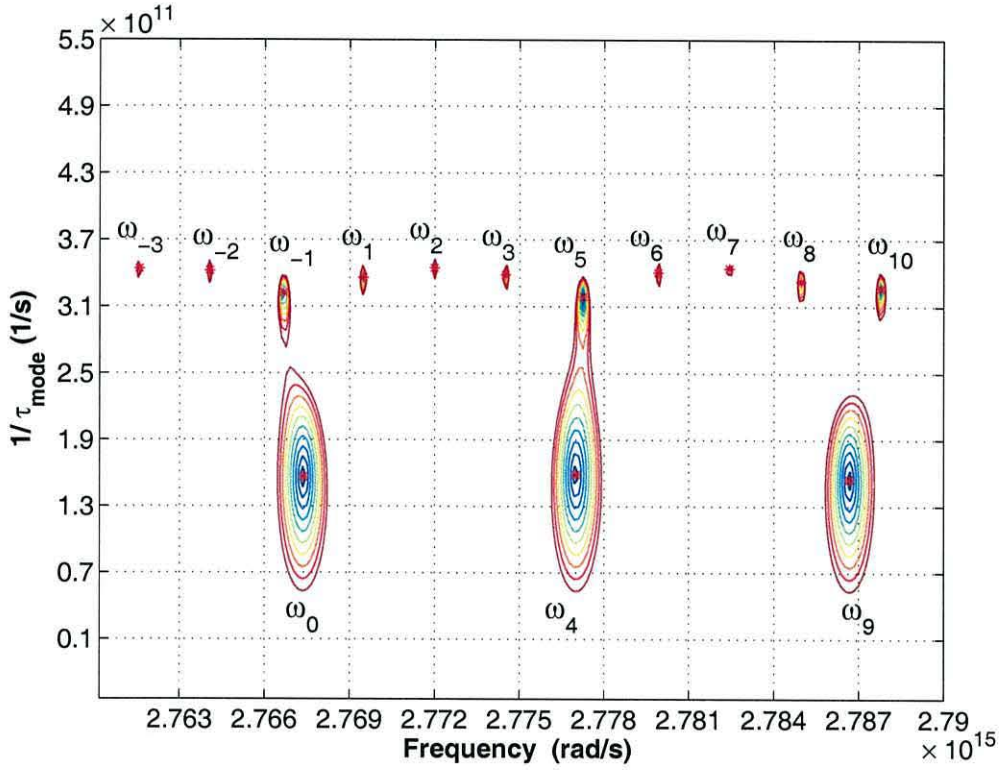

Figure 5.1: *A typical contour of a select spectral range, the stars (*) are solutions found by the APM. The external feedback level was set a -80dB. The larger contours with smaller values of $\Im\{\omega\}$ pertain to longer lifetimes and are the solitary laser modes.*

that of the laser were calculated using the APM. This refractive index gives a laser facet power reflectivity of approximately 30%.

For completeness figure 5.1 shows a contour plot of ω in a spectral area of interest, with the exact position of the roots denoted by stars (*) found using the APM. In this particular contour fourteen modes are supported by the coupled cavity system. The three most significant modes originate from the mode structure of the solitary laser diode. The other eleven modes are due to the feedback from the external cavity. The feedback level in figure 5.1 is set at -80dB, and as such the mode spectrum would, (with such small levels of optical feedback), be expected to be reminiscent of that of the solitary laser diode, comparisons can be drawn to Fig. 4.2 where only the solitary laser modes are shown.

It can be seen that as the feedback level is increased all the mode lifetimes become increasingly comparable, until at larger feedback levels one of the external cavity modes dominates. The central mode in figure 5.2, ω_0, can be identified as one of the longitudinal modes of the solitary laser and likewise the six other modes can be regarded as being external cavity modes. The four outermost modes exhibit very little change in their real frequency with increasing feedback, unlike the two modes adjacent (ω_{-1} and ω_{-2}) to the central mode. The mode lifetime increases for all the modes as the reflectivity is increased. For low external reflectivities the central mode has an appreciably longer mode lifetime, indicating that the solitary laser mode dominates the system; in contrast, for very large external reflectivities all the external cavity modes have longer mode lifetimes, indicating that they dominate the system, this switch of domination occurs at some intermediate value of external reflectivity. The dashed lines in Fig. 5.2 illustrates this increased variation in mode lifetime either side of the critical feedback level by connecting all the modes supported at a particular external reflectivity. For clarity only

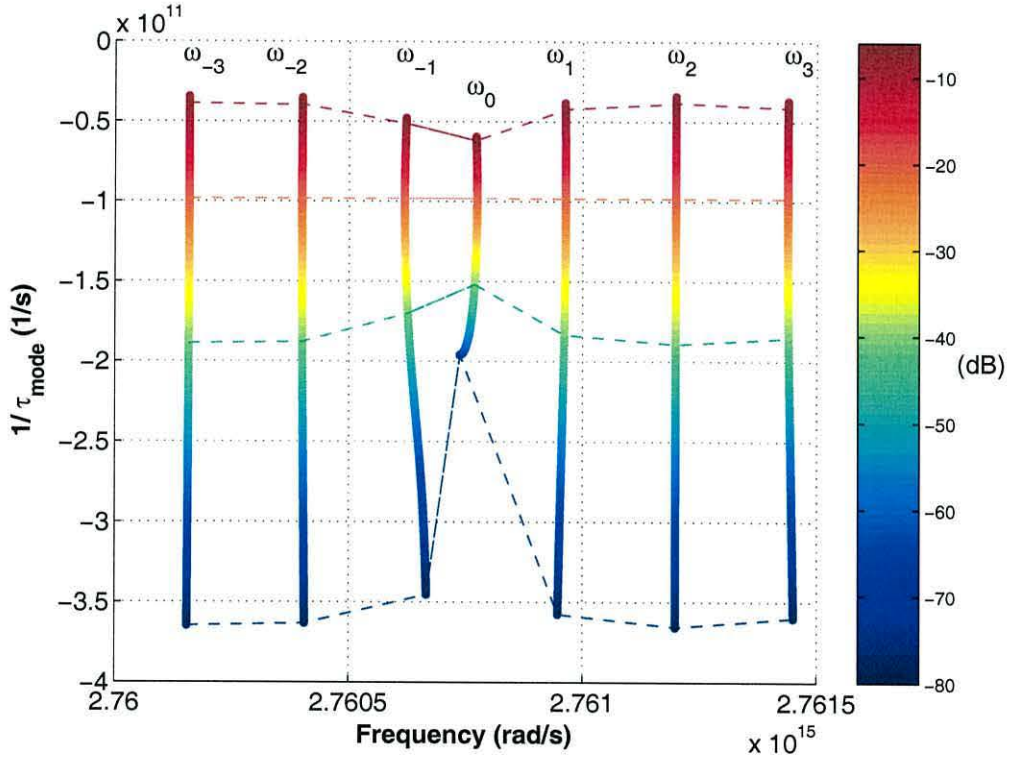

Figure 5.2: *Trajectories of the modes in the complex frequency plane as the external reflectivity is increased.*

four feedback levels have been considered $R = -80dB, -41dB, -20.5dB$ and $-6dB$.

5.2.1 External Cavity Length Sensitivity

The influence that the external reflectivity has on the lifetimes of all the modes in Fig. 5.2 is more clearly delineated in Fig. 5.3. In this figure the mode lifetimes are re-plotted of a subset of the modes shown in figure 5.2, as function of the external reflectivity. It can be seen that there is a critical feedback level at which the mode lifetime discrimination is essentially lost. This catastrophic loss of mode discrimination marks a change over in systems behaviour: below the critical feedback level the solitary laser mode structure and external cavity mode structure are essentially independent entities, and the solitary laser mode structure dominates the system; while above the critical feedback level the external cavity and solitary laser begin to merge to form the compound cavity modes, and the external cavity modes are more important.

The increased variation in the mode lifetime can be seen in Fig. 5.3 where dashed vertical lines have been introduced at the same four external reflectivities as those highlighted in Fig. 5.2. At low feedback levels the solitary laser mode has by far the longest mode lifetime but immediately after the critical feedback level it has the shortest mode lifetime of all the modes. The external cavity mode closest to solitary laser mode has a noticeably longer mode lifetime than the rest of the external cavity modes below the critical feedback level but does not maintain this advantage above the critical feedback level, where the external cavity mode ω_{-2} dominates.

The adjacent mode spacing of all the modes shown in Fig. 5.2 have been monitored as function of external reflectivity and plotted in Fig. 5.4. The frequency spacing between adjacent mode is neither uniform or constant, with the largest variation again

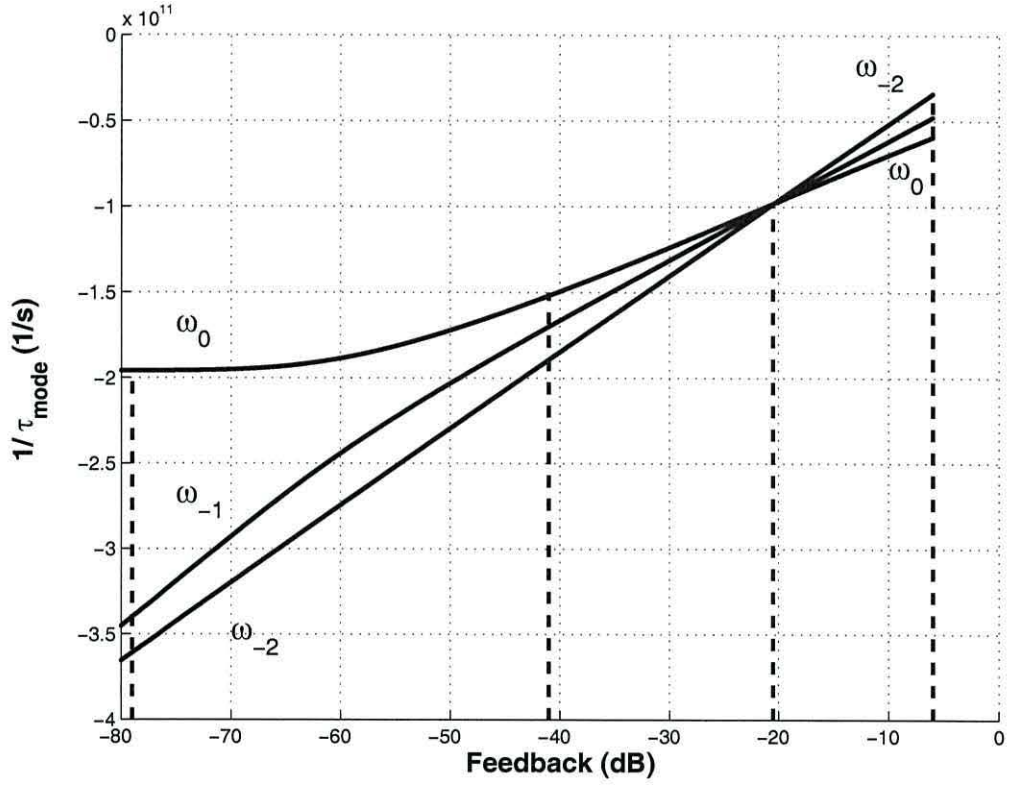

Figure 5.3: *The mode lifetime converge towards a point at the critical feedback level, indicating that all mode discrimination is lost.*

occurring between the solitary laser mode and the nearest external cavity mode. At the critical feedback level the mode separation was found to have reached a maxima or minima in all cases.

Up to this point variation in the external cavity length has not been considered. Having identified the existence of a critical feedback level the effect of sub-wavelength variations in the external cavity length will be investigated. These reveal that at the critical feedback level all the modes lose sensitivity to these small changes in the external cavity length, Fig. 5.5. This phase invariance means that at the critical feedback level the external cavity can no longer be tuned to enhance or reduce the mode lifetime. Moving away from the critical feedback level sees the re-emergence of usual phase resonance effect in the mode lifetime expected in Fabry-Perot cavities, however the behavior is inverted either side of the critical feedback level. The results shown in Fig. 5.5 are essentially the same for all the modes monitored.

Increasing the external cavity on a larger scale rapidly reduces the critical feedback level, Fig. 5.6. Hence, in most cases the transition from solitary laser mode to compound cavity mode structure is not visible experimentally. However, for integrated devices the transition should be discernible. The results shown in Fig. 5.6 are reminiscent of those obtained by Petermann in the short cavity limit, where below a certain external cavity length an exponential like increase in the optical feedback rate was required to obtain chaotic dynamics, [1]. The insert in Fig. 5.6 clearly demonstrates that the critical feedback level decreases exponentially with cavity length. This is essentially a manifestation of the fact that the critical feedback roughly corresponds to the lifetime of the external cavity modes exceeding that of the solitary laser mode.

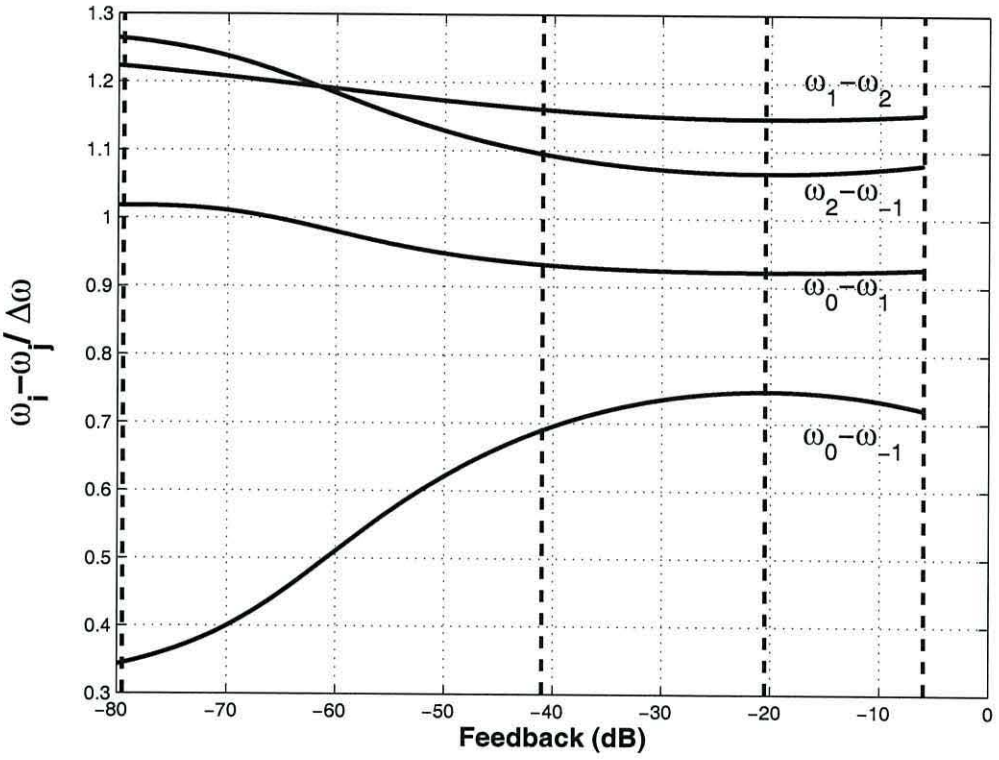

Figure 5.4: *The mode spacing between adjacent modes varies as the external feedback is increased. The mode spacing has been normalized with respect to the idealized coupled cavity spacing*

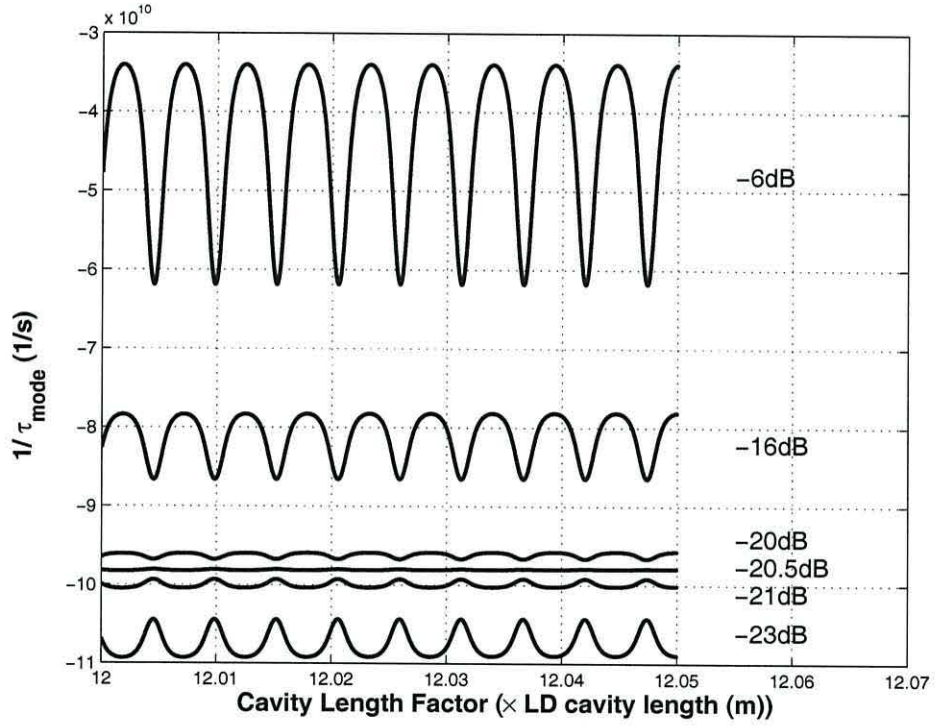

Figure 5.5: *Sub-wavelength increases in the external cavity length induce a modulation in the mode lifetimes. The magnitude of this Fabry-Perot cavity phase effect almost disappears at the critical feedback level.*

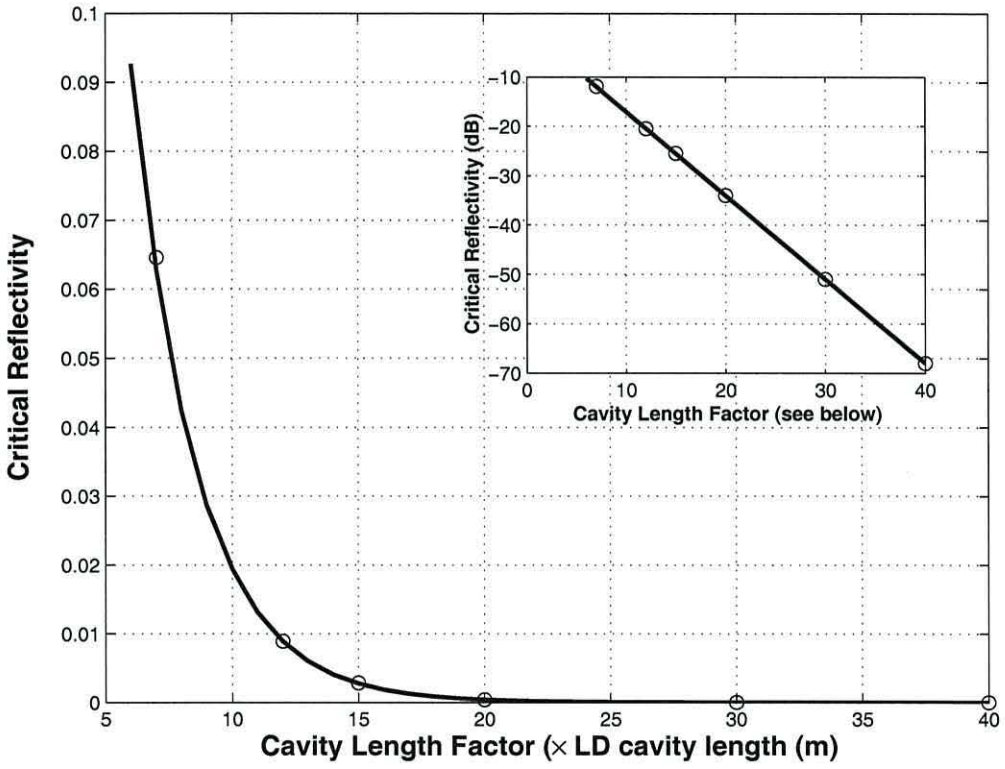

Figure 5.6: *An exponential decrease in the critical point is observed with an increasing in cavity length.*

5.2.2 Refractive Index Sensitivity

Varying the refractive index of the semiconductor has two effects: it changes the optical length of the laser cavity and it also changes the facet reflectivities. For very low external reflectivities and short cavities, increasing the refractive index causes the expected change in the longitudinal mode spacing of the solitary laser modes, but as the coupling to the external cavity is very weak, the external mode spacing is essentially unaffected, and sees the refractive index change as simply a sub-wavelength movement of the dielectric mirror (laser facet). For higher external reflectivities the two cavities are closely linked and hence a small change in the refractive index effects the mode frequencies and lifetimes of all the modes in a similar manner.

5.3 Discussion

The coupled cavity analysis above in the 'cold-cavity' limit has revealed some striking features, in particular, a critical feedback level has been identified where both phase discrimination and mode lifetime discrimination are lost. This critical feedback level has also been found to be sensitively dependent on the external cavity length when the two cavities are comparable in size.

The Lang-Kobayashi equations predicts, in the short cavity limit and under appropriate conditions, that a periodic picosecond pulse train will be generated. The coupled cavity analysis above offers further insight into this phenomenon; at the critical feedback level all the modes have essentially the same mode lifetime and thus are readily amenable to being mode locked, if a suitable gain medium is introduced to the 'cold cavity' and the close relation between modal lifetimes is retained at threshold. This cold-cavity analysis also predicts that the critical feedback limit rapidly decreases with

increasing external cavity length, thereby removing the possibility of generating pulses in longer cavities as spontaneous emission would prevent the necessary mode locking.

Duarte and Solari have studied a related system using a simplified coupled cavity based analysis, [2], in which they focussed their attention on the limit of validity of the single mode Lang-Kobayashi model. They concluded that the limit of validity was strongly influenced by the frequency dependence of the susceptibility, but only weakly dependent on the external cavity length. Figure 5.6 underlines this conclusion by indicating that for external cavities lengths greater that a few tens of laser cavity lengths the critical feedback level is essentially independent of external cavity size.

The Duarte and Solari analysis also predicts that the compound cavity modes will appear and disappear as the external reflectivity is increased. This effect is a consequence of including gain in the analysis, which essentially introduces another factor that will differentiate between modes.

The other main difference between the Duarte and Solari approach and this approach is in the relative importance of the laser facet adjacent to the external mirror. The highly asymmetric laser facet reflectivities assumed in [2] reduce the significance of the central dielectric mirror because the back laser facet has unity reflectivity. This will alter the mode frequencies and lifetimes significantly.

5.4 Summary

The coupled-cavity approach has shown that in the short cavity limit the exact nature of the mode structure will have an important role in determining the dynamics of the laser diode subject to external optical feedback. The interaction between the mode structure of the solitary laser and the external cavity results in a catastrophic loss of

mode discrimination at a critical feedback level. It has also shown that this critical feedback level decreases exponentially with external cavity length.

References

[1] K. Petermann. *Laser Diode Modulation and Noise*. Kluwer Academic, 1988. isbn 90-277-2672-8.

[2] A.A. Duarte and H.G. Solari. Metamorphosis of the monochromatic spectrum in a double-cavity laser as a function of the feedback rate. *Phys. Rev. A*, 58(1):614–619, July 1998.

Chapter 6

Optical Gain

6.1 Introduction

The study so far has revealed some very interesting phenomena in the modal structure of semiconductor laser diodes. The optical configuration has until this point been investigated in the *cold cavity* limit, this cold cavity limit is achieved by setting the optical gain (via the conductance) within the laser diode cavity to zero. The next obvious step in the development of the recast coupled cavity model is to introduce some optical gain into the structure.

This chapter presents an investigation into the modal structure of an semiconductor laser diode with optical gain. The significant result of the loss of mode discrimination in the cold cavity limit is shown to still be present with optical gain. Regions around the loss of mode discrimination will again be investigated.

In the passive case the long cavity limit also revealed the unexpected result that the longitudinal mode of the laser chip have shorter mode lifetimes than the external cavity modes. This occurs because in the passive cavity case the laser cavity is really just a

small perturbation on the mode of the much larger external cavity. Including gain will be shown to restore the dominance of the laser's longitudinal modes. In subsequent calculations the gain will be assumed to be frequency independent.

The work presented in this chapter uses the same optical configuration as in previous chapter. A laser diode is coupled to an external cavity, which is formed by a dielectric mirror, this then allows the external reflectivity to be varied, figure 4.3 shows the system of interest. The parameters used are also mirrored, except for the conductivity. The conductivity now offers a means of introducing optical gain into the laser diode's cavity and as a consequence k_m, where m is the cavity index, is made complex by the conductivity being greater than zero. The wavenumber must now be expressed in its entirety, where previously the imaginary component was assumed to be zero.

6.2 Loss of Mode Discrimination

The loss of discrimination seen in chapter 5, in figure 5.3 shows that with increasing external feedback the modes reach a critical point where the mode lifetimes are all the same, it also shows how the dominant mode before the critical point is switched to the least dominant mode after the critical point and vise-versa. The effect of introducing gain into the laser cavity will now be investigated.

Through a series of four figures the key features of the modal structure are investigated as the optical feedback is increased from the solitary laser limit to the low feedback case and then to just beyond the critical feedback level, and finally the strong feedback case is studied. All the figures follow the evolution of nine modes, one of which is a single laser mode and eight external cavity modes.

Figure 6.1 show the variation in the modes with increasing optical gain, for the case

when the configuration is tending toward that of a solitary laser, namely, R_{ext} is small ($-80dB$). The laser diode mode is easily distinguishable as the mode lifetime is considerably longer (the mode lifetime is inversely proportional to the imaginary frequency) than the external cavity modes. The longitudinal mode associated with the laser cavity dominates the system and shows the greatest sensitivity to increasing optical gain. All the modes exhibit mode bending, this is due to the contribution that the conductivity makes to the ω_{real}, see equation (4.6). As the optical gain is increased the mode lifetime of the laser longitudinal mode increases, while the mode lifetime of the external cavity modes decreases. Hence the external cavity modes are suppressed as the optical gain increases. If the external cavity reflectivity is increased such that the feedback is within *Regime I* of the Tkach and Chraplyvy classification and the optical gain is increased, Fig. 6.2 shows that the laser longitudinal mode still dominates the system. However, the external cavity mode lifetime does increase as the optical gain is increased, (unlike the previous case). As before all the modes experience mode bending and the laser mode is again the most sensitive to changes in the gain.

Figure 6.3 shows the effect of increasing optical gain when the optical feedback is just above the critical level that induces catastrophic loss of mode discrimination. As the optical feedback level is above the critical value the laser mode no longer dominates the mode structure in the passive cavity limit, but as the optical gain is gradually increased the mode lifetime difference is seen to reduce. It is worth noting the change of scale on the imaginary frequency axis, it can be seen that the variation in the lifetime is in fact very small by comparison to the previous two figures. It is evident from this figure that the loss of mode discrimination is not just a passive cavity phenomenon. Mode bending again occurs, and this time all the modes move to lower frequencies.

In the strong optical feedback limit the external cavity modes dominate the mode

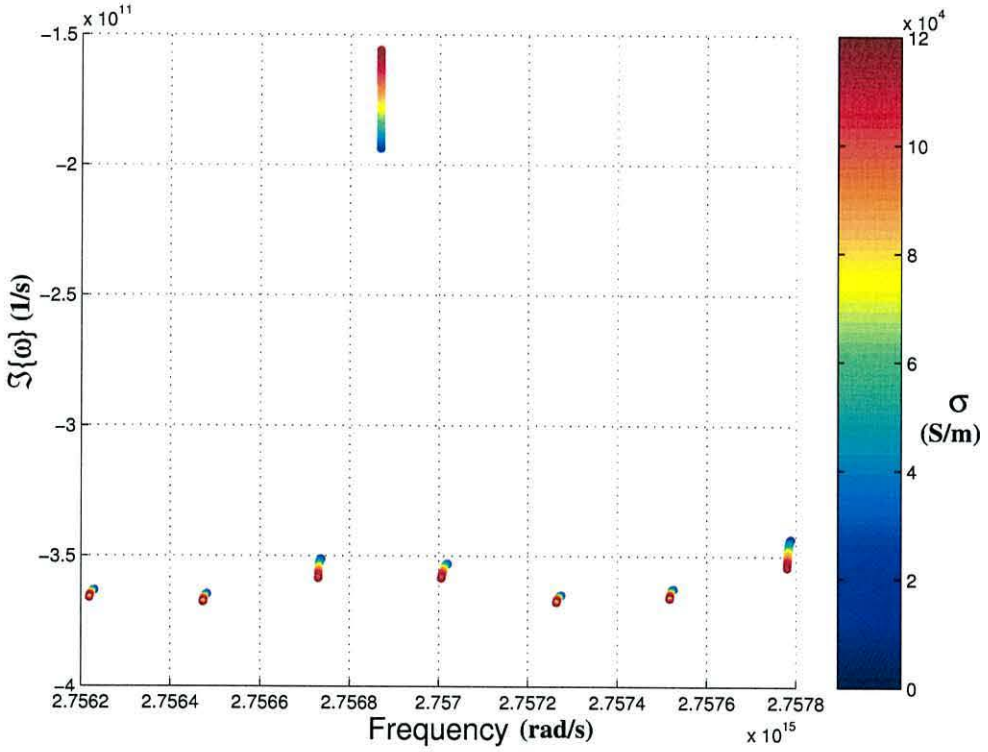

Figure 6.1: *The variation in the modal structure with increasing optical gain, the feedback is held very small ($R_{ext} = -80dB$)*

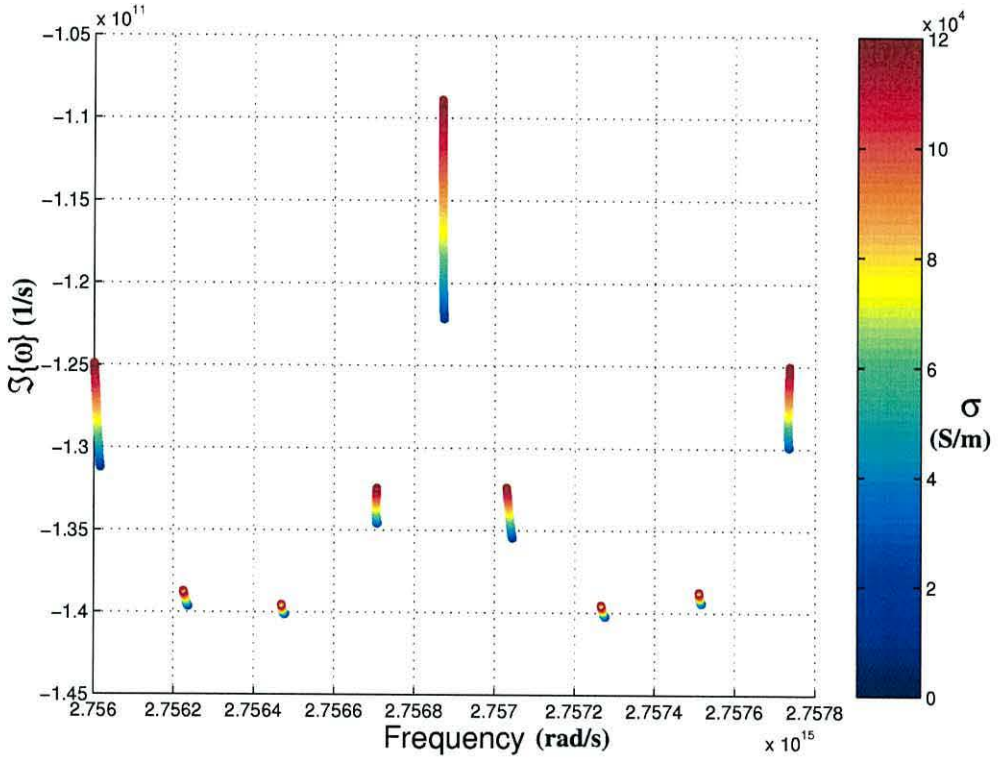

Figure 6.2: *The variation in the modal structure with increasing optical gain, the feedback is held at a reasonable level ($R_{ext} = -30dB$)*

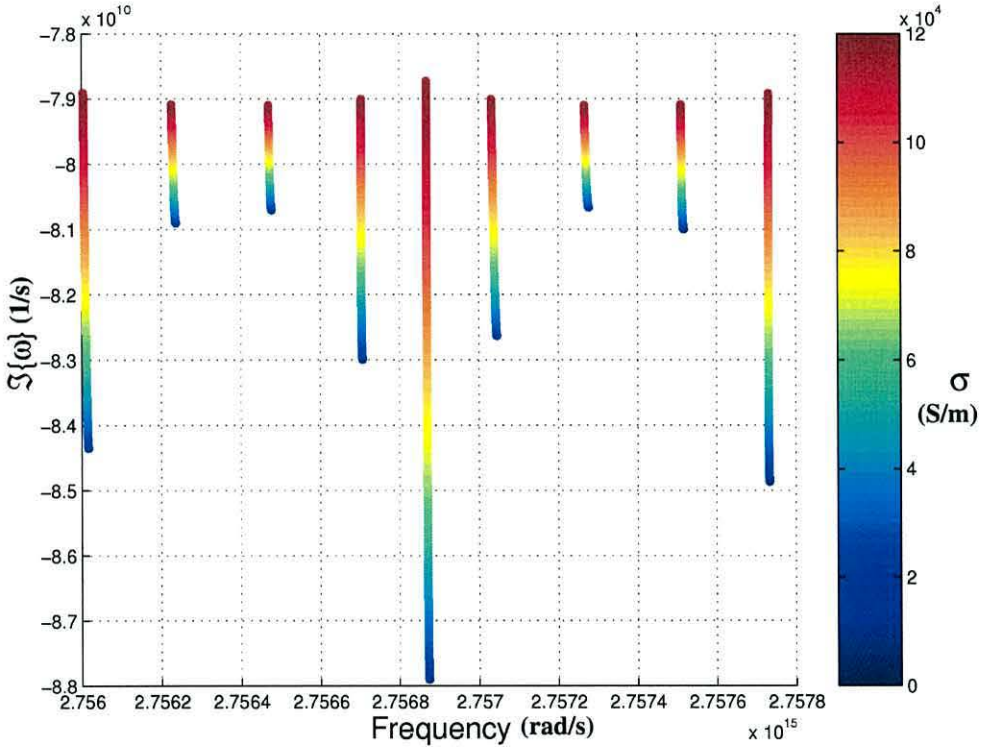

Figure 6.3: *The variation in the modal structure with increasing optical gain, the feedback is set to the critical point of loss of mode discrimination* ($R_{ext} = -16.5dB$)

spectrum for all gain values, Fig. 6.4. No one external cavity mode dominates because the optical gain has been assumed to have no spectral dependence. The laser cavity mode exhibits the greatest sensitivity to variation in the optical gain. This is to be expected as the mode satisfies the phase condition for resonant operation in the laser cavity and hence experiences the greatest interaction with the gain. As before all the modes move to a lower frequency as the gain increases.

6.2.1 Long Cavity Limit

All the results have so far been concerned with the short cavity limit. The focus will turn to the long cavity limit (five hundred times the laser length, $500L_1$) to see if the introduction of optical gain into the laser cavity restores the dominance of the laser cavity modes (c.f. Figure 4.5). Figure 6.5 shows that as the optical gain is increased the laser mode dominates the mode spectrum. In this case the external cavity reflectivity has again been reduced, so effectively modeling a solitary laser and hence the laser cavity mode must dominate. It is noticeable that all the external cavity modes bend toward the solitary laser mode, and have similar lifetimes at high gains.

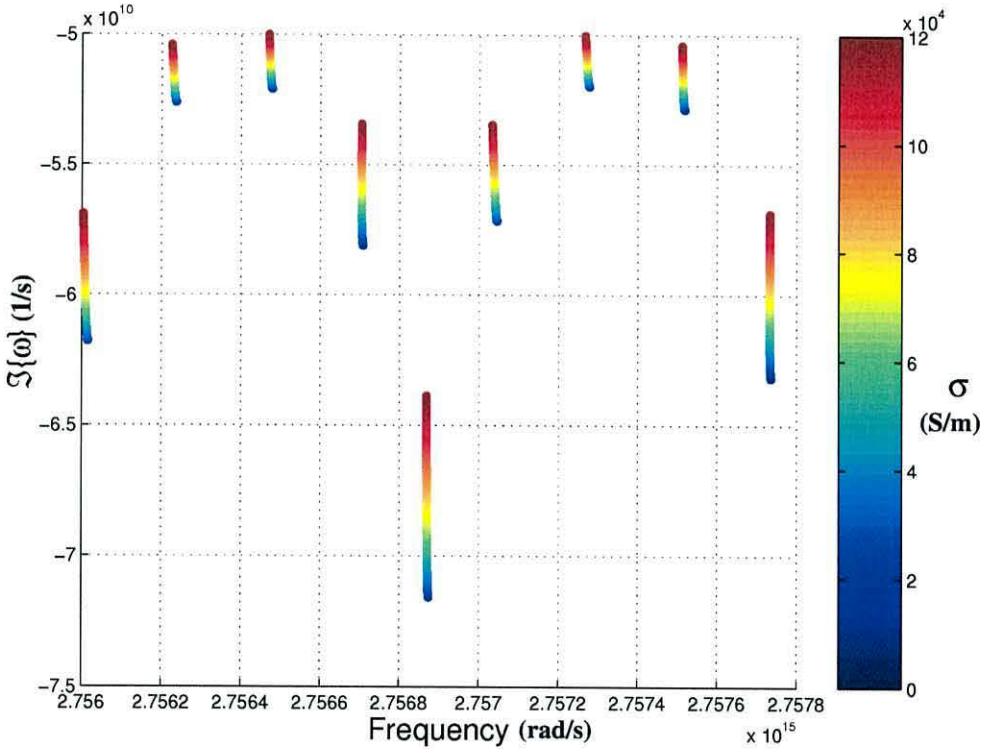

Figure 6.4: *The variation in the modal structure with increasing optical gain, the feedback is set to a high level ($R_{ext} = -10dB$)*

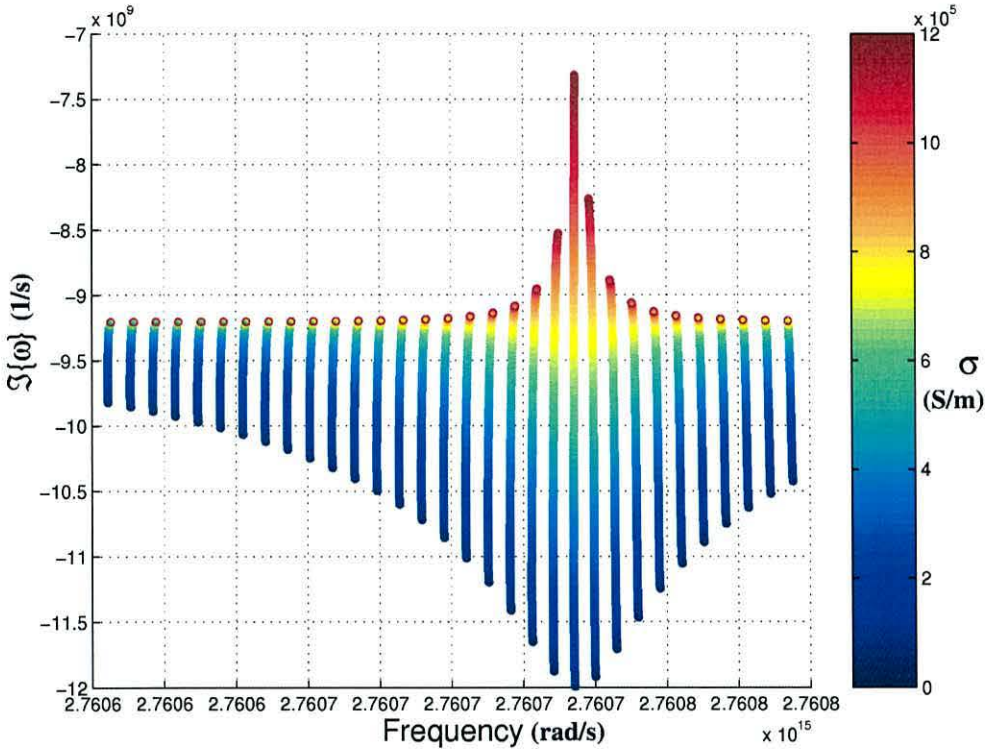

Figure 6.5: *The variation in the modal structure with increasing optical gain in the long cavity limit, the feedback is set to a low level ($R_{ext} = -80dB$)*

6.3 Summary

In the short cavity limit the regions around the point of catastrophic loss of mode discrimination have been investigated. It has been shown that the modes change as described in the case of the cold cavity limit for moderate levels of gain. However if the gain is increased sufficiently then the modes due to the laser diode can dominate. This result is expected because if enough gain is supplied then laser diode should dominate the optical configuration.

In the case of the long cavity limit it is shown that if the optical gain is increased sufficiently then the mode due to the laser diode can become the dominant mode in the spectrum. This result is especially important in light of the fact that in the cold cavity limit the mode is merely seen as a small perturbation to the mode structure.

Chapter 7

Cluster Development and Calculation

7.1 Introduction

Numerical computation has always been a very interesting field, not only is it evolving through the emergence of new technologies but also through increased use at home and in the work place. There has recently been a significant interest in the study of *Distributed Systems*, which addresses the increase of computing power, which can be situated in different physical locations, and how it can be exploited [1]. A *distributed system* is a set of interconnected, autonomous computers that cooperatively solve large single problems or facilitate parallel execution of separate and or possibly related tasks [2].

A 'Beowulf' cluster is essentially a distributed system for high performance parallel computing but built from commodity components [3]. Using commodity components the cost of a high performance computer is significantly reduced, thus allowing high performance computing to be available on modest budgets to fields other than Computer Science [4]. This chapter details the development of such Beowulf cluster for the parallel processing of a numerically laborious problems; the cluster is called "Mawrdwr".

Mawrdwr was design and build to facilitate the processing of numerical calculations involved in using the *Argument Principle Method* (APM) to locate the roots of a non-linear matrix equation, as outlined in chapter 4.

The primary objective of this work is to achieve a *user transparent distributed algorithm deployment software for legacy code*[1].This would then enable end users to produce legacy code to a predefined specification and deploy it on a distributed system without having a knowledge of the underlying system or architecture. Effectively allowing a cheap and powerful system for numerical calculation using legacy code.

7.2 Parallel Algorithms

7.2.1 Algorithm Identification

When trying to improve computational speed, you must determine whether the 'problem' is suitable for deployment on a distributed system. Does the algorithm lend itself to a parallel architecture [5, 6]? Due to the network speed limitations (the speed at which information can be passed between two or more machines by way of network connections), the computation to communication ratio [7, 8] is the paramount consideration. This is especially true when using a Beowulf cluster because of the commodity networking. Commodity networking is available at speeds of up to one gigabit per second ($1Gb/s$) but is expensive at this speed, Beowulf clusters tend to use one hundred megabit per second ($100Mb/s$) connections to reduce the costs involved. Mawrdwr was designed and created to run numerical models of semiconductor laser diodes. Execution of these models requires large *computational* needs relative to the *communication*

[1]Here the term *legacy code.* means not just existing or old code, but new code written in the end users preferred programming language

needs, thus the computation to communication ratio is large; only small amounts of data are passed over the network, thus removing the metaphorical 'bottle-neck' from the system, if the quantity of data is considerable then the network speed is the primary constraint on the execution times. Having a large computation to communication ratio is ideal for execution on a Beowulf cluster. As the algorithm is *massively parallel* which means that small amounts of data are passed between the processing nodes and cluster head, a simple divisional dynamic load balancing of the process distribution is sufficient, the processing is split into equal amounts and distributed to each of the processing nodes, however, more sophisticated schemes are possible (an example of improved load balancing can be seen in Fahringer's [9] work).

7.2.2 Cluster Relevance to The Grid

The Grid is a relatively new development, it primarily consists of a high speed network which interconnects a number of institutions (mainly academic at the moment) to enable them to share their computing resources. The primary aim of the Grid is to allow all of the institutions to have an arbitrary quantity of available processing in-house, which on its own is not significant, but, if all the institutions combine the available processing power, they form a formidable processing machine which has as much processing power as and when it is required. The main aim is that no one institution has a great deal of processing power other than is required to perform every day tasks, but when larger tasks are required and the institution's own resource are over stretched, it then automatically sends the task to be processed on the grid, in a similar way to how electricity is supplied now. Clusters of course are not on the same scale as the Grid but can be regarded as analogous to small scale 'Grid Computation', they take computers that

on their own do not amount to a very powerful system, but if many of them are linked together and used in collaboration then they become an extremely useful tool. This analogy can be extended to argue that through the development of cluster technologies and an awareness of the Grid, they can be later extended, either over the Grid directly or used as the basis for other Grid application(s) [10].

To ensure the 'Grid relevance' of any cluster, use of *Transmission Control Protocol/Internet Protocol* (TCP/IP) must be made. This not only makes development applicable to the Grid but also allows connections via the Internet as well. TCP/IP is the protocol used over the Internet and the Grid, it allows *packets* of data to be transmitted via *Sockets* (this is a virtual 'socket' on the host) to sent to a host at a specific *IP* address (an IP address is a number, eg. 192.168.1.3). Through the use of a *Domain Name Service* (DNS) names can be used instead of the IP numbers, eg. www.bangor.ac.uk.

Encompassing this idea of cluster extensions leading to the idea of a Grid technology ensures longevity of the cluster implementation while allowing the development to benefit both fields of research.

Clusters can not only be used for Grid development but also used as a pool resource within an institution for 'Grid Computation' [10, 11]. Small and large scale high performance distributed systems, including clusters, can be incorporated in to the Grid and are known as *virtual organisations*[2] [12].

The overall objective of Grid computation is to make computing power available as a commodity, allowing users to have as much computational power available as and when it is required [11]. The whole mechanism allows real-world problems to be solved [12] in a efficient and fast way.

[2]Virtual Organisations also can mean literal organisations, so a cluster could be a resource in a virtual organisation as well as be one in its own right

7.3 Application

The primary objective of this work is to calculate the solutions of the *Coupled Cavity model* [13, 14](derived in chapter 4) to find the solutions of the optical configuration defined by the matrix equation. The configuration is described by the following equation:

$$\begin{pmatrix} A_3 \\ B_3 \end{pmatrix} = Q(t_3)Q(t_2)Q(t_0)\begin{pmatrix} A_0 \\ B_0 \end{pmatrix} \tag{7.1}$$

where

$$Q(t_m) = \begin{pmatrix} \alpha, & \beta \\ \gamma, & \delta \end{pmatrix} \tag{7.2}$$

The solution of equation (7.1) is non-trivial, so to find the solutions the Argument Principle Method (APM)[15] (also outlined in chapter 4) is employed. The APM can only be applied to any analytic complex function, and is able to count the number of solutions in a given region of interest. This is achieved by evaluating the contour around the required area using equation (4.27). Establishing the number of solutions is one of the APM's greatest advantages because once the number of solutions is known any root finding algorithm could then be deployed. Knowing that all the solutions have been found is a unique feature not found in other root finders (where mainly heuristics are used to examine the function and determine roots). Once the number of solutions is known a summation of the function for each root is performed using equation (4.26), these summations are then used to construct an equivalent polynomial from equation (4.28), which is known to have zeros in the same places as the function of interest and can then be solved using standard numerical methods.

The APM requires a definition of the complex contour around the area under study, this single contour can be broken up into smaller multiple contours in which the same solutions exist. The APM can then be applied to each of the smaller contours in turn, the solutions in each of the contours are then found and combined to produce the solutions of the initial larger contour.

The smaller contours are evaluated in parallel, thus the execution times are reduced. For each solution there is a single summation of equation (4.26) so if say twenty summations are required, execution in a serial fashion would say take twenty minutes, but, if the contour is split into four smaller contours (five solutions in each) for instance, then the summations would still be evaluated in one minute, but because they are now executed in a parallel fashion, the execution time would be about five minutes. This is of course a simplification of the process but it illustrates the means by which execution times are reduced.

7.4 Theory

7.4.1 Complex Contours

The solutions to the matrix equation (7.1) are in the from of a complex variable. The contours are also in the complex plane, the contour is defined by complex variables. Figure 7.1(a) shows the complex plane, the real component is along the x-axis and the imaginary is along the y-axis. Figure 7.1(a) shows a single complex contour that has nine solutions. The contour has a rectangular shape, this has been chosen because it means the contour can be conveniently divided into sub-contours that encapsulate all of the solution; this process would be far from trivial if circular contour were used. Fig-

ure 7.1(b) illustrates how the contour is divided smaller contours. The choice of rectan-

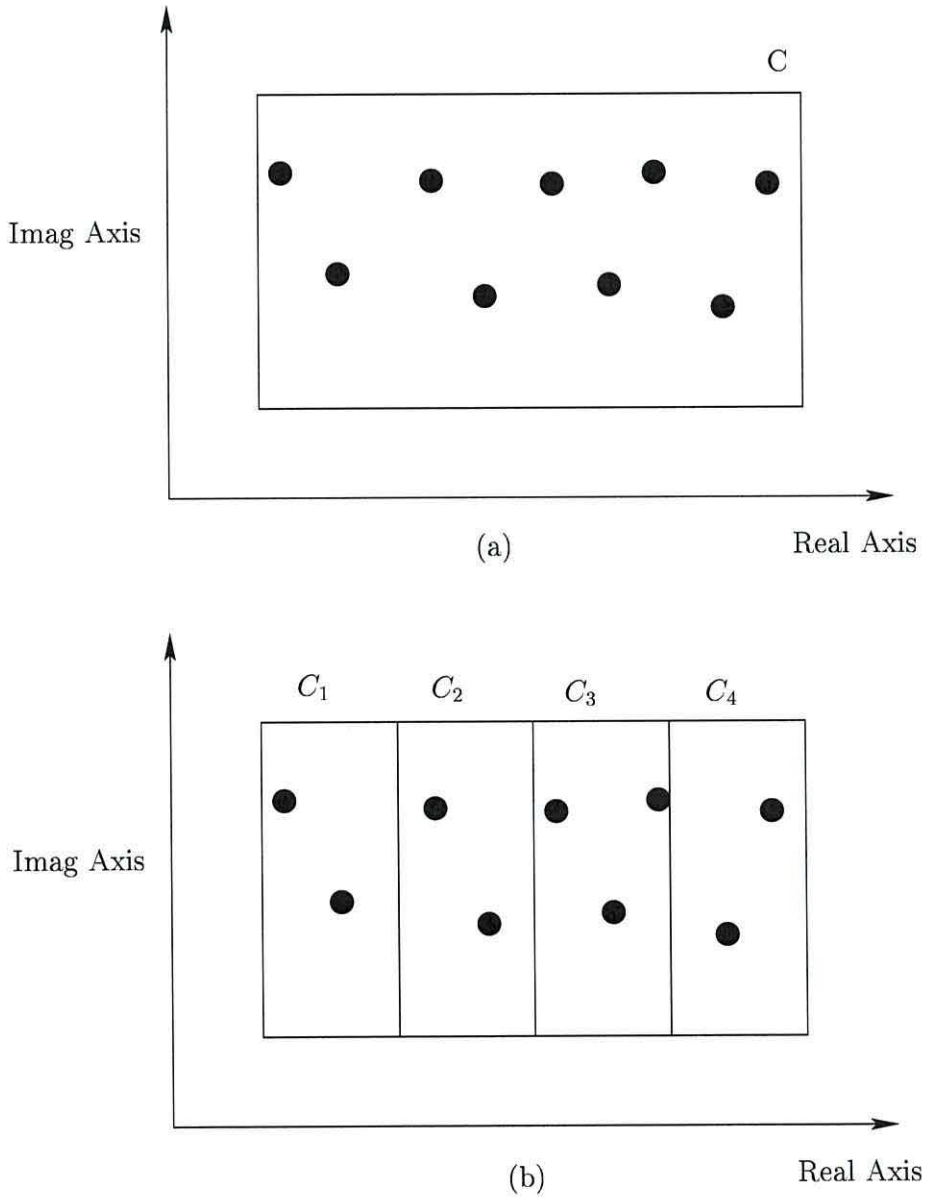

Figure 7.1: *A schematic showing how the rectangular contours can be split. (a) has a single contour C around nine solutions (the black circles). (b) has four contours coving the same area as C in (a).*

gular contours then also lends itself to rectangular coordinates, but again if the problem

is suitable then a polar coordinate system could be used. The use of polar coordinates can be very useful when a single contour is used, this is because the integration can be implemented to only require a single value, the angle to be varied.

As can be seen in equations (4.26) and (4.27) there is a division in the APM integrals, it is thus essential that the contour does not pass through a zero, this could result in a divide by zero error. In the initialisation of the APM the contour must be checked to ensure that it does not pass through any zeros, if this situation does arise then the contour must be adjusted, the adjustment must increase the contour otherwise a solution may be missed. This process must be undertaken automatically, by evaluating the function at intervals around the contour, the magnitude can be compared to a limit (this is problem dependent) and if the limit is breached then the contour must be adjusted.

7.4.2 Contour Integration

The APM relies purely on the contour integral of equation (4.26), shown here again for clarity,

$$S_m = \frac{1}{2\pi i} \oint_C z^m \frac{f'(z)}{f(z)} dz. \tag{7.3}$$

There is a vast amount of literature available on numerical method to conduct integration. It is, however, worth mentioning the method used in this work. Initially the simplest form of line integration was used, the *Trapezoid Rule*, this indeed did work but required the *step of integration* to be very small. In order to ensure sufficient accuracy steps in the order of quarter of a million per side of the contour were needed. To reduce the number of steps required *Simpson's Rule* was used, this only required one hundred thousand step for the entire contour, an order of magnitude reduction.

As can be seen from equation (7.3) the derivative of the function is divided by the

function itself, thus requiring the function and the derivative to be evaluated at each of the hundred thousand steps.

7.4.3 Derivative

In equations (7.3) and (4.27) the derivative, $f'(z)$ of $f(z)$ is required. To make the APM as generic as possible the derivative must be obtained through numerical methods, this can be achieved using the *Cauchy Integral Formula*:

$$f'(z_0) = \frac{1}{2\pi j} \oint_D \frac{f(z)}{(z - z_0)} dz, \tag{7.4}$$

where D is an arbitrary analytic contour around the point z_0. Again the most appropriate contour system should be chosen.

The evaluation of each of these contours requires at least one hundred thousand evaluations of the function, to again achieve the required accuracy in the derivative. Simpson's rule was applied over a hundred thousand steps. A consequence of having to evaluate the derivative numerically is to square the number of required function evaluations for each contour integral in the APM.

Removing these extra function evaluations from the APM would entail the derivative being analytically derived and then be directly used in the calculations, this would considerably reduce the computational time, it however removes the generality of the APM implementation.

7.4.4 Computational Requirements

Analysis of the equations and method already reveals a large computational requirement. For instance, the contour of interest must be initially evaluated to determine how

many solutions exist, this would itself require one hundred thousand function evaluations and may possibly require the same number of evaluations of the derivative. Once the number of solutions is known then the contour integral must be evaluated once again for every solution.

Figure 7.2 outlines the algorithm used to deploy the APM technique. Initially the process starts on the cluster's main node, this then sets the overall contour as defined by the user. It then divides the contour in to the required number of smaller contours, this is usually the number of nodes in the cluster. Once the smaller contours have been defined, the main node sends the smaller contours to each of the nodes, where the node checks the contour for zero crossings (the contour is assumed to cross a zero if the absolute value of the function drops below 10^{-5}, this threshold was obtained through trial and error, if reduced then numerical errors start to play a significant role in the results); if this situation does occur duplication may result, two contours may contain a single solution and the duplicate must be remove via post processing of the data. The APM is then applied to each of the individual contours where the number of solutions, and then their locations are found. This data is then sent back to the main node, where it is collected and saved to disk.

The APM's computational requirement is dramatically affected by the use of numerical derivative computation, as explained in section 7.4.3.

Method	Contour Steps	Evaluations of $f(z)$
Analytic	1×10^5	2×10^5
Numerical	1×10^5	1×10^{10}

Table 7.1: *Typical function evaluations per contour summation, for numerical and analytic derivative, values are typical realistic values*

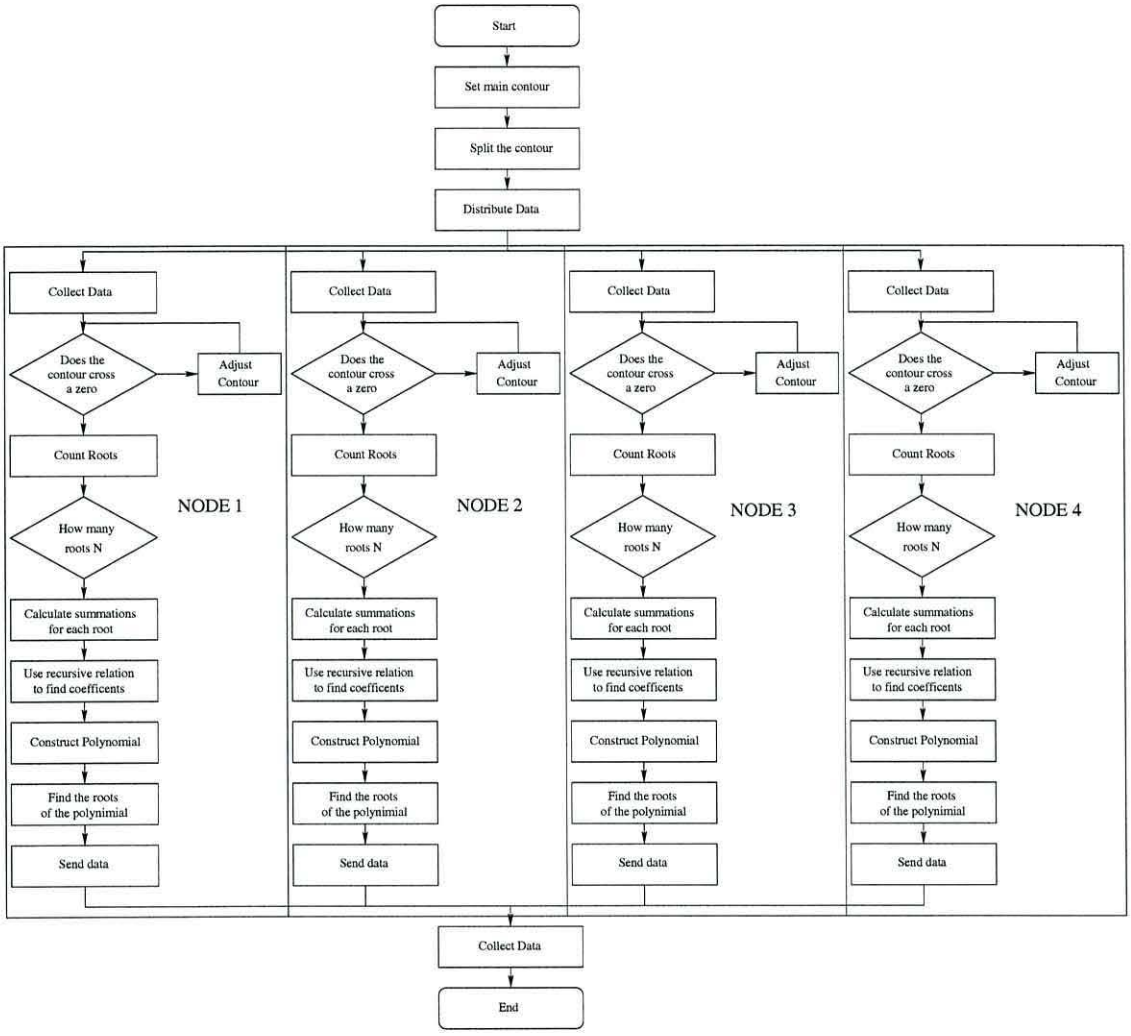

Figure 7.2: *A flow diagram of the computational algorithm in deploying the APM on a cluster. Here the method has been executed on a four node cluster.*

Table. 7.1 clearly demonstrates the additional computational cost due to numerical evaluation of $f'(z)$, this computational cost needs to be balanced against using the analytic derivative, since using the analytic expression for $f'(z)$ will remove the generic nature of the APM.

7.5 Stages of Development

7.5.1 Language Choice

Platform independence.

Beowulf clusters have primarily been used as a means of keeping costs down. One way of ensuring this ethos is maintained is by the use of an *open source* operating system (OS), Linux is an example of an open source OS an is available at no cost and was hence chosen a the preferred OS. It is of course the case that most people buy their OS (Microsoft's Windows for example). Ensuring the final implementation to be platform independent make the final program more accessible to any perspective user. A language that offers both platform independence and proven network communications is Java [16]. The *Byte Code*, as Java programs are known, uses the *Java Virtual Machine* (JVM) to execute the Byte Code. There are many OS variants of the JVM, thus offering the platform independence required. To then deploy the Byte Code on a cluster, each node simply needs a JVM [17].

Multi-Threading.

Multi-Threading is a desirable tool in any programming language, it is however, not necessary in this instance because the process division will be handled explicitly, it

could be used for testing by simulating multiple processors on a single machine. This would only be of use in the debugging phase of the implementation because Mawrdwr is a *distributed memory multi-processor machine*(DMMPM) not a *shared memory multi-processor machine*(SMMPM). This in short means that the APM does not have access to the same memory, thus global variables must be stored independently by each node. To exploit the architecture of a SMMPM multi-threading along with a JVM would be required. Java offers a good multi-threading package, it has been shown however that it does not offer high performance in comparison to sequential code [18], when run on a single processor machine.

Object Orientation.

An Object Oriented(OO) language is preferred, as it can offer decreased development time, but it can also offer increased code reuse [19]. Java is again a valid choice for this type of development, it has an extensive array of computational libraries that are continually being developed.

Java as a Development Tool.

Java was chosen as the obvious language for development of the system, it does, however have some issues that needed to be addressed. Firstly the lack of numerical libraries when compared with other languages. This can be overcome by porting well known algorithms to Java [20]. The second hurdle is Java's relative speed compared with other languages. Java is regarded as being very slow by comparison with Fortran, C++ etc, but there have been a number of studies that now show that as Java becomes more mature, the platform dependent virtual machines are improving Java's performance [21], some of these studies have also undertaken comparisons between older more estab-

lished languages that were designed for numerical computation, they have shown that if standard optimizations are used then Java can achieve 85% of the fastest run of a native language performing the same calculations [22] this is using the highest precision available but does not include complex numbers. For the initial proof of principle of the cluster, the numerical functions required were fairly trivial, so the necessary routines were re-written in a new Java Numerical Library(JNL) developed for this work, and used in conjunction with a *complex number* class which was also written for this work.

7.5.2 Initial proof of Principle

The Java client and server ran in a windows environment on just two machines. This proved the system would work. It was then deployed on the undergraduate computing laboratory, on 40, 500MHz personal computers. This showed the expected improvement in performance and demonstrated scalability(see figure 7.3). This was deemed only a proof of principle because there was no realistic way of being able to use the machines on a regular basis. The available machines also needed to be setup and initiated on every trial, the time taken for this would be prohibitive in a final solution, at two hours. The program was also executed on a cluster of 10 nodes, figure 7.3 shows the runtime versus the number of nodes, it also shows an exponential decay in processing time with an increase in nodes, this result was not unexpected.

Initial Algorithm

The initial development stages of the cluster where aimed at executing a *Quadrature Detection* algorithm. Quadrature detection (or lock-in amplifier [23]) method, is much used in experimental system identification and can be used to determine the nonlinear

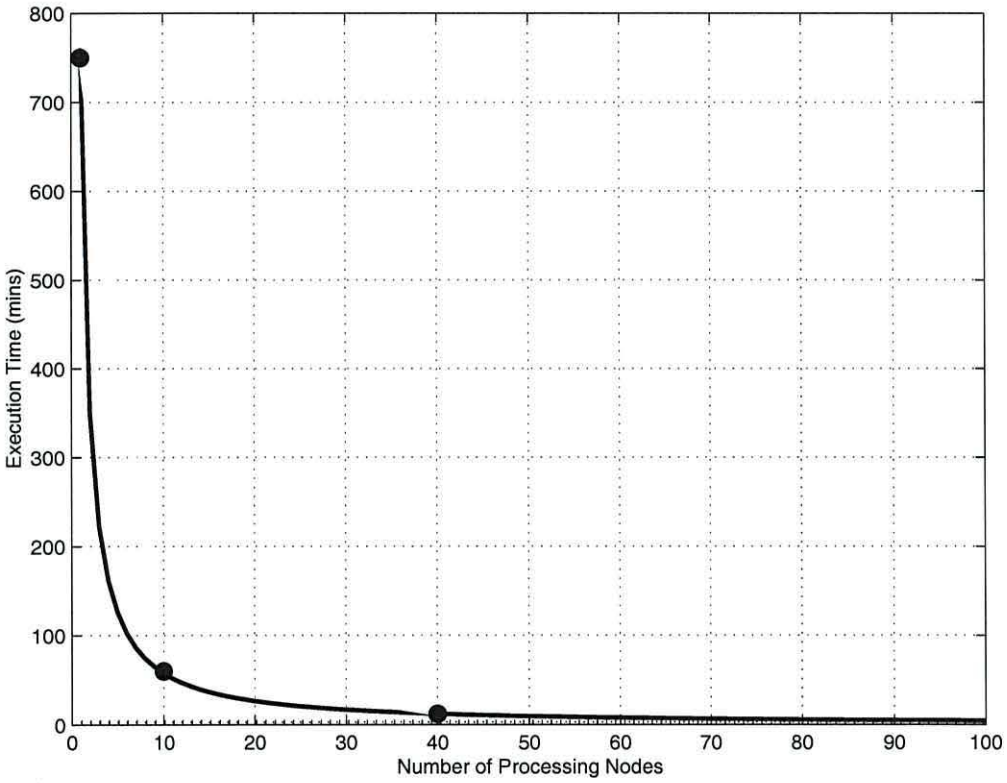

Figure 7.3: *Showing the improvement in process time, with an increase in cluster nodes, the line shows the minimum time in which the process could be run*

modulation response of a semiconductor laser diode model. A systematic characterisation of the nonlinear modulation response in the laser model is undertaken by varying the dc-bias current and the amplitude of an applied sinusoidal modulation signal, see Fig. 7.4. By locking to harmonics of the excitation signal information about the degree of nonlinearity in the system can be gained, with a view to predicting the chaotic synchronisation behaviour of the laser diode when used in a chaotic communication system. Applying a sinusoidal signal to the system under test (S.U.T.) and then mixing

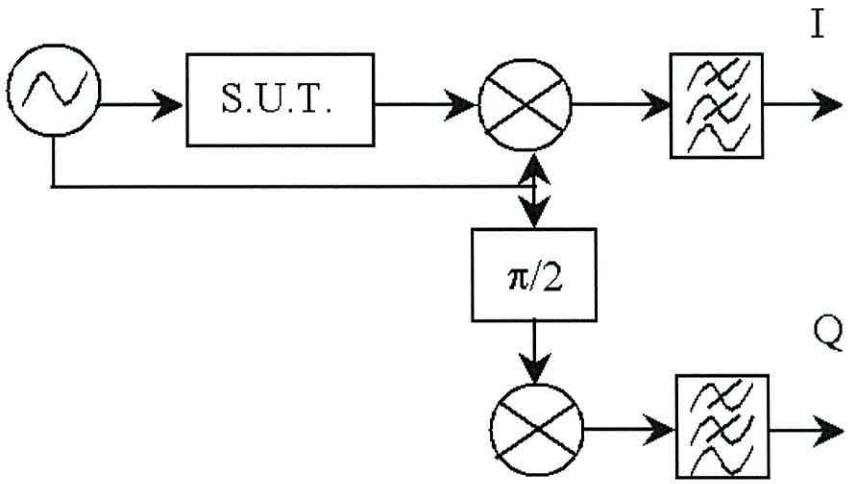

Figure 7.4: *Schematic of a quadrature detection system.*

the output with the same signal as the input, valuable information about the phase and amplitude to be gained from channels I and Q. For the development of this process in Java there was a *complex* class written, this was required to encapsulate complex numbers into a Java object.

The quadrature detection technique proved to not offer any assistance in the analysis of the non-linear output of a laser diode. The primary reason for this was that the filtering required was not good enough to completely remove the DC element of the

signal, and as such the analysis failed.

However, the quadrature technique requires large amounts of data to be processed, this requirement helped in the development of the cluster software and allow a successful demonstration of the cluster.

Execution Times

Figure 7.3 shows the process time as a function of number of nodes, it is not unexpected that the execution times decrease with more nodes, the offset in processing time is the single process runtime, and is the minimum time the system will take to execute (this is the time a single node would take to execute one contour for the APM or a single data-run of the quadrature detection). Once the overall execution time meets the offset more nodes would be redundant as the minimum process time would be achieved. The execution time could then only be improved if the actual speed of the nodes were increased. Figure 7.5 shows cost to speed relationship it can be seen that a minimum exists not at the greatest number of nodes but after a few tens of machines, showing that an optimum cluster for this particular problem would have about 15 nodes. This optimum number of nodes would be different for each different parallel algorithm and a similar analysis would need to be performed. Of course if the nodes are available then they should all be used to reduce runtime as far as possible.

7.5.3 Legacy Code

Java offers the *Java Native Interface* (JNI), this allows there to be a link formed between a native programming language (native language is one that needs explicit compilation depending on OS). To try and make the architecture as transparent as possible the pro-

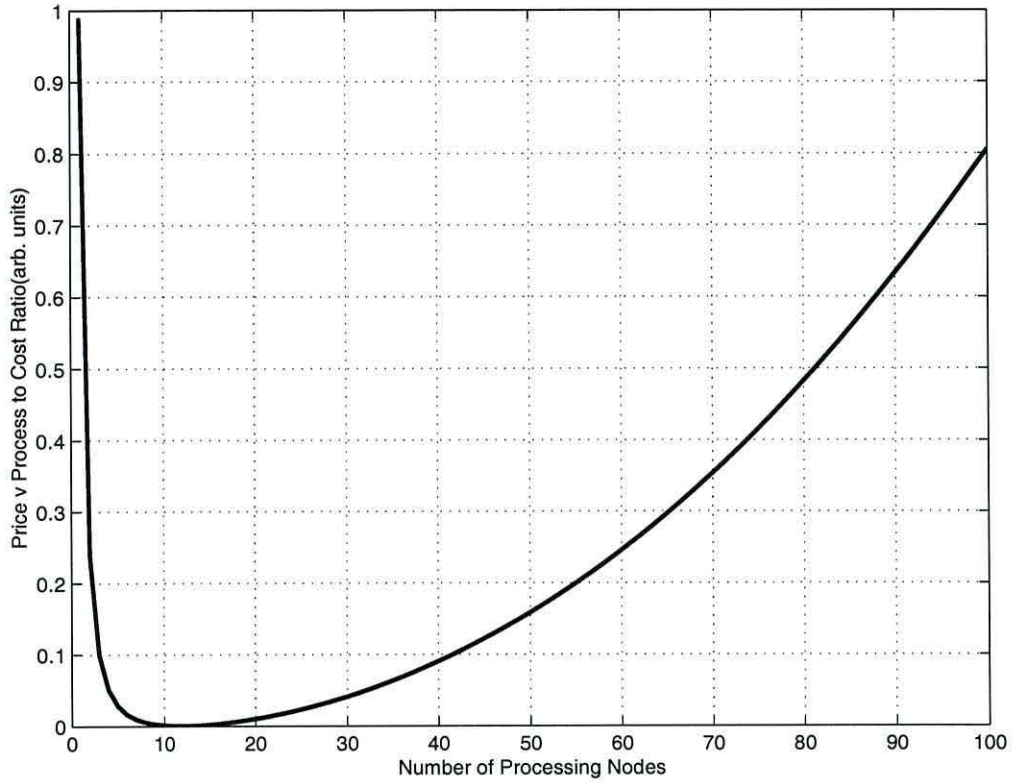

Figure 7.5: *Shows the optimum number of nodes required for this particular problem, the minimum reflects the point where any more nodes would reduce the cost efficiency of the system. For this particular problem approximately 15 nodes would be optimum, meaning and further nodes purchased for this problem would not justify the financial commitment.*

gram source code should never be altered, it should offer a generic interface independent of language choice or program to be run. Also due to Java's sparse inherent routines and data types with regards to numerics, it is not the preferable language for scientists. Fortran or C are popular choices of language offering vast numerical libraries that not only offer what is needed, but also has decades of proven reliability. Ultimately Legacy Fortran was used for the numerical parts of the program due to the large amounts of preexisting code, whilst still using Java as the environment controller or high level operating system. This was already known to function as desired as the prototype had used purely Java.

Java has numerous methods for integration of other languages. One of these is the JNI, already mentioned , this was demonstrated by Getov *et.al.* [24] but just with C++ libraries. However, to link Java to Fortran it must be accessed through a C++ interface called a *Wrapper Class*, it allows the different ways in which Java and Fortran address memory to be compatible. The Java Runtime Environment (JRE) being an alternative, allows control of the external legacy programs directly by the JVM. In this scenario variable passing can be carried out using either Java's *streams* for sending directly to the program through the OS, or file passing. It was decided to use the JRE as this offered the most convenient way to handle the legacy Fortran.

The JRE allows Java's streams to 'pipe' information to the standard input/output of Fortran, these standard input/output streams mean that Java would 'catch' the screen output of the Fortran program and receive it as a stream of bytes; the input is achieved by sending bytes to Fortran's standard input which is usually the keyboard. This type of synchronized communications can lead to overly complicated checking of the passed data. It was decided, due its simplicity, that legacy to Java communication would be carried out using parameter file passing. As stated earlier the level of communication

between processes is low so parameter file passing would not add a significant increase in process time. If the communication required were to increase then the Java use of streams through the standard input/output would be utilised for maximum performance. Alternatives to the standard JRE such as *Gabi* as reported by Chen and Hou [25], Gabi is an implementation of the JVM, this new JVM implements its own JRE that removes complexity from the standard JVM, the change thus reduces the memory footprint and as a consequence reductions in the execution times is achieved.

The use of legacy code gives Mawrdwr a more generic architecture type, it is able to use solely Java code, or any combination of Java and natively complied executable. With a much larger target of end users, and because Mawrdwr uses Internet protocols the final system could be deployed on the Grid [26]. Mawrdwr as it stands still requires user decomposition of the algorithm, the parallel section of execution must be implemented separately to the pre and post processing of the loop. The user must therefore be aware that the program will be executed on a parallel machine and as such, take account of this fact in the coding development. The development of automated decomposition is a vast area of study, decomposition can be broadly split into two main areas of interest SMMPMs and DMMPMs. The difference in communication methods (communication between parallel serial code fragments) of the former, shared memory architectures, and the later, the distributed memory architectures is significantly diverse. It has already been stated that the communication speeds are of little consequence in the problems being solved and it is therefore not addressed any further in this work.

7.5.4 Implementation

In the first version of the Java deployment software each node still needed direct initialisation. To overcome this problem the system was changed from client/server to server/client, this means that instead of the processing node initializing the communication channels used, the controlling node would initialize the communication, the processing nodes became 'dumb', and need to know nothing except what the controller node tells them. Hence, servers are now running as Linux Daemons (Daemons are processes running on the node as background processes and are started up at boot) on the processing nodes and no initialisation is necessary, making each of the nodes fully independent. The resultant effect of this modification was to improve productivity and also reduce the administration of the cluster. Fault tolerant node software [8] enhances usage because each node handles errors, therefore no user intervention is necessary, it is however possible to view the daemon logs to allow faults to be found.

The node daemon waits for a class to upload, it then executes the class using a specifically designed *interface* (interfaces allows decoupling of the object oriented architecture, giving much more cohesive code design and implementation) and simply returns the class to the 'Controller' Node, where the results are collated. This type of architecture can be regarded as a type of *message passing* paradigm, other systems use *Remote Method Invocation*(RMI), which allows a method to be called remotely from a pre-established communication channel. Examples of the RMI paradigm have been used to a similar end by [9, 17]. The system can be schematically seen to have an architecture as shown in figure 7.6, the Java being the 'Middleware' for the cluster and the Fortran sitting between the Java and the OS on each of the nodes.

In an early version of the Mawrdwr software a *Graphical User Interface*(GUI) was

used for user interaction. If the end user is local to the *controller node* then this has been shown to be an excellent means of user interaction [27], if, however, the system is to be accessed remotely then the GUI can cause a massive 'bottle-neck' over a dial up connection for instance due to large amounts of data needing to be transmitted and received over a very slow network connection. To overcome this the user interface was redesigned to be a terminal type interface (text based menu system), this had the benefit of allowing 'local' and 'remote' use due to minimal communication requirements.

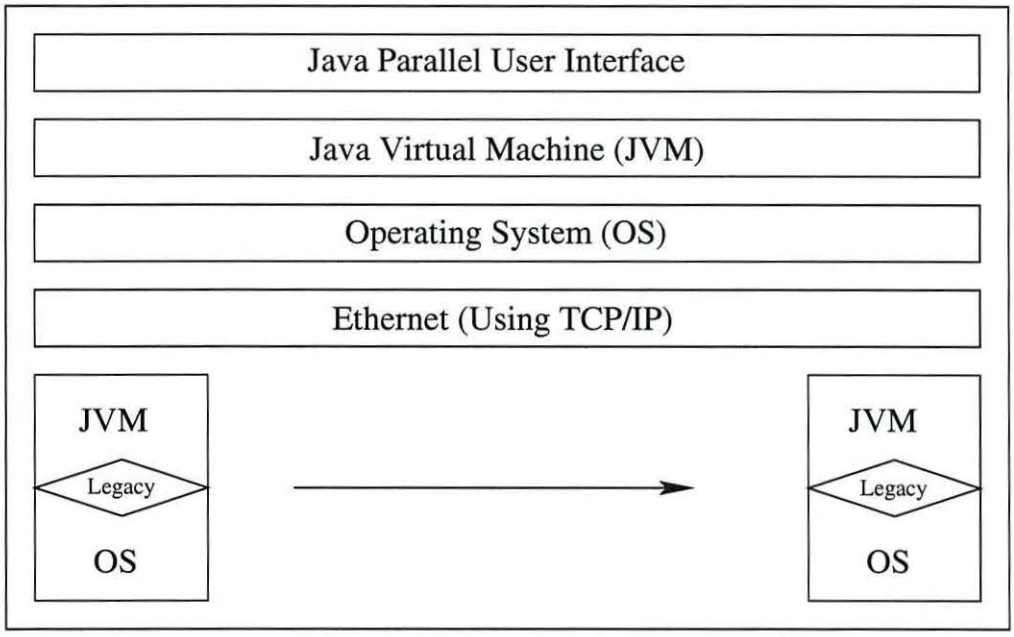

Figure 7.6: *The architecture of the implemented system*

7.5.5 Using Mawrdwr

Once the end user has written the legacy code, an executable can be produced, which can then be uploaded to the nodes using the cluster software, this removes having to individually transfer the program to each of the cluster nodes individually. Once this

is complete a 'bank' of parameters must be set up, these could be the parameters that the user wishes to change on different runs of the program, for instance a parameter commonly varied in this thesis is the cavity length, this would be stored in the parameter bank and can be changed on each run by editing the parameter 'bank'. The bank is like a set of pseudo-CPU registers that can be accessed by all of the nodes, for ease, the parameter bank can be saved and loaded and modified at any point. The bank must also contain a 'range' parameter, this range is used for the automated distribution, in this work the range is the real frequency for contour division. Once the bank is complete the system then instantiates a class for each of the nodes. These classes are then deployed upon the cluster, upon reaching the cluster node the class is executed. The class executes the legacy program, then once it is complete the classes are returned to the controller with the legacy results in it. The results can then be collated and saved, ready for analysis.

7.6 Conclusions

The work described here has been undertaken to facilitate the computation of semiconductor laser models. Upon developing the cluster and its Java *Middleware* a number of issues surrounding distributed systems have been addressed. It has been explained that if the 'problem' to be solved has a large computation to communication ratio then it is ideal for parallel deployment. It has also be explained that the use of legacy applications called by the JRE proved a simple, yet, effective mechanism to avoid code rewriting.

A very generic implementation of a parallel algorithm deployment system written in Java was produced, that allows legacy applications to be deployed on an open source operating system. It uses self instantiating Java executables that run on the node's fault

tolerant daemons, providing full node independence.

Limitations of the current system occur when the computation to communication ratio is small, the communication then becomes the restriction to execution speeds. Overcoming this leads to the legacy linking being re-evaluated and a more direct link employed. The current system uses parameter file passing, this requires the application to read the local disk and as a consequence would need to be eliminated to reduce runtimes; this could perhaps be achieved using JRE *streams* to link to the legacy code.

Further to this work, legacy pre/post processing functionality could be added, thus allowing the legacy code to control the cluster, and also allowing the legacy code to post process the returning results. With this addition to the system, the end user would be able to implement a complete solution and be able to test it without using the deployment software, in effect the system would be completely transparent.

References

[1] J.M. Crichlow. *The Essence of Distributed Systems*. Essence of Computing. Prentice Hall, 1st edition, 2000. ISBN: 0130-15167-X.

[2] L.D. Wittie. Computer networks and distributed systems. *IEEE Computer*, 24(9):67–76, September 1991.

[3] D.J. Becker, T. Sterling, D. Savarese, J.E. Dorband, U.A. Ranawake, and C.V. Packer. Beowulf: A parallel workstation for scientific computation. *Proceedings of the 1995 International Conference on Parallel Processing(ICPP)*, 1:11–14, August 1995.

[4] R. Buyya. *High Performance Cluster Computing*, volume 1. Prentice Hall, 1999. ISBN: 0-13-013784-7.

[5] A. Grama, A. Gupta, G. Karypis, and V. Kumar. *Introduction to Parallel Computing*. Addison Wesley, 2nd edition, 2003. ISBN: 0-201-64865-2.

[6] C.D. Wang and Jr.M.J. Gonzalez. Matching algorithms with parallel architectures: a quantitative approach. *Proceedings of the Scalable High Performance Conference*, pages 215–220, May 1994.

[7] L.A. Barroso, J. Dean, and U. Holzle. Web serch for a planet: The google cluster architecture. *IEEE Micro Magazine*, 23(2):22–28, March 2003.

[8] G. Tel. *Introduction to Distributed Algorithms*. Cambridge, 2nd edition, 2000. ISBN: 0-521-79483-8.

[9] T. Fahringer. Javasymphony: A system for develpment of locality-oriented distributed and parallel java applications. *Proceedings. IEEE International Conference on Cluster Computing*, pages 145–152, November 2000.

[10] I. Foster. The grid: A new infastructure for 21st century science. *Physics Today*, 55(2):42, Feburary 2002. URL: http://www.aip.org/pt/vol-55/iss-2/p42.html.

[11] W. Gentzsch. Grid computing, a vendor's vision. *2nd IEEE/ACM International Symposium of Cluster Computing and the Grid*, pages 323–324, May 2002.

[12] T. Myer. Grid computing: Conceptual flyover for developers. May 2003. URL: http://www.106.ibm.com/developerworks/library/gr-fly.html.

[13] K.J. Ebeling and L.A. Coldren. Analysis of multielement semiconductor lasers. *J.Appl Phys*, 54(6):2962–2968, June 1983.

[14] I. Pierce, P. Rees, and P. S. Spencer. Multimode dynamics in laser doides with optical feedback. *Phys. Rev. A*, 61:053801, 2000.

[15] G.F. Barlow and K.A. Shore. Application of the argument principle method to the calculation of dfb laser diode modes. *International Journal of Numerical Modeling - Electronic Networks, devices and fields*, 14(4):291–302, July 2000.

[16] J.L. Webber. *Using Java 2 Platform*. Que, special edition edition, 1999.

[17] A. Shah and D. Kafura. Symphony: A java-based composition and manipulation framework for distributed legacy resources. *Proceedings. International Symposium on Software Engineering for Parallel and Distributed Systems*, pages 2–12, May 1999.

[18] M.J. Baxter and S. Hope. Java for real-time process control systems. *15th Triennial World Congress of the International Federation of Automatic Control, Barcelona*, July 2002.

[19] S. Hope. Applying object-oriented techniques. *Proceedings of IASTED, International Symposium on Applied Informatics*, pages 174–176, May 1993.

[20] B. McCollum, V. Purnell, P.H. Corr, and P. Milligan. The improvement of a software design methodology by encapsulating knowledge from code. *Proceedings of 24th Euromicro Conference*, 2:913–918, August 1998.

[21] R.F. Boisvert, J. Moreira, M. Philippsen, and R. Pozo. Java and numerical computing. *Computing and Science Engineering*, 3(2):18–24, March 2001.

[22] J.E. Moreira, S.P. Midkiff, and M. Gupta. A comparison of java, c/c++, and fortran for numerical computing. *IEEE Athennas and Propagation Magazine*, 40(5):102–105, October 1998.

[23] E.R. Davies. *Electronics, noise and Signal Recovery*. Academic Press, London, 1993.

[24] V. Getov, S. Flynn-Hummel, S. Mintchev, and T. Ngo. Massively parallel computing in java. *Proceeding of Third Working Conference on Massively Parallel Programming Models*, pages 112–117, November 1997.

[25] F.G. Chen and Ting-Wei Hou. Design, and implementation of a java execution environment. *International Conference on Parallel and Distributed Systems*, pages 686–692, December 1998.

[26] K. Mani Chandy, Adam Rifkin, Paolo A.G. Sivilotti, Jacob Mandelson, Matthew Richardson, Wesley Tanaka, and Luke Weisman. A world-wide distributed system using java and the internet. *Proceedings of 5th IEEE International Symposium on High Performance Computing*, pages 11–18, August 1996.

[27] X. Shen, G. Thiruvathukal, W. Liao, A. Choudhary, and A. Singh. A java graphical user interface for large-scale scientific computations in distributed systems. *Prodceedings. The fourth International Conference on High Performance Computing in the Asia-Pacific Region*, 1:478–484, May 2000.

Chapter 8

Conclusion

This thesis has presented numerical results produced with a coupled cavity model about the modal structure of a semiconductor laser diode subject to coherent optical feedback. The results were generated using a purpose built cluster, the development of which is also presented, the use of commodity components allowed this to be achieved at considerably less cost than commercial clusters. The thesis also reports on the development of the software to utilize the cluster.

Chapters 2 and 3 give an overview of semiconductor laser diodes, and how the lasing action can be achieved under certain conditions, once met allows wavelengths larger than that of the band-gap of the semiconductor to lase. To complete laser diode, a cavity of some form must also be used which contains the semiconductor media to allow reflections in the cavity to build into a standing wave which together with the gain spectrum defines the lasing spectrum.

Chapter 3 gives an overview of the method in which laser diodes are numerical simulated and derives a basic rate equation model which, although very simple gives a good insight into the mechanisms of a laser diode. The addition of external optical feedback

is then introduced using the model developed by Lang and Kobayashi. The problem with most laser diode models is the assumption of a single lasing frequency or single longitudinal mode operation, whereas experimental observations have highlighted a multi-frequency spectrum or multimode nature. This was then addressed through the development of multimode models, they are however limited to weak feedback in the case of the multi-mode Lang and Kobayashi model, or weak to moderate feedback in the iterative model. This limitation in feedback level can be addressed using the coupled cavity model. The coupled cavity model allows any system of cavities to be modeled, and no limitations on the feedback level are made. However, due to the complexity of the model the computational requirement is large and the problem is inherently difficult to solve due to the discontinuous independent variable.

Chapter 4 introduces a new version of a coupled cavity model, instead of a temporally harmonic Fourier analysis, the analysis is conducted using spatial harmonics. This results in a model that has a continuous variable. The continuous variable then allows application of the *Argument Principle Method*(APM), the APM conducts complex contour integrals that can be used to count the possible solutions that exist in a given region. The location of the solution can then be calculated by further application of the APM. A comparison between the analytic solutions for a solitary laser diode and the numerical results obtained using the coupled cavity model was performed. This confirmed that the model is accurate. The configuration of the system was then changed to include optical feedback. The results showed a striking mode 'bending', and significant changes in the lifetimes of the modes.

The effect of increasing in the cavity length results in the expected reduction in the frequency separation between adjacent modes. The longer cavity sees the relatively small diode cavity as a perturbation to the external cavity mode. In the long external

cavity limit the external laser cavity modes dominate at all the optical feedback levels, the modes due to the laser diode are least dominant.

Small variations in refractive index of the laser diode were also investigated and three modes were examined in the short cavity limit, the solitary laser mode and the two adjacent modes. It was found that at very low levels of feedback the laser diode mode exhibits periodic variation in the mode lifetime as expected, but the external cavity modes see the variations as a sub-wavelength perturbation and thus a elliptical movement in the complex frequency plane is seen. However, as the feedback is increased the external cavity modes begin to behave as a laser mode varying in periodic manner with changing refractive index.

Chapter 5 investigated the transitions from one type of mode behavior to another. It was seen that at a certain level of feedback there is a catastrophic loss of mode discrimination and a switching of mode dominance before and after this point. The mode bending is investigated, it was seen that the variation in the modes is most significant between the two closest external modes to that of the solitary laser diode mode. It was also seen that the mode bending reaches a minimum or maximmum at the point of loss of mode discrimination.

Small variations in the cavity length were then examined at different set values of feedback. They showed there is a periodic variation with length, however, at the optical feedback level of the critical point of loss of mode discrimination, no variation the imaginary part of the frequency occurs; the mode becomes phase invariant, this means the mode lifetime does not vary with changes in the cavity length.

The point of loss of mode discrimination was then investigated to show a linear (log scale) or exponential drop with the increasing length of the external cavity. This significant result means that at cavity lengths in excess of forty times that of the laser

cavity the point of catastrophic loss of mode discrimination is unattainable in a realistic devices due to the tiny levels of feedback, this result could then explain why only certain dynamics are observed in the short cavity limit.

Chapter 6 introduced the idea of having gain in the laser's cavity. The effects of adding gain to a short external cavity laser diode are studied. Regions around the point of catastrophic loss of mode discrimination are shown to reflect the result seen in earlier chapter, hence the cold cavity limit results are still valid under gain conditions.

The perturbation caused to the external cavity modes by the laser mode seen in chapter 4, is shown to only be true in low gain conditions. Increasing the gain in the long cavity limit is shown to make the laser mode dominate the structure, rather than the other way around, the laser mode dominates under high gain conditions.

Chapter 7 details the development of a cluster for the deployment of the APM to perform the calculations on the coupled cavity model. Java is used to develop a cluster management tool to allow a transparent system for end user to execute native program. The native program (executable compiled specifically for a particular machine in any language) can the be distributed and executed through a terminal type interface, this has a two fold effect of allowing remote operation and it offers a simple interface.

8.1 Objectives

The primary objective of this work is to study the coupled cavity model's modal structure. Having ascertained the salient features of the modal structure in the 'cold-cavity' limit the work then needs to establish the relevance and context of the results, this will be achieved through the addition of gain in the laser diode's active region.

The cold cavity limit of the coupled cavity model has been studied, and some strik-

ing results have been seen, these include a point of catastrophic loss of mode lifetime discrimination, and as a consequence short/long cavity limits are defined. A phase invariance is seen under certain circumstances making the mode lifetime insensitive to cavity length variation. It is also seen that in the cold cavity limit with long external cavities that the external cavity has complete dominance over the laser cavity; the laser cavity is only seen as a small perturbation to the cavity system. Through the addition of gain into the laser cavity, the cold cavity limit results are shown to be relevant, furthermore in the long cavity case the addition of gain can be seen to cause the laser the establish dominance over the external cavity.

The secondary objective is to observe any relationships between the static and dynamic solutions. This may allow dynamical boundaries to be defined by the static solutions.

The static solutions are seen to be possibly linked to the regimes of laser dynamics. This may mean the the static solutions play a more integral role than previously thought. In is in light of this that study into the static solutions should be made before running any dynamical model, thus offering a firmer grounding into the dynamical system.

The third objective of the work is to examine the advantages of using a distributed system for the processing of the numerical models. This also requires a full appreciation of the parallel processing paradigm.

The use of a purpose build commodity cluster is made for performing the calculations within this work. They are many issues which need to be addressed whilst developing of such a system. The work here explores some of these issues, one such issue is looking at what type of problem is suitable for different types of distributed architecture. Having developed a suitable architecture and suitable software, the cluster is used extensively and has shown that additional computing power allows otherwise

prohibitively extensive problem to be addressed.

The objectives laid out in the introduction have been met. The results presented in this thesis have opened some proverbial doors to other areas of interest. Through the usage of a cluster to examine static solutions of the coupled cavity model, there have been numerous observations they are previously unseen. It is hoped that the results will be used in future work and that this thesis may form the basis of more study.

8.2 Future Work

The work in this thesis looks at the modal structure of the laser diode subject to external optical feedback. The most obvious and useful next step would be to use the results of this work to carry out some dynamical simulations. These could be carried out on the cluster once the pre and post processing legacy modules have been added.

The development of the coupled model has been furthered through the addition of gain to the system. This however could be improved by the development of a introducing a frequency dependent gain.

Appendix A

Standard Coupled Cavity Formalism

A.1 Electromagnetic Model

The fundamental quantities of the electromagnetic model are the electric field and the magnetic field, these are expressed as $\boldsymbol{E}$ and $\boldsymbol{H}$ respectively; the field vectors. They also have associated flux densities, $\boldsymbol{D}$ the Electric Flux Density or Electric Displacement and $\boldsymbol{B}$ the Magnetic Flux Density [1]. These vectors are related through Maxwell's equations:

$$\nabla \times \boldsymbol{E}(t) = -\frac{\partial \boldsymbol{B}(t)}{\partial t}, \tag{A.1}$$

$$\nabla \times \boldsymbol{H}(t) = \boldsymbol{J}(t) + \frac{\partial \boldsymbol{D}(t)}{\partial t}, \tag{A.2}$$

$$\nabla.\boldsymbol{D} = \rho_v \tag{A.3}$$

$$\nabla.\boldsymbol{B} = 0 \tag{A.4}$$

The proportional relationships between the field and flux densities of the electromagnetic model are related by the proportionality constants μ and ϵ, the material permitivity

and permiability respectively. Both the permitivity and permeability are equal to the respective quantity in free space multiplied by the relative quantity, thus the following exists:

$$\epsilon = \epsilon_0 \epsilon_r \tag{A.5}$$

$$\mu = \mu_0 \mu_r \tag{A.6}$$

These terms are related to the velocity of the wave propagation - the material characteristic - in the following way:

$$u_p = \frac{1}{\sqrt{\mu\epsilon}} \tag{A.7}$$

If the wave propagation is in free space then $\mu_r = 1$ and $\epsilon_r = 1$, giving the new relationship:

$$\epsilon = \epsilon_0 \tag{A.8}$$

$$\mu = \mu_0 \tag{A.9}$$

Thus the velocity of the wave in free space can be written:

$$u_p = \frac{1}{\sqrt{\mu_0 \epsilon_0}} \tag{A.10}$$

This is the speed of an electromagnetic wave in free space, which is the speed of light c, thus:

$$c = \frac{1}{\sqrt{\mu_0 \epsilon_0}} \tag{A.11}$$

Knowing $\mu_0 = 4\pi \times 10^{-7}(H/m)$ and $c = 3 \times 10^8(m/s)$ are fixed then:

$$\epsilon_0 = \frac{1}{c^2\mu_0} = \frac{1}{36\pi} \times 10^{-9} = 8.854 \times 10^{-12}(F/m) \tag{A.12}$$

Using these proportionality constants and defining a *conductivity*, σ relating the current density and the electric field density, the following stand true:

$$\boldsymbol{D(t)} = \epsilon \boldsymbol{E(t)} + \boldsymbol{P(t)}, \tag{A.13}$$

$$\boldsymbol{B(t)} = \mu \boldsymbol{H(t)}, \tag{A.14}$$

$$\boldsymbol{J(t)} = \sigma \boldsymbol{E(t)}, \tag{A.15}$$

Assume there are no free charges, then $\rho_v = 0$ and also assuming static polarization, $\boldsymbol{P(t)} = 0$. (A.1) cam be rewritten using (A.14); (A.2) can also be rewritten using (A.13) and (A.15), thus eliminating both the electric and magnetic flux. Maxwell's equations reduce to:

$$\boldsymbol{\nabla} \times \boldsymbol{E(t)} = -\mu \frac{\partial \boldsymbol{H(t)}}{\partial t}, \tag{A.16}$$

$$\boldsymbol{\nabla} \times \boldsymbol{H(t)} = \sigma \boldsymbol{E(t)} + \epsilon \frac{\partial \boldsymbol{E(t)}}{\partial t}, \tag{A.17}$$

$$\boldsymbol{\nabla}.\boldsymbol{D} = 0, \tag{A.18}$$

$$\boldsymbol{\nabla}.\boldsymbol{B} = 0. \tag{A.19}$$

The electromagnetic wave equation can now be derived.

A.2 The Electromagnetic Wave Equation

The general form of the electromagnetic wave equation can be derived using Maxwell's equations. Firstly take the curl of both sides of (A.16) giving:

$$\nabla \times \nabla \times \boldsymbol{E}(t) = -\mu \frac{\partial}{\partial t}(\nabla \times \boldsymbol{H}(t)), \tag{A.20}$$

Using the *vector identity* $\nabla \times \nabla \times \boldsymbol{E}(t) = \nabla(\nabla.\boldsymbol{E}(t)) - \nabla^2\boldsymbol{E}(t)$ and because of (A.18) it can be shown that $\nabla.\boldsymbol{E}(t) = 0$ by substitution from (A.13) with static polarisation. So now $\nabla \times \nabla \times \boldsymbol{E} = -\nabla^2\boldsymbol{E}$, now substituting into (A.20):

$$\nabla^2\boldsymbol{E}(t) = \mu \frac{\partial \nabla \times \boldsymbol{H}(t)}{\partial t^2}, \tag{A.21}$$

Using (A.17) to rewrite (A.21) in terms of electric field, $\boldsymbol{E}(t)$:

$$\nabla^2\boldsymbol{E} = \mu\sigma \frac{\partial \boldsymbol{E}(t)}{\partial t} + \mu\epsilon \frac{\partial^2 \boldsymbol{E}(t)}{\partial t^2}, \tag{A.22}$$

giving the general form of the wave equation:

$$\nabla^2\boldsymbol{E}(t) - \mu\sigma \frac{\partial \boldsymbol{E}(t)}{\partial t} - \mu\epsilon \frac{\partial^2 \boldsymbol{E}(t)}{\partial t^2} = 0. \tag{A.23}$$

A.3 Plane Electromagnetic Waves

The electromagnetic wave equation can be used in any orthogonal coordinate system. In Cartesian coordinates $\boldsymbol{E}(t)$ can then be defined as:

$$\boldsymbol{E}(t) = \boldsymbol{a}_x E_x(t) + \boldsymbol{a}_y E_y(t) + \boldsymbol{a}_z E_z(t). \tag{A.24}$$

Consequentially the electromagnetic wave equation can be expressed as three scalar wave equations, here the x component is shown as an example:

$$\frac{\partial^2 E_x}{\partial x^2} + \frac{\partial^2 E_x}{\partial y^2} + \frac{\partial^2 E_x}{\partial z^2} - \mu\sigma\frac{\partial E_x(t)}{\partial t} - \mu\epsilon\frac{\partial^2 E_x(t)}{\partial t^2} = 0. \tag{A.25}$$

Without loss of generality a rectangular coordinate can be oriented so that $E_y(t) = E_z(t) = 0$, the wave is defined as being perpendicular to the x-y plane and traveling in the z direction. In thus doing, the spatial variables are reduced. This then reduces $\boldsymbol{E(t)}$ to:

$$\boldsymbol{E(t)} = \boldsymbol{a}_x E_x(t) \tag{A.26}$$

A plane wave front traveling in the z direction is defined as infinite and unbounded in the $x - y$ plane, then:

$$\frac{\partial}{\partial x} = \frac{\partial}{\partial y} = 0. \tag{A.27}$$

The first term of the generic electromagnetic wave equation (A.23) can be rewritten as:

$$\boldsymbol{\nabla^2 E(t)} = \left(\boldsymbol{a}_x\frac{\partial^2}{\partial x^2} + \boldsymbol{a}_y\frac{\partial^2}{\partial y^2} + \boldsymbol{a}_z\frac{\partial^2}{\partial z^2}\right)E_x(t), \tag{A.28}$$

Because of (A.26) and knowing (A.27) the first term reduces to:

$$\boldsymbol{\nabla^2 E(t)} = \frac{\partial^2 E_x(z,t)}{\partial z^2} \tag{A.29}$$

Substituting (A.29) into the generic electromagnetic wave equation, (A.23), gives the plane one-dimensional electromagnetic wave equation:

$$\frac{\partial^2 E_x(z,t)}{\partial z^2} - \mu\sigma\frac{\partial E_x(z,t)}{\partial t} - \mu\epsilon\frac{\partial^2 E_x(z,t)}{\partial t^2} = 0. \tag{A.30}$$

A.4 The Time Harmonic Plane Wave Equation Solution

If we assume the waves to be time harmonic, the fields can be expressed as a Fourier component:

$$E_x(z,t) = E_x(z)e^{j\omega t} \tag{A.31}$$

The following equation is of the from required to satisfy the 'standard' wave equation solution.

$$\frac{\partial^2 E_x(z)}{\partial z^2} + k^2 E_x(z) = 0, \tag{A.32}$$

a complex propagation coefficient k is included, this contains all the material parameters, by substituting (A.31) into (A.30) the following is obtained:

$$\frac{\partial^2 E_x(z)}{\partial z^2} + \left(\omega^2\mu\epsilon - j\omega\mu\sigma\right)E_x(z) = 0 \tag{A.33}$$

The *free space propagation coefficient* k_0 is defined along with a complex permitivity $\hat{\epsilon}$. The following relationships are obtained by defining k^2 as:

$$k^2 = k_0^2\hat{\epsilon} \tag{A.34}$$

giving:

$$k_0^2 = \omega^2\mu_0\epsilon_0 = \frac{\omega^2}{c^2} \tag{A.35}$$

$$\hat{\epsilon} = \epsilon_r - j\frac{\sigma}{\omega\epsilon_0} \tag{A.36}$$

Resulting in a key relationship of:

$$k = k_0 \sqrt{\hat{\epsilon}} \tag{A.37}$$

This one dimensional electromagnetic plane wave equation,(A.32), it can readily show that the solution is of the form:

$$E(z) = Ae^{-jkz} + Be^{jkz} \tag{A.38}$$

Using equation (A.16) a similar expression for the magnetic field can be obtained. As the electric field is harmonic so to must be the magnetic field, rewriting (A.16) gives:

$$\nabla \times \boldsymbol{E}(z) = -j\mu\omega \boldsymbol{H}(z) \tag{A.39}$$

substituting into the L.H.S. of (A.39) gives:

$$\nabla \times \boldsymbol{E}(z) = \begin{vmatrix} \boldsymbol{a}_x & \boldsymbol{a}_y & \boldsymbol{a}_z \\ 0 & 0 & \frac{\partial}{\partial z} \\ E(z) & 0 & 0 \end{vmatrix} = \boldsymbol{a}_y \frac{\partial}{\partial z} E(z), \tag{A.40}$$

The magnetic field can also be expressed as three vector scalar products:

$$\boldsymbol{H}(z) = \boldsymbol{a}_x H_x(z) + \boldsymbol{a}_y H_y(z) + \boldsymbol{a}_z H_z(z), \tag{A.41}$$

which leads to:

$$H_y = \frac{1}{-j\omega\mu} \frac{\partial}{\partial z} E(z), \tag{A.42}$$

and by substituting (A.38) into (A.42) we get:

$$H(z) = \frac{Ak}{\mu\omega}e^{-ikz} + \frac{Bk}{\mu\omega}e^{ikz}. \tag{A.43}$$

Giving the electromagnetic field solutions for the one dimensional plane wave equation as:

$$E(z) = Ae^{-jkz} + Be^{jkz} \tag{A.44}$$

$$H(z) = \frac{Ak}{\mu\omega}e^{-ikz} + \frac{Bk}{\mu\omega}e^{ikz} \tag{A.45}$$

. (A.46)

Traditionally in optical systems the main parameter of interest is the refractive index. In a simple system, where the conductivity, $\sigma = 0$ the refractive index is real related to the permitivity by $n = \sqrt{\epsilon_r \mu_r}$, where $\mu_r \approx 1$, giving $n = \sqrt{\epsilon_r}$. However the system described here, the conductivity is not equal to zero and as a consequence the permitivity is complex, then so to must the refractive index be complex as it is dependent upon the complex permitivity, from:

$$\hat{n} = \sqrt{\hat{\epsilon}}. \tag{A.47}$$

The complex refractive index is then defined as:

$$\hat{n} = \eta + j\kappa \tag{A.48}$$

The complex propagation coefficient can now be written in terms of a complex refractive index:

$$k = k_0\hat{n} = k_0(\eta + j\kappa) = \frac{\omega}{c}(\eta + j\kappa). \tag{A.49}$$

Relating κ to the system gain is also necessary, the expression for *power* is used:

$$P(z) = P_0 e^{\gamma z} = |E_f|^2 = |A|^2 e^{2\Im\{k\}z} \tag{A.50}$$

where E_f is the forward propagating field, γ is the absorption, this equal to $-g$ the system gain, then (A.50) can be rewritten as:

$$P(z) = P_0 e^{-gz} = |A|^2 e^{2\Im\{k\}z} \tag{A.51}$$

therefore,

$$2\Im\{k\} = -g = 2\kappa\frac{\omega}{c} \tag{A.52}$$

giving us the relationship between k and the g as:

$$\kappa = -\frac{g}{2}\frac{c}{\omega} \tag{A.53}$$

A.4.1 Coupled Cavity System

Up until this point the the system has been in linear, isotropic, homogeneous medium of infinite extent. Now consider a boundary between two semi-infinite linear isotropic media. The boundary under consideration is at z, from medium m to medium $m + 1$:

$$E_m = E_{m+1}, \tag{A.54}$$

$$H_m = H_{m+1}. \tag{A.55}$$

Substituting in equations (A.38) and (A.43) into (A.54) and (A.55) respectively we get:

$$A_m e^{-ik_m z} + B_m e^{ik_m z} = A_{m+1} e^{-ik_{m+1} z} + B_{m+1} e^{ik_{m+1} z} \tag{A.56}$$

and,

$$k_m A_m e^{-ik_m z} - k_m B_m e^{ik_m z} = k_{m+1} A_{m+1} e^{-ik_{m+1} z} - k_{m+1} B_{m+1} e^{ik_{m+1} z} \tag{A.57}$$

Now rearrange (A.56) in terms of B_{m+1} to get:

$$B_{m+1} = \frac{A_{m+1} e^{-ik_{m+1} z} + B_{m+1} e^{ik_{m+1} z} - A_m e^{-ik_m z}}{e^{ik_m z}} \tag{A.58}$$

We then substitute (A.58) in (A.57), giving:

$$A_{m+1} = A_m \left(\frac{k_{m+1} + k_m}{2k_{m+1}} \right) e^{-i(k_{m+1} - k_m) z} + B_m \left(\frac{k_{m+1} - k_m}{2k_{m+1}} \right) e^{i(k_{m+1} + k_m) z} \tag{A.59}$$

Similarly the process can be repeated for B_{m+1}, giving:

$$B_{m+1} = A_m \left(\frac{k_{m+1} - k_m}{2k_{m+1}} \right) e^{-i(k_{m+1} + k_m) z} + B_m \left(\frac{k_{m+1} + k_m}{2k_{m+1}} \right) e^{-i(k_{m+1} - k_m) z} \tag{A.60}$$

Matrix Equations

These equations are more conventionally expressed as a matrix equation:

$$\begin{pmatrix} A_{m+1} \\ B_{m+1} \end{pmatrix} = Q(z_m) \begin{pmatrix} A_m \\ B_m \end{pmatrix} \tag{A.61}$$

where

$$Q(z_m) = \begin{pmatrix} \frac{k_{m+1}+k_m}{2k_{m+1}} e^{i(km+1-k_m)z}, & \frac{k_{m+1}-k_m}{2k_{m+1}} e^{i(km+1+k_m)z} \\ \frac{k_{m+1}-k_m}{2k_{m+1}} e^{-i(km+1+k_m)z}, & \frac{k_{m+1}+k_m}{2k_{m+1}} e^{-i(km+1-k_m)z} \end{pmatrix}$$

This matrix can then be used at multiple boundaries in a coupled cavity system to

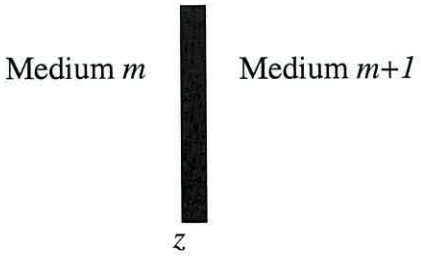

Figure A.1: *A semi infinite system with only one boundary.*

calculate any number of results. Figure A.1 depicts the single boundary semi-infinite system from the derivation. If a complete system is defined then the matrix can be applied at each boundary. Figure A.2 a simple Fabry-Perot laser in air shown as an example of the coupled cavity application. Equation (A.62) shows the system equation

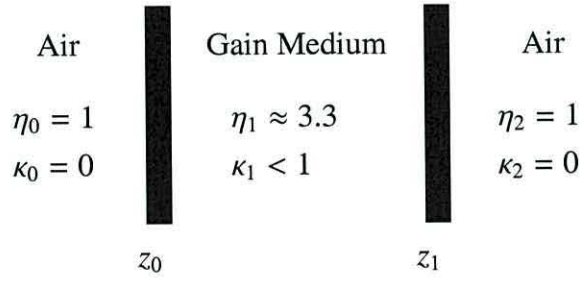

Figure A.2: *A cavity system, with three boundaries.*

for the Fabry-Perot laser in Figure A.2.

$$\begin{pmatrix} A_3 \\ B_3 \end{pmatrix} = Q(z_1)Q(z_0) \begin{pmatrix} A_0 \\ B_0 \end{pmatrix} \tag{A.62}$$

Solution Method

The solution of (A.62) aims to establish the standing waves in the system, this corresponds to *resonant modes* of the optical system. To locate the resonant modes $A_0 = 1$, this is arbitrary, $A_3 = 0$ set to zero, the point of solution. The resonant modes of interest are in the laser medium, therefore the solutions must be found between boundary 0 and 1, the dependent variable here is the complex wave number, k_1. By resolution of the real and imaginary components the desired results can be obtained. The real part yields the the solution of the frequency of the resonant mode,

$$\omega_{mode} = \frac{c}{\eta}\mathscr{R}\{k_1\} \tag{A.63}$$

the other desired optical result of interest is the threshold gain, g_{th} this is related to k_1 in the following way:

$$g_{th} = -2\mathscr{I}\{k_1\} \tag{A.64}$$

References

[1] David K. Cheng. *Fundamentals of Engineering Electromagnetics*. Addison Wesley, 1993. ISBN: 0-201-60071-4.

Appendix B

Publications

B.1 Journal

- Cold Cavity analysis of the longitudinal mode structure of laser diodes subject to external optical feedback. (with Paul S. Spencer and Paul Rees) *submitted to Phys. Rev. A. June 2004*
- Polychromatic Coupled Cavity Model of Passive Structures (with Paul S. Spencer and Paul Rees) *accepted for publication by IEE proc. Optoelectronics November 2004*
- Mawrdwr - A High Speed Distributed System for Numerical Computation (with Paul S. Spencer and Sian Hope) *submitted to J. Sys. Arch. April 2004*

B.2 Conference

- Catastrophic Loss of Mode Discrimination in Coupled Cavity Systems. (with Paul S.Spencer, Iestyn Pierce and Paul Rees) *SPIE Fluctuations and Noise, Gran*

Canaria, Spain, 25-28 May 2004

- Coupled Cavity multi-mode model of laser diode subject to optical feedback. (with Paul S. Spencer and K. Alan Shore) *SIOE 03, Cardiff, April 2003*

- Determination of nonlinear modulation response of semiconductor laser diodes by quadrature detection. (with I. Pierce, P. Rees, P.S. Spencer and K.A.Shore) *IOP Quantum Electronics and Photonics 15, Glasgow, September 2001*

- Quadrature detection method for determination of non-linear response of semiconductor laser diodes. (with I. Pierce, P. Rees. P.S. Spencer and K.A. Shore) *SIOE 01, Cardiff, April 2001*